A STUDY OF SEMICONDUCTING OXIDE OXYGEN ELECTRODES IN ALKALINE MEDIA.

A thesis submitted for the
degree of
Doctor of Philosophy

by

N. P. RASIYAH.

at

Department of Chemistry
The City University
London.

This work was carried out under the supervision of
Professor A.C.C.Tseung.

ACKNOWLEDGEMENT

I would like to express my sincere and grateful thanks to Professor A.C.C.Tseung for his guidance and encouragement throughout this work. My thanks are also extended to [redacted] for providing invaluable guidance at the early stages of this work. I am also grateful to my student colleagues in the Electrochemistry group for many valuable discussions, to The City University library and technical staff for helping on numerous aspects of the work and to [redacted] for persisting with a difficult manuscript.

I would also like to acknowledge the receipt of an SRC assistantship for carrying out the studies reported in Chapter 7. The financial support by the NRDC for patenting the work relating to the Li doped Co_3O_4 system is also acknowledged.

Finally I would like to extend my deepest gratitude to my parents for their encouragement and financial support throughout my studies.

ABSTRACT.

The oxygen electrode is highly irreversible and is the main cause of efficiency losses in many electrochemical systems. In recent years the use of oxides as oxygen electrodes have been suggested and many oxide electrodes were studied in this respect. Of such oxides, the spinel structured $NiCo_2O_4$ was shown to be an active oxygen electrode in alkaline medium.

This study reports the work that was carried out to investigate the reasons for the good activity of $NiCo_2O_4$ as an oxygen electrode. Studies on the oxygen evolution aspects were carried out by investigating the oxidation state transitions of the surface compounds formed before oxygen is evolved and ascertaining the Tafel and reaction order parameters for oxygen evolution. The results of such studies and a knowledge of the transition metal cationic sites on $NiCo_2O_4$ enabled the postulation of a mechanism, suggesting that trivalent cations of Ni and Co are more active for oxygen evolution rather than the divalent ones. This postulation was confirmed by carrying out oxygen evolution studies on similar lines, on 4 oxides of the Li doped Co_3O_4 system. This work enabled the development of a better oxygen evolution electrocatalyst than $NiCo_2O_4$. The performance of a Teflon bonded 10 at. % Li doped Co_3O_4 electrode was found to be 1.52V vs the dynamic hydrogen electrode at a current

density of 1A cm^{-2} in 5 mol dm^{-3} KOH at $70^{o}C$. This performance is significantly better than that obtained on $NiCo_2O_4$.

This thesis also discusses some factors that govern the selection of oxides for oxygen evolution, such as the role of the lower metal oxide/higher metal oxide couple and the corrosion stability of oxides.

Since the efficiency of an oxygen evolving electrode is determined by the electrocatalyst characteristics and the electrode characteristics, some effort was also directed in comparing the efficiency of porous non Teflon bonded and Teflon bonded electrodes. The effectiveness factor of Teflon bonded electrodes for oxygen evolution was found to be higher than the non Teflon bonded porous electrodes.

On oxygen reduction aspects, the potentiostatic pulse technique was used to study the mechanism of oxygen reduction on $NiCo_2O_4$. A mechanism has been proposed by considering the experimentally observed values of the kinetic parameters and the nature of the cation sites on $NiCo_2O_4$

Oxygen reduction studies were also carried out on composite $NiCo_2O_4$/graphite electrodes. In these electrodes the HO_2^- formed by oxygen reduction on graphite is broken down by $NiCo_2O_4$, thus, bringing about a synergetic

enhancement in performance. This study establishes by means of simple models, the factors that govern the attainment of the maximum oxygen reduction performance in composite electrodes. It also establishes that the peroxide decomposition activity of oxides such as $NiCo_2O_4$ is sufficient to bring about the maximum possible oxygen reduction performance, if the two electrocatalysts are in a state of interparticulate mix.

CONTENTS

Page

CHAPTER THREE

STUDY OF SURFACE COMPOUND FORMATION AT POTENTIALS BELOW OXYGEN EVOLUTION POTENTIALS.

CHAPTER FOUR

OXYGEN EVOLUTION STUDIES ON $NiCo_2O_4$ AND ON THE Li DOPED Co_3O_4 OXIDES.

Page

Page

LIST OF FIGURES

Page

Page

LIST OF TABLES

ABBREVIATIONS

BET	Brunauer Emmett and Teller.
dhe	dynamic hydrogen electrode.
she	standard hydrogen electrode.
rhe	reversible hydrogen electrode.
E	potential.
E_e	equilibrium potential.
E_e^o	standard equilibrium potential.
E^1	potential of lower oxide/higher oxide couple.
i	current density.
i_t	transient current density.
i_o	pseudo exchange current density.
FEP	fluorinated ethylene propylene.
C	concentration.

CHAPTER ONE

INTRODUCTION.

1.1 Introduction.

The energy problems facing many nations has led to considerable interest in electrochemical energy conversion and storage devices. An important part of most such devices is the oxygen electrode.

$$O_2 + 4H^+ + 4e \rightleftarrows 2H_2O \qquad (1.1)$$

(acid medium, $E_e^o = 1.229V$)

$$O_2 + 2H_2O + 4e \rightleftarrows 4OH^- \qquad (1.2)$$

(alkaline medium, $E_e^o = 0.401V$)

Unfortunately the oxygen electrode is highly irreversible, causing excessive voltage losses and restrictions on power densities of the cells.

The pronounced irreversibility of the oxygen electrode reaction at moderate temperatures has severely complicated mechanistic studies. The exchange current density of the oxygen electrode is very low (typically 10^{-10} to 10^{-11} A cm^{-2}) on an effective unit surface. Consequently the current densities near the reversible potential are generally too low to permit measurements under conditions where the kinetics are sensitive to the reverse as well as the forward reactions. Further, the experimentally obtainable portions of the cathodic and anodic branches of the polarisation curves are sufficiently separated

in potential so that the surface conditions differ very substantially. Therefore the cathodic and anodic processes are generally not the reverse of each other. To complicate the situation further the oxygen electrode reaction proceeds through a large number of reaction paths. This explains why the mechanism of oxygen generation and reduction are still not fully understood even on Pt, the most studied oxygen electrode.

1.2 Oxygen Evolution.

The oxygen evolution reaction is one of the most fundamental anodic reactions. It is the anodic process in water electrolysis, electrowinning of certain metals and in the charging cycle of metal-air batteries. However, it is a difficult and complicated reaction to study. It takes place with the formation of unstable surface intermediates such as hydroxides, oxides, dioxides or peroxide by stepwise consecutive reactions. The number and type of intermediates will depend on the electrode surface and the last formed intermediate decomposes to give oxygen.

In recent years much research effort has been directed towards the development of efficient and suitable anodes for water electrolysis. These efforts have been motivated due to the belief that hydrogen is a suitable source of secondary energy for the future[1,2,3,4], and the simplest method of producing hydrogen is by water

electrolysis. The anode materials in conventional alkaline electrolysers are generally nickel plated iron sheets or ferronickel alloy sheets [5]. The oxygen evolution overvoltages on these anodes are 0.25 to 0.30V at a current density of 0.2A cm^{-2} at $80^{o}C$. These metalic anodes also show deterioration in performance on a long term basis, which is attributed to the formation of poorly conducting oxide films on the surface[79] and anodic dissolution, thus limiting the anode life. To overcome these disadvantages of low efficiency and poor long term stability, transition metal oxides were selected as suitable material and oxygen evolution studies have been carried out on many oxides[63-71,78,79]. Furthermore, oxide electrodes were prepared in porous forms to increase the effective electrode area. Research efforts directed in these lines have been fruitful in developing stable oxygen evolution anodes with fairly low overvoltages. For example, the overvoltage of a porous Teflon bonded $NiCo_2O_4$ electrode is $\sim$ 0.4V for an oxygen evolution current density of 1 A cm^{-2} in 5 mol dm^{-3} KOH, at $70^{o}C$. The long term stability of these electrodes were also found to be good[7]. The use these novel anodes in electrolysers will reduce energy consumption and will enable electrolysers to perform at higher efficiencies.

1.3 Oxygen Dissolution.

The electrochemical dissolution of oxygen presents

one of the challenging problems in electrochemistry. It is the cathodic process in most fuel cells and metal-air batteries which are very important energy converters. The air cathode also has potential use in the chloro-alkali industry[6]. The replacement of the hydrogen evolving cathode by a air depolarised cathode in diaphragm cells can reduce the equilibrium potential for chlorine evolution from 2.15V to 0.95V, and therefore could bring about a considerable saving in energy. The present day air cathodes use expensive platinum group of metals as electrocatalysts in an effort to achieve acceptable level of performance. To reduce the electrocatalyst cost it is necessary to use high surface area forms of the platinum group of metals. However, the performance of such electrodes are difficult to maintain over long operating times due to loss of surface area of electrocatalyst[8,9]. These short comings are some of the reasons for the retarded development of energy converters such as fuel cells and restricting its application to specialist purposes such as space programs. The development of efficient, inexpensive oxygen reduction electrocatalysts is an imperative task if electrochemical energy converters are to be successful. The possible use of transition metal oxides for this application is rated as high.

It has been found that on most of the substrates the oxygen dissolution process takes place by the formation of peroxide as an intermediate, by

$$O_2 + 2H^+ + 2e \rightarrow H_2O_2 \qquad (1.3)$$

(acid medium, $E_e^o = 0.682V$)

$$O_2 + H_2O + 2e \rightarrow HO_2^- + OH^- \qquad (1.4)$$

(alkaline medium, $E_e^o = -0.076V$)

On most substrates other than graphite the peroxide is further reduced electrochemically by

$$H_2O_2 + 2H^+ + 2e \rightarrow 2H_2O \qquad (1.5)$$

(acid medium, $E_e = 1.77V$)

$$HO_2^- + H_2O + 2e \rightarrow 3OH^- \qquad (1.6)$$

(alkaline medium, $E_e^o = 0.88V$)

or decomposed chemically by

$$2H_2O_2 \rightarrow 2H_2O + O_2 \qquad (1.7)$$

(acid medium)

$$2HO_2^- \rightarrow O_2 + 2OH^- \qquad (1.8)$$

(alkaline medium)

The oxygen formed is recyled through reactions 1.3 or 1.4 to obtain an overall reaction of 4 electrons.

There are three possible ways of improving the kinetics of oxygen dissolution -

(1) To speed up the rate of electrochemical reduction of peroxide. This is not likely to be successful since this step is known to be highly irreversible.

(2) To speed up the rate of chemical decomposition of peroxide. This approach has been used by many workers. Graphite is known to reduce oxygen only upto the formation of peroxide. By incorporating peroxide decomposition catalysts like Ag and spinel oxides into graphite electrodes[10,11,12], the peroxide has been decomposed chemically and the oxygen formed is recycled to obtain enhanced performance.

(3) The third approach is to induce the oxygen reduction process to bypass the peroxide formation step. Isotopic studies carried out by Davis, Clark, Yeager and Hovorka[13] showed conclusively that the 0 = 0 bond of the oxygen molecule remains unbroken on conversion to peroxide. Thus, the key to this approach may lie in the electrocatalyst's ability to dissociatively chemisorb oxygen. If this condition is fulfilled, peroxide will not be formed as an intermediate and oxygen reduction will go directly to OH^- ions via a 4 electron process. This method of approach has been successful on certain oxides[14,15], but only at high temperatures.

1.4 The aim of this work.

The mixed spinel $NiCo_2O_4$ has been found to be a good electrocatlyst for oxygen evolution[78] and reduction[130] in alkaline medium. This work investigates the mechanism of oxygen evolution and reduction on $NiCo_2O_4$. The oxygen evolution studies on $NiCo_2O_4$ are reported in chapters 3 and 4 together with mechanistic studies on a more efficient oxygen evolution electrocatalyst, Li doped Co_3O_4.

The investigation carried out to establish certain guidelines for choosing transition metal oxides for oxygen evolution in alkaline medium is reported in chapter 5. Also reported in chapter 5 are the transient studies carried out to compare the efficiencies of porous Teflon bonded and porous non Teflon bonded electrodes for oxygen evolution.

Chapter 6 reports the work carried out to determine the mechanism of oxygen reduction on $NiCo_2O_4$ in alkaline medium. In chapter 7 the investigation carried out to optimise $NiCo_2O_4$/graphite composite electrodes for oxygen reduction is reported. This chapter highlights certain important characteristics that governs the fabrication of efficient composite electrodes for oxygen reduction.

The mechanisms postulated in this study are based on kinetic indicators such as Tafel slopes and reaction order parameters, obtained by steady state current-potential measurements. In instances where there were doubts to the

Tafel dependence of the current-potential characteristics obtained by steady state measurements, potentiostatic transient studies were carried out to confirm the Tafel behaviour. Thus, it was necessary to carry out all electrochemical measurements by potentiostatic transient technique to study the mechanism of oxygen reduction on $NiCo_2O_4$.

Although mechanistic pathways are generally postulated on the basis of electrochemical indicators, it is also essential to consider mechanistic paths from the point of view of the nature of the active site (transition metal ion) of the electrocatalyst. The characteristics of the transition metal cation that could influence the mechanistic path are; the oxidation state of the cation at rest, the highest oxidation state the cation could attain, the number of cations, the relative abundance of the cations if more than one is present and the cation environment, etc. Therefore, when mechanisms were postulated in this study, the site characteristics were taken into account as much as possible. For this purpose an ionic model was chosen to relate the property of the oxide to the electrochemical process, rather than a collective (band) model. It is hoped that this simple approach will facilitate a better understanding and development of electrocatalysts.

CHAPTER TWO

EXPERIMENTAL ASPECTS AND SOME STRUCTURAL ASPECTS OF THE ELECTROCATALYSTS.

2.1 Introduction.

This thesis reports the work carried out on the electrochemistry of oxygen on certain oxides. The experimental procedures that were used for material preparation, electrochemical testing and material characterisation, in this study, have already been well established by previous workers in the Electrochemistry Laboratory of The City University. These experimental procedures have been well documented in numerous Ph.D theses and published literature. Therefore, such procedures will only be described in short and will be referred to the original literature.

This chapter describes the preparation and characterisation of all electrocatalysts used in this study, and the galvanostatic steady state and potentiostatic pulse methods of electrochemical evaluation of the electrodes. The electrodes used in this study are of the hydrophobic type and their preparatory method is also included here. However, some electrochemical techniques and some precautions taken in electrode preparation are described in the relevant chapters for the sake of clarity. This chapter also includes a short description of structural aspects of the electrocatalysts.

2.2 Preparation of Electrocatalysts:

2.2.1 Freeze Drying.

The preparation of oxide electrocatalysts by the

method of freeze drying has been discussed in three research publications[113,114,115]. The method involves rapidly cooling a solution of two or more precursor metal salts, therefore bringing about freezing without fractional crystalisation, thus retaining the random ordering of ions of the solution. The ice is sublimed in vacuum and hence the solutes are effectively immobilised during the drying process, thus, the degree of homogeneity found in solution will be retained. The dried salts are vacuum decomposed and heat treated in air to obtain the oxide. The atomic mixing brought about during freeze drying helps to form a homogenous product and lowers the heat treatment temperature and time, thus producing high surface area powders.

$NiCo_2O_4$[157,92], 10 at. % Li doped NiO[113], Co_3O_4 and the 3 Li doped (4, 7 and 10 at .%) cobalt oxides used in this study were prepared by freeze drying. A solution of 35g of $Co(No_3)_2.6H_2O$ containing the appropriate quantity of Li in the form of $LiNo_3$ in 150 cm^3 of water was freeze dried to obtain the oxides of Co. The heat treatment conditions were 400°C for 10 hours for $NiCo_2O_4$ and the Li doped NiO, and 500°C for 5 hours for the 4 oxides of cobalt.

2.2.2 Preparation of IrO_2, RuO_2, PtO_2 and PdO.

These four oxides were prepared by the thermal

treatment of the respective chlorides.

Preparation of IrO_2[67]; 0.7g of $IrCl_3 . 3H_2O$ was dissolved in ∿ 10 cm^3 of 20% HCl and to this solution 4 cm^3 of 30% H_2O_2 was added. The resulting solution was dried at 100°C for 1 hour and then heated at 450°C for 1 hour.

Preparation of RuO_2[155]; About 1g of $RuCl_3 . 3H_2O$ was dissolved in a minimum quantity of 20% HCl. To this solution, 5 cm^3 of 30% H_2O_2 was added. The resulting solution was dried at 100°C for 1 hour and heated at 450°C for 1 hour.

Preparation of PtO_2[63]; About 1g of chloroplatinic acid ($H_2PtCl_6 . 6H_2O$) was dissolved in a minimum amount of water. To this solution, 5 cm^3 of 30% H_2O_2 was added. The resulting solution was dried at 100°C for 1 hour and heated at 450°C for 1 hour.

Preparation of PdO; About 1g of $PdCl_2$ was dissolved in a minimum amount of water. This solution was dried at 100°C for 1 hour and heated at 450°C for 4 hour.

2.2.3 Preparation of high surface area graphite.

High surface area graphite was prepared by a vacuum grinding method[164]. This method was optimised by Kent[158] and was used extensively by Jasem[157]. Basically the method

involves vacuum grinding about 20g of low surface area graphite (B.P. Chemicals Ltd., Sunbury, 5 M^2 g^{-1}) in a vibratory ball mill (Mega Pact Laboratory Mill, Pilamec Ltd., Gloucestershire) for 14 hours using nickel shots as grinding elements.

2.3 Characterisation of the Electrocatalysts.

2.3.1 Determination of the Specific Surface Area of the Electrocatalysts.

The Brunauer, Emmet and Teller (BET) specific surface areas of the electrocatalyst powders were measured using a laboratory built apparatus which incorporated a microbalance. The description of the apparatus and the method of measurement is given else where[157,159,161]. Table 2.1 gives the BET specific surface areas of the electrocatalysts.

2.3.2 Electrical Resistivity.

The D.C. electrical resistivity of the powder samples were measured using a Teflon cell similar to that employed by Bevan[159] and Goldstein[161]. The cell consisted of a Teflon ring in which the powder sample was compressed between two stainless steel discs. When the powder is compressed, it's electrical resistance (measured by a multimeter at the two discs) fell to a minimum as the mutual contact among the particles increased. The

Table 2.1: Brunauer, Emmet and Teller specific surface areas of electrocatalyst.

Oxide	Specific surface areas $M^2 g^{-1}$
$NiCo_2O_4$	43
Co_3O_4	8
10 at.% Li doped NiO	47
4 at. % Li doped Co_3O_4	8
7 at. % Li doped Co_3O_4	8
10 at. % Li doped Co_3O_4	8
*10 at. % Li doped Co_3O_4	38
PdO	9
RuO_2	17
IrO_2	14
PtO_2	14
Graphite	490

*heat treatment conditions; 400°C, 10 hours in air.

electrical resistivity of the powder was calculated using the minimum value of the resistance and the dimensions of the compact powder. The resistivity of the powder obtained by this method is not very reliable. However, adequate reproducibility could be achieved by using similar compression treatment and a fixed mass of the powder. Table 2.2 gives the electrical resistivities of the oxides and compares them with the values quoted in the literature

2.3.3. X-ray Analysis.

X-ray characterisation of the $NiCo_2O_4$ powder produced by the freeze drying technique was carried out by Jasem[157] and showed complete spinel phase formation. Similar analysis was carried out for Co_3O_4 and the Li doped cobalt oxides. This confirmed complete spinel phase formation in each case. The lattice spacings of the Li doped cobalt oxides were very similar to that of Co_3O_4. The Debye-Scherrer powder technique[162] was used for this analysis. The equipment (Phillips PW 1010 X-ray generator) and the method of analysis is similar to that described by Jasem[157].

3.4 Electrochemical Evaluation.

All electrochemical measurements reported in this study were carried out in alkaline KOH electrolyte at 25°C. The electrolyte was prepared from Analar pellets

Table 2.2: Room Temperature electrical resistivities of some oxide.

Oxide	Restivity ohm - cm Experimental	Literature*
$NiCo_2O_4$	<10	<10 (157)
Co_3O_4	4×10^3	$10^3 - 10^4$ (153)
4 at. % Li doped Co_3O_4	10	
7 at. % Li doped Co_3O_4	1	
10 at. % Li doped Co_3O_4	1	
PdO	25	10 - 1000 (181)
RuO_2	<0.1	5×0^{-5} (180)
IrO_2	<0.1	6×10^{-7} (179)
PtO_2	14	10^6 (179)
10 at.% Li doped NiO	60	

* Literature reference in parenthesis.

of KOH and doubly distilled deionised water. The dynamic hydrogen electrode[163] (dhe) was used as the reference electrode in this study. A large piece of 100 mesh Ni wire was used as the counter electrode. The electrocatalysts were studied in the form of hydrophobic electrodes[156,164,157,92,119] for both oxygen evolution and dissolution. A three comparment glass cell[157] (figure 2.1) was used for oxygen evolution studies. Oxygen dissolution studies were carried with the hydrophobic electrode in the floating mode i.e. placed on the surface of the electrolyte, in an experimental setup[154,159] shown in figure 2.2.

2.4.1 Fabrication of Hydrophobic Electrodes[165,164,157,92,119]

Weighed quantities of electrocatalyst powder and aqueous particulate Teflon dispersion were slurried in distilled water. The mixture was then dispersed in an ultrasonic bath for five minutes and finally painted on to a 1 cm^2 100 mesh Ni screen current collector previously degreased using acetone. The electrode was then dried at 100°C for one hour, and cured at 300°C for another hour. It is important that the slurry is rapidly transferred to the screen in order to prevent the partial separation of the slurry. If partial separation occurs the Teflon/catalyst ratio will be higher than intended as the catalyst settles in the dispersion. It is also important to coat both sides of the screen equally, in order to prevent the

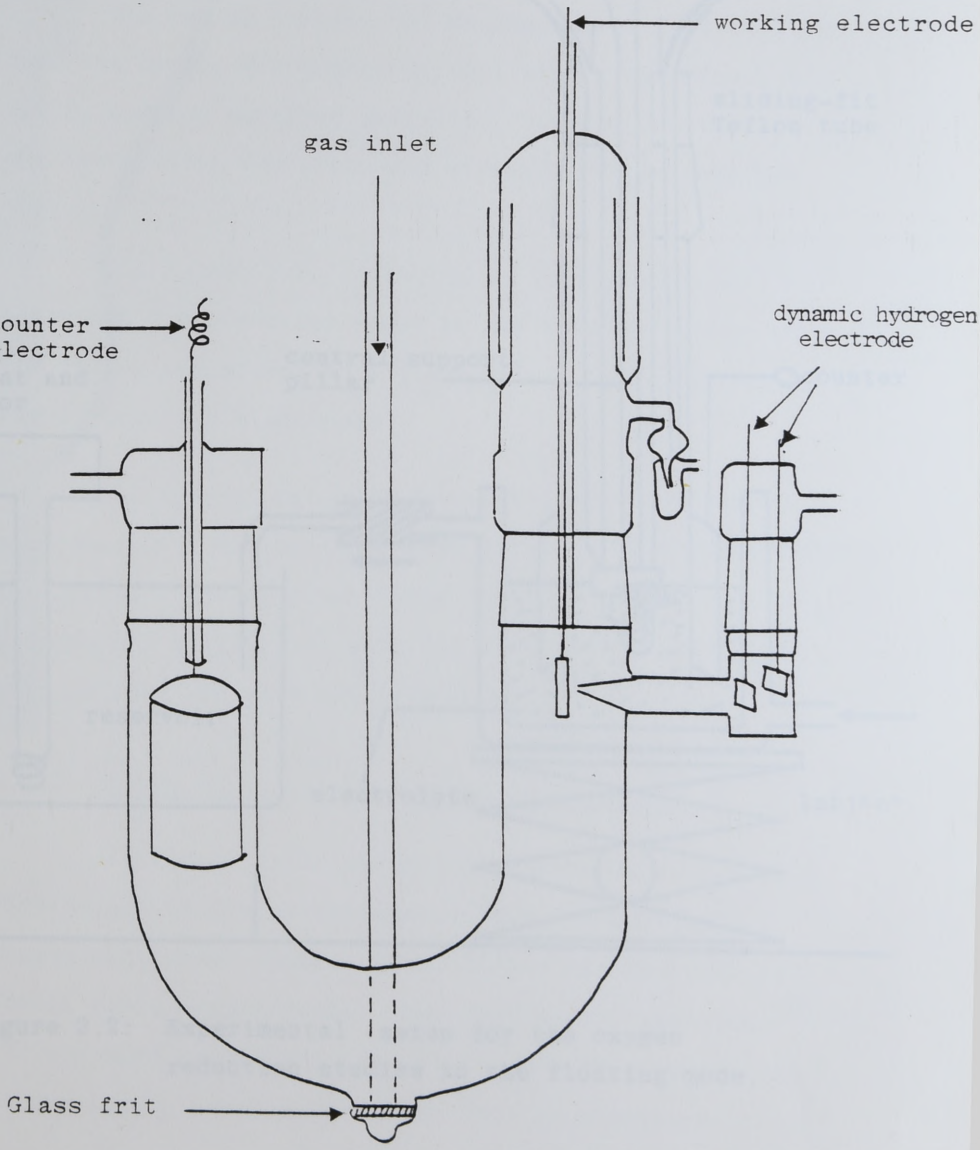

Figure 2.1: Three compartment glass cell.

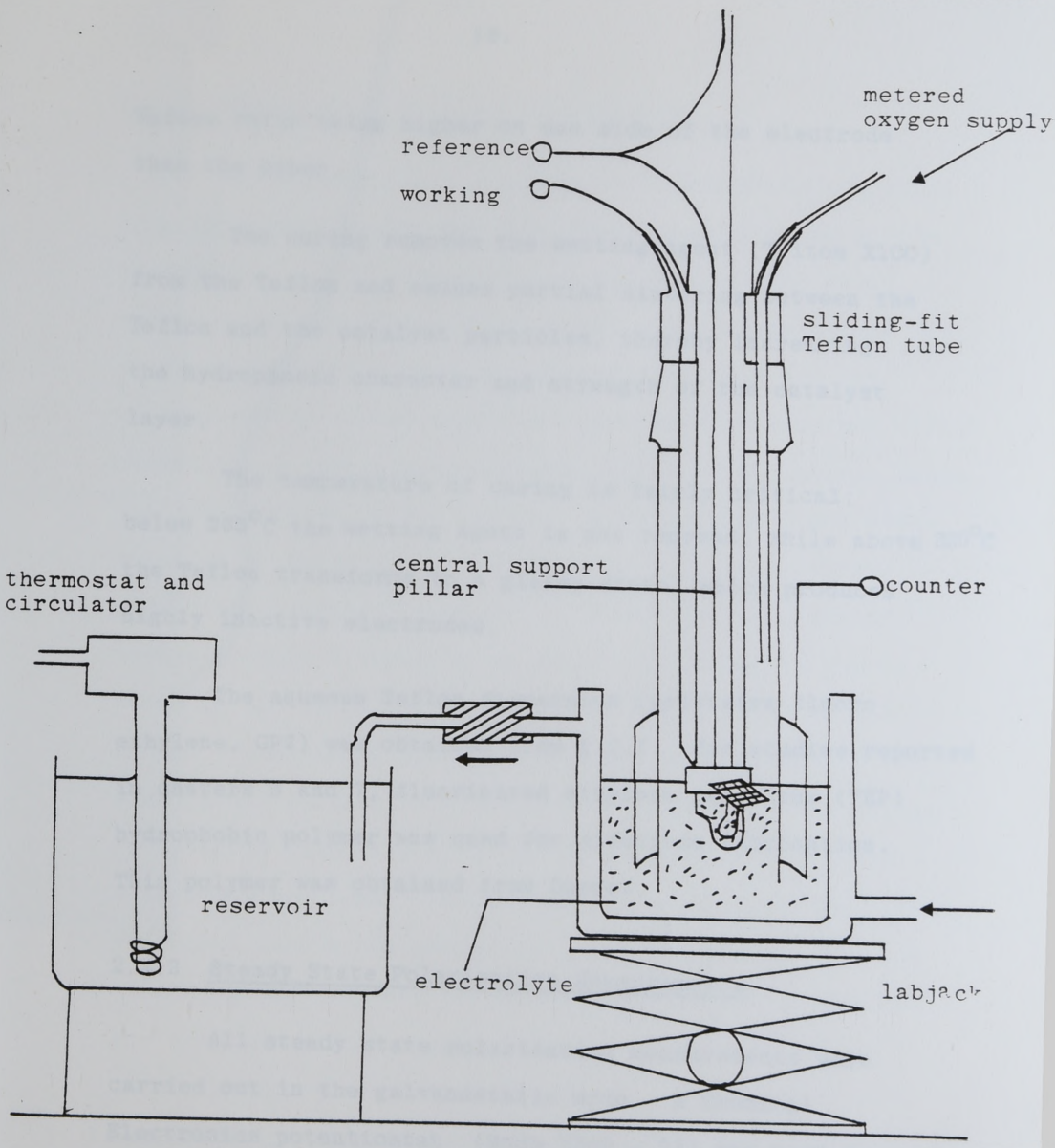

Figure 2.2: Experimental setup for the oxygen reduction studies in the floating mode.

Teflon ratio being higher on one side of the electrode than the other.

The curing removes the wetting agent (Triton X100) from the Teflon and causes partial sintering between the Teflon and the catalyst particles, thereby increasing the hydrophobic character and strength of the catalyst layer.

The temperature of curing is fairly critical; below 265°C the wetting agent is not removed, while above 330°C the Teflon transforms to a glassy state, which produces highly inactive electrodes.

The aqueous Teflon dispersion (polytetra fluoro ethylene, GP2) was obtained from I.C.I. For studies reported in chaters 5 and 7, fluorinated ethylene propylene (FEP) hydrophobic polymer was used for electrode fabrication. This polymer was obtained from Dupont.

2.4.2 Steady State Polarisation Measurements.

All steady state polarisation measurements were carried out in the galvanostatic mode. A Chemical Electronics potentiostat (Mode 3R40 - 3A) was used to obtain these measurements. The interrupter technique[157, 166] was used to measure the ohmic drop between the tip of the Luggin Capillary and the working electrode.

2.4,3 Potentiostatic Pulse Measurements.

It is difficult to interpret steady state polarization measurements for gas dissolution reactions on porous electrodes, due to complications associated with mass transfer and non-evenly distributed ohmic drops within the pores of the electrode i.e. current densities are not uniform within porous media because the diffusion and ohmic overvoltages vary throughout the length of the pores, hence the contribution of activation, diffusion and ohmic overvoltages to the total is different at different points within the porous structure[167]. Moreover the study of oxygen evolution reaction on solid electrodes is complicated by the formation of oxides on the surface as well as the formation of gas bubbles which will block off significant amounts of the electrode surface. The amount of blockage will vary with current density. If porous electrodes are used, apart from the above problems, gases generated inside the pores will push the electrolyte out of the pores, reducing the amount of surfaces available for electrochemical reaction as the current increases[82, 168]. Therefore, we have a situation whereby apart from concentration polarization, the amount of surface area available is continuously changing with potential, thus, causing doubts to Tafel behaviour of the steady state E-logi plots. In this study potentiostatic pulse studies were carried out in instances where there were doubts to the Tafel behaviour of E-logi steady state measurements.

The potentiostatic pulse technique has been used by many workers in the past, in the author's laboratory to study gas evolving[120,168,169.157,82,170,171] and oxygen dissolving porous electrodes[154] in order to indentify the electron transfer overvoltge from mass transfer and ohmic effects.

At the instant of applying an overvoltage to the electrode, the mass transfer effects are neglibible, and the i - E relationship will be governed solely by the charge transfer (neglecting ohmic and double layer charging effects). Mass transfer effects become more significant as the reaction time increases. After an infinite time the steady state conditions will be attained. The electrode behaves as a "leaky" condenser, and at the instant of applying the potential a very small but finite time is required to charge the electrode. So it is not possible to take measurements at exactly zero time due to double layer charging effects. This time depends on the capacity of the electrode double layer, and consequently on the electrode surface area. For planar electrodes, the current transient can be predicted by mathematical analysis[172,173] assuming semi-infinite diffusion[173]. However, for porous electrodes, the situation is far too complex, because it is unlikely to obey the laws of semi-infinite linear diffusion[120,157]. It is more realistic to take measurements at the shortest time interval after the double layer charging is complete and

accept a small amount of concentration polarization. The experimenal procedure[157] is as follows:-

The electrode was left to equilibrate in the chosen test conditions until the open circuit voltage (o.c.v.) was steady. The potentiostat (Wenking) was set to this value and switched to the cell and a single potential jump applied to the electrode by means of a pulse generator (Chemical Electronics type - 01). The change in current with time was measured across a one ohm standard resistor in series with the cell, and the voltage-time trace was recorded on an x-y-t recorder (Bryans 29000 A4). The signal from the pulse generator was fed to the x-y-t recorder through a transient recorder (Data Lab. DL 901).

This procedure was repeated for varying values of potential jump. The potentiostatic transient currents were noted after double layer charging had been completed (200 μ sec).

A schematic circuit diagram of the potentiostatic pulse system is shown in figure 2.3.

The transient currents were corrected for the ohmic-drop using a galvanostatic pulse technique (at different current values). The traces were displayed on an oscilloscope (Rem scope type S01, Cawkell Ltd.) in which the storage facility was used. A schematic circuit diagram of the galvanostatic pulse system is shown in figure 2.4.

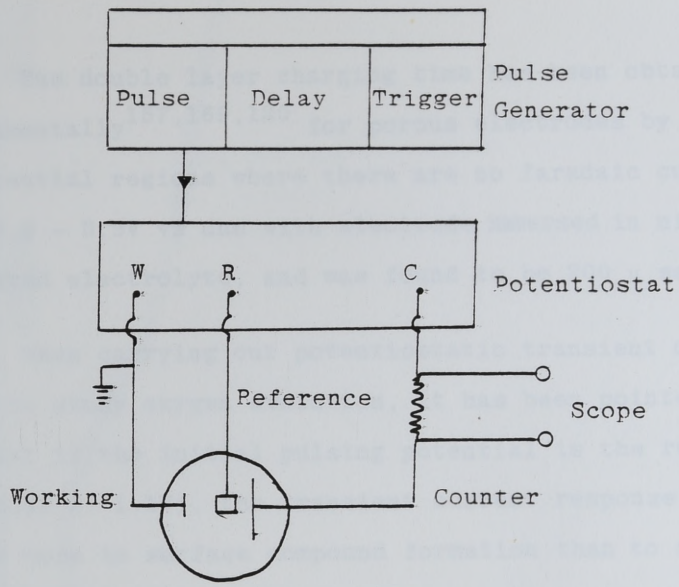

Figure 2.3: Schematic circuit digram for potentiostatic pulsing.

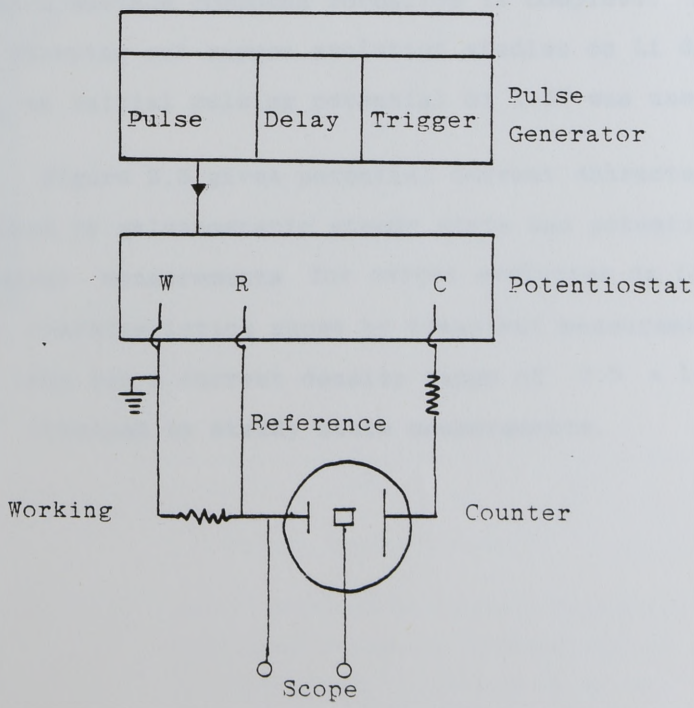

Figure 2.4: Schematic circuit diagram for galvanostatic pulsing.

The double layer charging time has been obtained experimentally[157,169,120] for porous electrodes by pulsing in potential regions where there are no faradaic currents e.g. 0.8 - 0.9V vs dhe with electrode immersed in nitrogen saturated electrolyte, and was found to be 200 μ sec.

When carrying out potentiostatic transient measurements to study oxygen evolution, it has been pointed out[157, 82], that if the initial pulsing potential is the rest potential (∿ 1.1V), the transient current response will relate more to surface compound formation than to oxygen evolution. Therefore, it was suggested that the initial pulsing potential should be slightly above the potential at which surface compound formation is complete. Hence, when carrying out oxygen evolution studies on Li doped Co_3O_4 an initial pulsing potential of 1.5V was used.

Figure 2.5 gives potential current characteristics obtained by galvanostatic steady state and potentiostatic transient measurements for oxygen evolution on Li doped Co_3O_4. Tafel characteristics shown by transient measurement is only true for a current density range of $0.5 \times 10^{-3} - 10^{-2}$ A cm^{-2} obtained by steady state measurements.

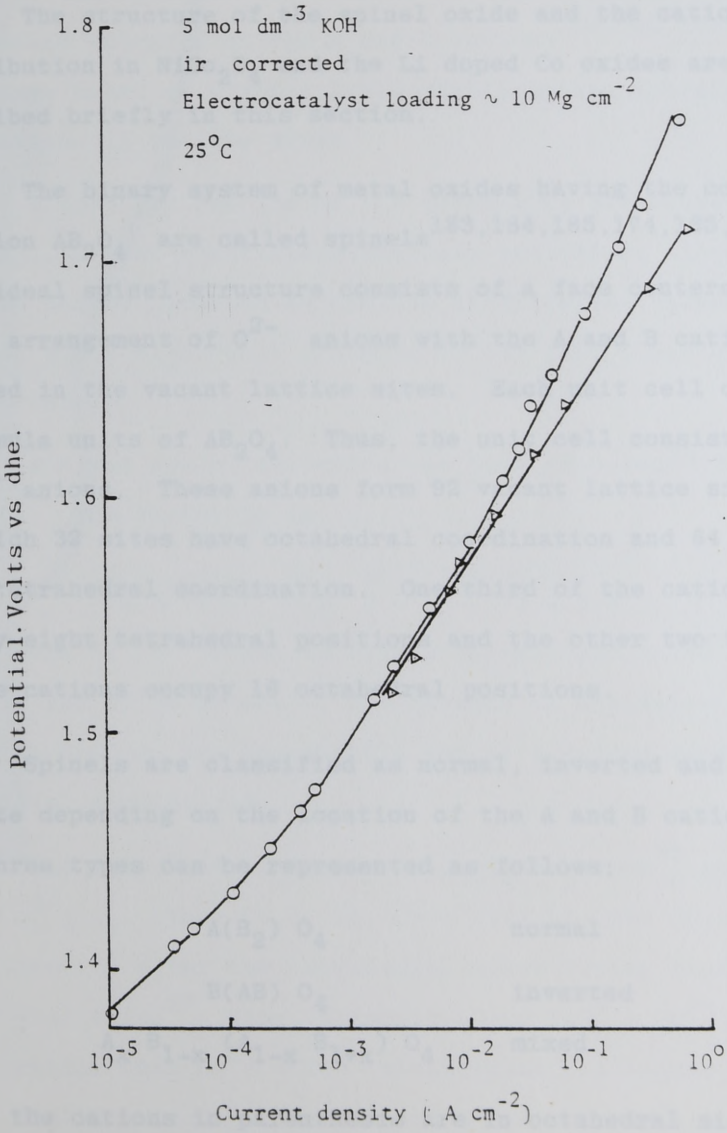

Figure 2.5: Oxygen evolution current potential characteristics on preanodised 10 at. % Li doped Co_3O_4 obtained by steady state (o) and potentiostatic pulse (Δ) technique.

2.5 Structural Aspects of the Electrocatalysts.

The structure of the spinel oxide and the cation distribution in $NiCo_2O_4$ and the Li doped Co oxides are described briefly in this section.

The binary system of metal oxides having the composition AB_2O_4 are called spinels[183,184,185,174,165,161]. The ideal spinel structure consists of a face centered cubic arrangement of O^{2-} anions with the A and B cations located in the vacant lattice sites. Each unit cell contains 8 formula units of AB_2O_4. Thus, the unit cell consists of 32 O^{2-} anions. These anions form 92 vacant lattice sites, of which 32 sites have octahedral coordination and 64 sites have tetrahedral coordination. One third of the cations occupy eight tetrahedral positions and the other two thirds of the cations occupy 16 octahedral positions.

Spinels are classified as normal, inverted and intermediate depending on the location of the A and B cations. The three types can be represented as follows;

$A(B_2)\ O_4$	normal
$B(AB)\ O_4$	inverted
$A_x\ B_{1-x}\ (A_{1-x}\ B_{1+x})\ O_4$	mixed

where the cations in parenthesis are in octahedral sites and those outside are in tetrahedral sites. The oxidation states of the cations in a spinel can be 1, 2, 3, 4 or 6.

The cation distribution in spinels has been explained in terms of the relative tetrahedral and an octahedral site preference energies of the A and B cations[147,148,149,146], which are based on crystal field stabilisation energies of the cations in the two sites.

A specific feature of the crystaline structure of spinels, is that crystallographically equivalent sites in the lattice can be occupied by cations of different valancies, between which electronic transitions can take place with very little energy

A mixed spinel structure has been proposed[96] for $NiCo_2O_4$. The structure is

$$Co^{2+}_{0.9}Co^{3+}_{0.1}(Ni^{2+}_{0.9}Ni^{3+}_{0.1}Co^{3+})\ O^{2-}_{3.2}O^{-}_{0.8}$$

where some of the oxygen is singly charged and loosely bound. The mixed nature of the cations in equivalent lattice sites in $NiCo_2O_4$ are responsible for it's fairly good intrinsic electrical conductivity.

The cation distribution of Co_3O_4 is known[85] to be $Co^{2+}(Co^{3+}_2)\ O_4$. When Co_3O_4 is doped with Li, the dopant is postulated to enter the tetrahedral sites rather than octahedral sites[87], thus, bringing about $Co^{2+} \rightarrow Co^{3+}$ transitions rather than $Co^{3+} \rightarrow Co^{4+}$ transitions. A higher crystal field stabilisation of the oxidation state transitions in the tetra hedral sites, having a lower ionisation potential, compared to the $Co^{3+} \rightarrow Co^{4+}$ transition supports this preference.

CHAPTER THREE

STUDY OF SURFACE COMPOUND FORMATION AT POTENTIALS BELOW OXYGEN EVOLUTION POTENTIALS.

3.1 INTRODUCTION

Considerable interest has accompanied the use of semiconducting oxide electrocatalysts for the evolution of oxygen in alkali medium. However, the mechanism of evolution on these electrodes have proved difficult to establish, not only due to the inherent complexity of the oxygen evolution reaction but also due to the nature of the catalysts themselves. If O_2 is evolved by a direct 4 electron process on the active sites, which are the transition metal ions, on the oxide catalyst, then, oxygen evolution should take place at 1.23V at 25°C. However, this is not the case. The active sites have a more complicated role, in that oxides of higher oxidation states are formed and these eventually decompose to give oxygen. Therefore, it is essential to ascertain the types of oxides and the potentials at which they are formed on the electrocatalyst before oxygen evolution takes place.

The formation of oxides at potentials before oxygen evolution takes place has been studied on many metals such as platinum[16-20] and other precious metals[21-29]. Work has also been carried out on other transition metals, such as, iron[30-33], molybednum[34], tungsten[35], titanium[36,37], manganese[38], nickel[39,40] and cobalt[41,42]. However, oxide formation studies on bulk oxides at potentials before oxygen evolution takes place are not very common.

This chapter describes the investigation carried out on the formation of higher oxidation state compounds and the potentials at which they are formed on $NiCo_2O_4$ and 4 at.% Li doped Co_3O_4. The techniques used for this study are constant potential coulometry, charging curves and cyclic voltammetry.

3.2 Experimental

Pre-anodised Teflon bonded, $NiCo_2O_4$ and 4 at.% Li doped Co_3O_4 electrodes were used for this study. All experiments were carried out at 25°C and in 5N KOH. The potentials were measured against the dynamic hydrogen electrode.

3.2.1 Constant Potential Coulometry

The quantity of electricity that is required to form surface compounds from the rest potential of the electrode to the oxygen evolution potential was measured in steps of small potential increments (eg 25mV). This was carried out by means of a simple circuit as shown in Figure 3.1. A Chemical Electronics potential-time integrator was used to monitor the quantity of electricity, and a current-time plot was recorded simultaneously on a XT servoscribe (model RE511.20) recorder.

To carry out an experimental run, the working electrode was maintained at its rest potential by use of the potentiostat for 30 minutes. The time of 30 minutes

was obtained from previous determinations as the time required to reduce electrochemically all surface compounds formed during anodic polarisation when the working electrode is maintained at its rest potential. The complete reduction of surface compounds is indicated by the stable rest potential voltage when the potentiostat is switched off. Next, the potential at which coulometry is to be carried out is set on the potentiostat by means of a dummy cell and the working electrode is raised to this potential by switching on the potentiostat. The current-time plot was recorded and the quantity of electricity was noted with time. The electrode was then held at the rest potential for a further 30 minutes and the procedure was repeated for different potentials. The range of potentials studied was 1.25V to 1.50V for both types of electrodes. Up to potentials of 1.41V the residual currents of constant potential coulometry (cpc) was of the order of 10^{-4} to 10^{-5}A. At potentials greater than 1.41V the total charge was corrected for oxygen evolution. This procedure becomes more unreliable as the evolution current increased and as such cannot be used above 1.5V.

Experiments were carried out to ascertain the reproducibility of the cpc technique. For example, the cpc procedure as described, when carried out on a Teflon bonded $NiCo_2O_4$ electrode at 1.36V gave for five successive determinations, integrated charge values of 1.392, 1.394,

1.391, 1.397 and 1.388 coulombs. Therefore the mean and standard deviation is 1.392 ± 0.002 coulombs. However at potentials greater than 1.41V the error margin was greater. For example, at a potential of 1.455V the total charge values were 2.878, 2.840, 2.821, 2.806 and 2.951 coulombs for five successive determinations having a mean and standard deviation of 2.859 ± 0.044 coulombs. The larger error in charge measurements at potentials greater than 1.41V was due to the correction that were necessary due to oxygen evolution.

3.2.2 Anodic Charging Curves

The potentiostat was used on a galvanostatic mode to pass a small anodic current (eg 0.1 mA cm^{-2}) between the electrode under study at rest, and the secondary electrode. The change in potential of the working electrode with time was recorded at a XT recorder. The surface compounds formed on the preanodised electrodes were electrochemically reduced by imparting a potential of 1.1V for 30 minutes before anodic charging curves were obtained.

3.2.3 Cyclic Voltammetry

The potential of the electrode under study was swept from its rest potential to a potential of 1.55V and the current output was measured on a XY (Bryans, model 29000 A4) recorder. A potentiostat (Wenking) and a wave form generator (Chemical Electronics, Type - 01) were

used to set the upper and lower limits of the potential. The circuit diagram for this technique is shown in Figure 3.2.

3.3 Results and Discussion

3.3.1 Constant Potential Coulometry

Figures 3.3 and 3.4 give the integrated charge vs potential relationship for the Teflon bonded $NiCo_2O_4$ and Li doped Co_3O_4 electrodes respectively. For $NiCo_2O_4$, 3 plateaux are observed corresponding to the completion of surface compound formation at 1.31V, 1.38V and 1.45V. Furthermore, the ratios of charges passed to form each surface compound is approximately 1:1:2. In the case of Li doped Co_3O_4, two peaks were obtained at potentials of 1.36V and 1.44V. The ratio of the integrated charges under the peak potentials are approximately 1:3, therefore indicating that the charge required to form surface compounds at potentials of 1.36V and 1.44V are approximately in the ratio of 1:2. The integrated charge-potential trends obtained by the cpc technique are reproducible. Cpc carried out on three $NiCo_2O_4$ electrodes gave similar trends, but the integrated charges were found to vary depending on the $NiCo_2O_4$ loading.

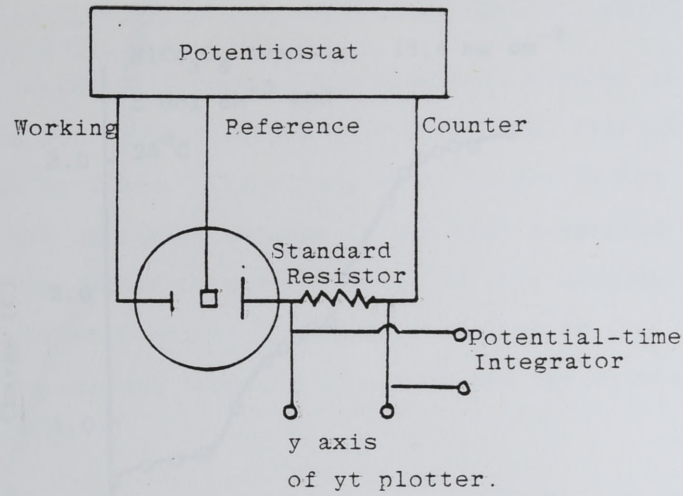

Figure 3.1: Circuit for constant potential coulometry.

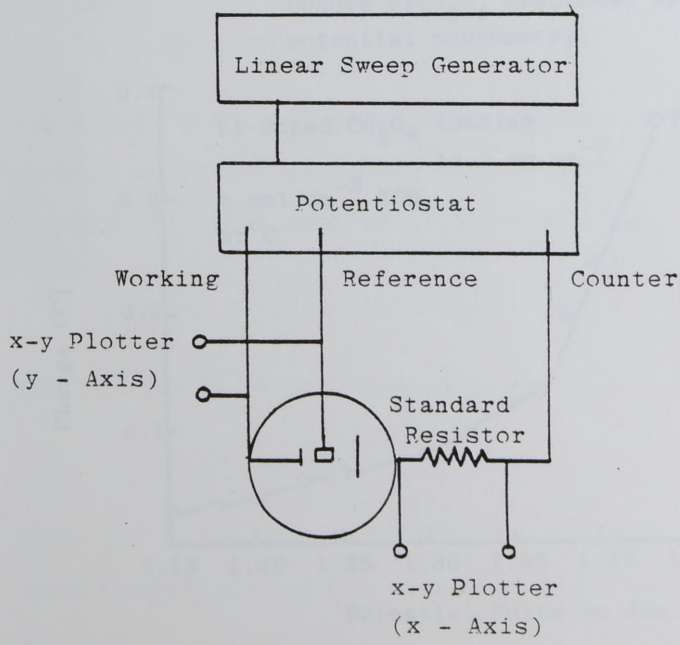

Figure 3.2: Circuit for cyclic voltammetry.

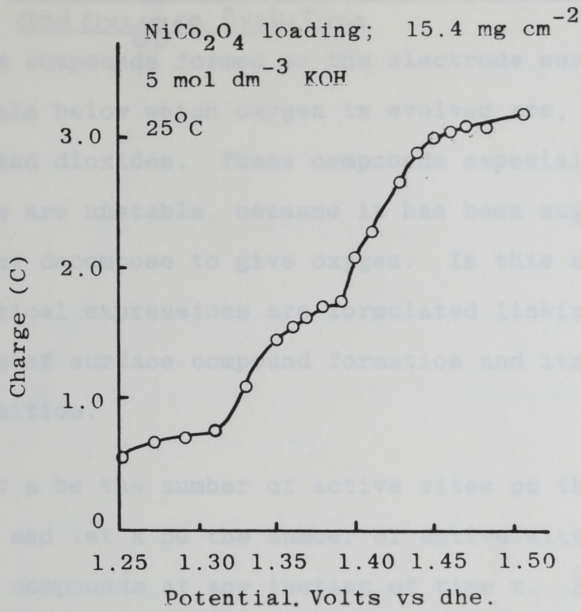

Figure 3.3: Integrated charge measured on a Teflon bonded $NiCo_2O_4$ electrode by constant potential coulometry.

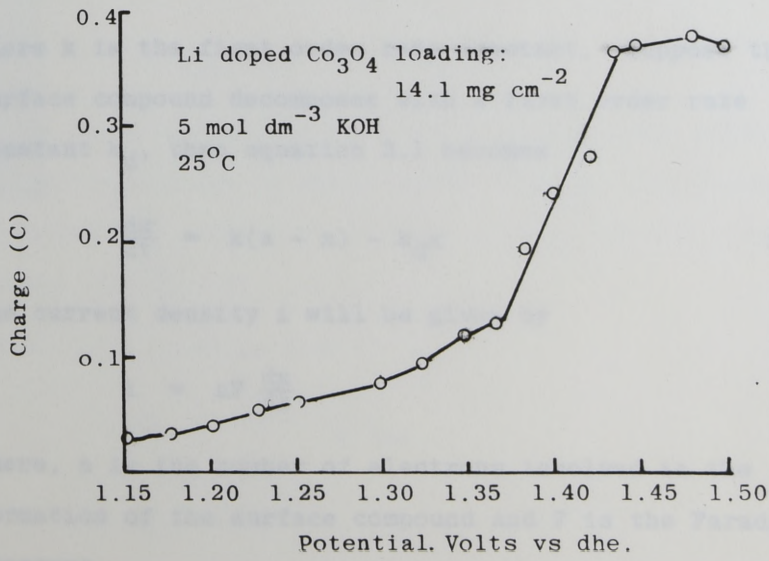

Figure 3.4: Integrated charge measured on a 4 at.% Li doped Co_3O_4 electrode by constant potential coulometry.

3.3.2 Kinetics of Surface Compound Formation, Decomposition and Oxygen Evolution

The compounds formed on the electrode surface at potentials below which oxygen is evolved are, hydroxides, oxides and dioxides. These compounds especially the dioxides are unstable, because it has been suggested that they decompose to give oxygen. In this section mathematical expressions are formulated linking the kinetics of surface compound formation and its chemical decomposition.

Let a be the number of active sites on the electrode surface and let x be the number of active sites forming surface compounds at any instant of time t. For first order kinetics of formation:

$$\frac{dx}{dt} = k(a - x) \qquad 3.1$$

where k is the first order rate constant. Suppose the surface compound decomposes with a first order rate constant k_d, then equation 3.1 becomes

$$\frac{dx}{dt} = k(a - x) - k_d x \qquad 3.2$$

The current density i will be given by

$$i = nF \frac{dx}{dt}$$

where, n is the number of electrons involved in the formation of the surface compound and F is the Faraday Constant

$$\text{i.e. } i = nFk(a - x) \qquad 3.3$$

This is because k_d involves a chemical step.

Now, rearranging Equation 3.2, we have

$$\frac{dx}{dt} = ka - (k + k_d)x \qquad 3.4$$

Equation 3.4 can be expressed as:

$$\frac{dx}{ka - (k + k_d)x} = dt$$

Integrating with respect to x and t, and taking R to be equal to $k/(k + k_d)$, we have,

$$-\ln(Ra - x) = (k + k_d)t + C$$

where C is the constant of integration. When t = 0, x = 0 and C = -ln(Ra).

Therefore,

$$\ln \frac{Ra}{(Ra - x)} = (k + k_d)t \qquad 3.5$$

It is to be noted that as $t \to \infty$ a steady state current is postulated due to oxide decomposition. Now considering Equation 3.4, as $t \to \infty$, $i \to i_\infty$, $x \to x_{ss}$ (ss for steady state) and $\frac{dx}{dt} \to 0$.

Thus, from Equation 3.4

$$ka = (k + k_d)x_{ss} \qquad 3.6$$

$$\text{i.e } x_{ss} = Ra \qquad 3.7$$

Thus the term Ra in Equation 3.5 represents the steady state amount of surface compound on the electrode at a given temperature and potential.

Further, it also follows from Equation 3.5, that

$$x = Ra(1 - e^{-(k + k_d)t}) \qquad 3.8$$

Now substituting for x in Equation 3.3, we have

$$i = nFka - nFkRa + nFkRa\ e^{-(k + k_d)t} \qquad 3.9$$

Also, if $t \to \infty$, $i \to i_\infty$ and from Equation 3.9

$$i_\infty = nFka(1 - R) \qquad 3.10$$

It is to be noted that Equation 3.10 obeys the concept, that, when $k_d \to 0$, $R \to 1$ and $i_\infty \to 0$. This implies that the current will tend to zero, if the oxide is stable. If i_∞ is positive, the current is due to oxygen evolution due to the decomposition of higher oxide

Further, from Equations 3.9 and 3.10, we have

$$i = i_\infty + nFkRa\ e^{-(k + k_d)t} \qquad 3.11$$

or

$$\ln(i - i_\infty) = \ln(nFkRa) - (k + k_d)t \qquad 3.12$$

The expression obtained has to be modified so that the kinetics of formation could be studied by constant potential coulometry considerations.

If only the formation of the oxides are considered, then, it implies that $k_d \to 0$, i.e. $R \to 0$ and $i_\infty \to 0$ then Equation 3.11 becomes,

$$i = nFka\, e^{-kt} \qquad 3.13$$

where i is the current density due to oxide formation and is expected to decay exponentially with time.

Integrating Equation 3.13 to obtain charge terms

$$i \int_0^t dt = nFka \int_0^t e^{-kt} dt \qquad 3.14$$

From Equation 3.14,

$$C_t = nFa(1 - e^{-kt}) \qquad 3.15$$

where C_t is amount of charge corresponding to surface compound formation at any instant of time t.

Also if C_∞ is taken to correspond to the amount of charge when surface compound formation is completed, then

$$C_\infty = nFa \qquad 3.16$$

Therefore Equation 3.15 could be written as,

$$C_\infty - C_t = C_\infty\, e^{-kt} \qquad 3.17$$

As predicted by Equation 3.13, the current decayed exponentially with time during cpc, on both the oxides, and at all the potentials. Figure 3.5 is a current-time plot for a $NiCo_2O_4$ electrode at a potential of 1.33V showing the exponential decay of current with time. Similar behaviour was observed on Li doped Co_3O_4 electrodes.

Equation 3.17 can be rearranged as

$$\log (C_\infty - C_t) = -\frac{k}{2.303} t + K \qquad 3.18$$

where K is a constant.

Since C_∞ is equal to the integrated charge at the potential at which the formation of a surface compound is complete and also since C_t and t are known for each potential at which cpc was carried out, the validity of Equation 3.18 to the kinetics of surface compound formation could be put to the test. The kinetics of surface compound formation on both $NiCo_2O_4$ and Li doped Co_3O_4 electrodes obeyed Equation 3.18 indicating that the kinetics of surface compound formation is first order. Figure 3.6 and Figure 3.7 give the log $(C_\infty - C_t)$ vs t plots for the formation of the first surface compound on $NiCo_2O_4$ and Li doped Co_3O_4 electrodes respectively at different potentials. The rate constants (given in figures) were found to increase with increase in potential, indicating that the kinetics of surface compound formation increases with potential.

3.3.3 Anodic Charging Curves

Figures 3.8 and 3.9 give the anodic charging curves on Teflon bonded, preanodised $NiCo_2O_4$ and Li doped Co_3O_4 electrodes. The charging curve on $NiCo_2O_4$ indicates that the potentials corresponding to the completion of formation of the surface compounds are the same as that obtained by

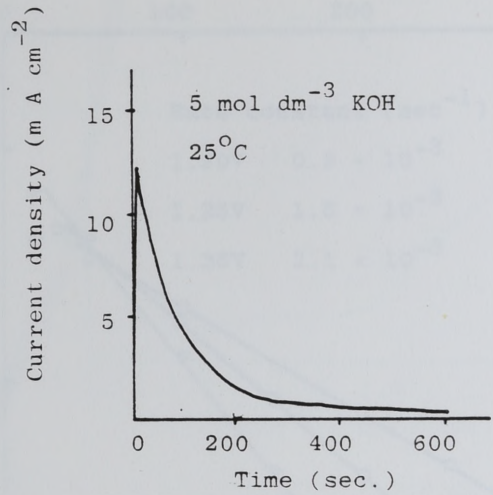

Figure 3.5: Decay of current density with time on raising the potential of a Teflon bonded $NiCo_2O_4$ electrode from rest (1.1V) to 1.33V.

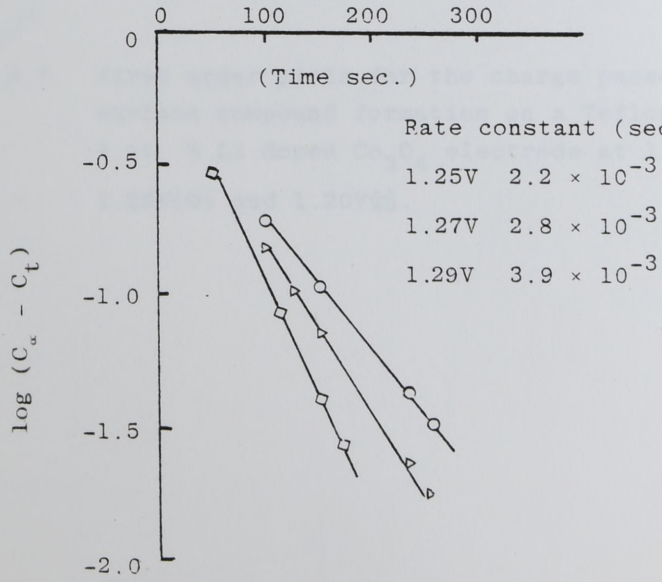

Figure 3.6: First order plots for the charge passed during surface compound formation on a Teflon bonded $NiCo_2O_4$ electrode at 1.29V(□), 1.27V(△) and 1.25V(○).

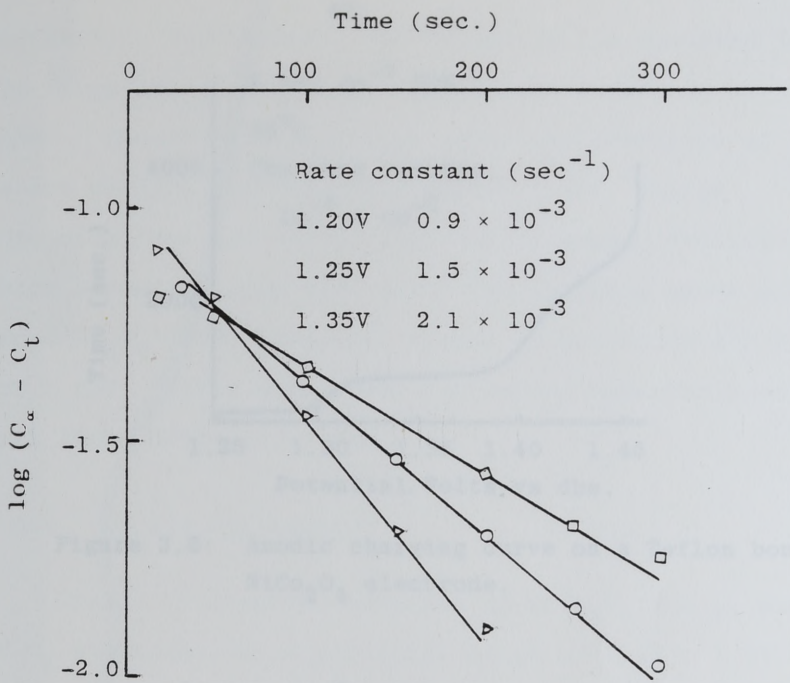

Figure 3.7: First order plots for the charge passed during surface compound formation on a Teflon bonded 4 at. % Li doped Co_3O_4 electrode at 1.35V(△), 1.25V(○) and 1.20V(□).

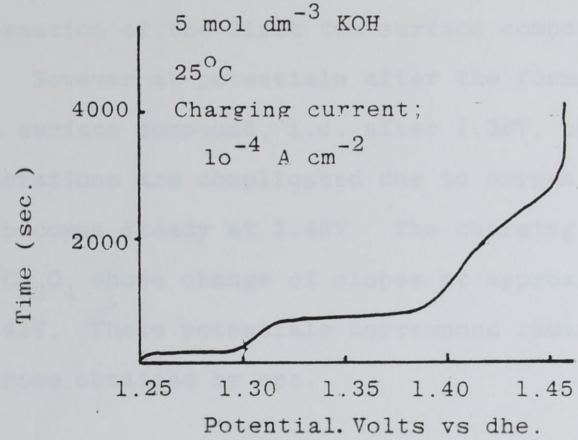

Figure 3.8: Anodic charging curve on a Teflon bonded $NiCo_2O_4$ electrode.

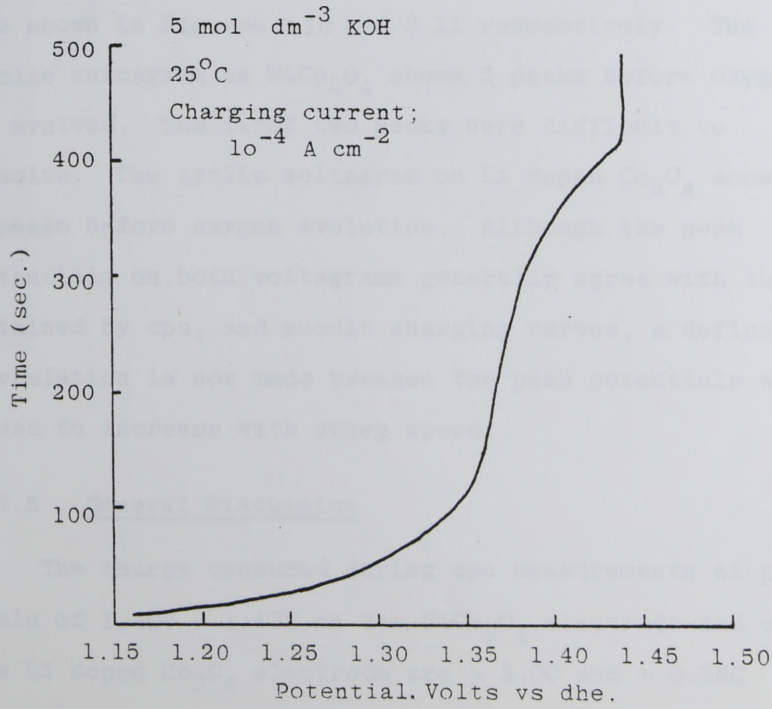

Figure 3.9: Anodic charging curve on a Teflon bonded 4 at. % Li doped Co_3O_4 electrode.

cpc study. Furthermore, the charge ratios required for the formation of the first two surface compounds are equal. However at potentials after the formation of the second surface compound, i.e. after 1.38V, charge considerations are complicated due to oxygen evolution which becomes steady at 1.49V. The charging curve on Li doped Co_3O_4 shows change of slopes at approximately 1.36V and 1.43V. These potentials correspond remarkably well with those obtained by cpc.

3.3.4 Cyclic Voltammetry

Cyclic voltagrams obtained on $NiCo_2O_4$ and Li doped Co_3O_4 electrodes at a potential range of 1.1V - 1.55V are shown in Figures 3.10 and 3.11 respectively. The cyclic voltagram on $NiCo_2O_4$ shows 3 peaks before oxygen is evolved. The first two peaks were difficult to resolve. The cyclic voltagram on Li doped Co_3O_4 shows 2 peaks before oxygen evolution. Although the peak potentials on both voltagrams generally agree with those obtained by cpc, and anodic charging curves, a definite correlation is not made because the peak potentials were found to increase with sweep speed.

3.3.5 General Discussion

The charge consumed during cpc measurements at potentials of 1.40V - 1.43V on the $NiCo_2O_4$ electrode and on the Li doped Co_3O_4 electrode are $\sim$ 3.0C and $\sim$ 0.36C respectively. The electrocatalyst loading of the two

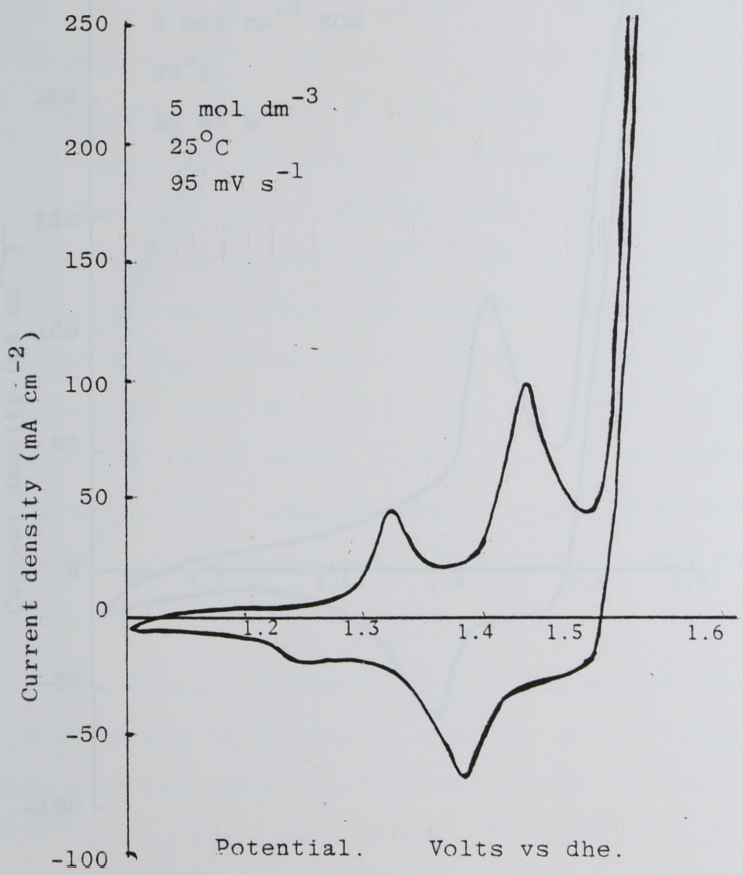

Figure 3.10: Cyclic voltagram on a Teflon bonded $NiCo_2O_4$ electrode.

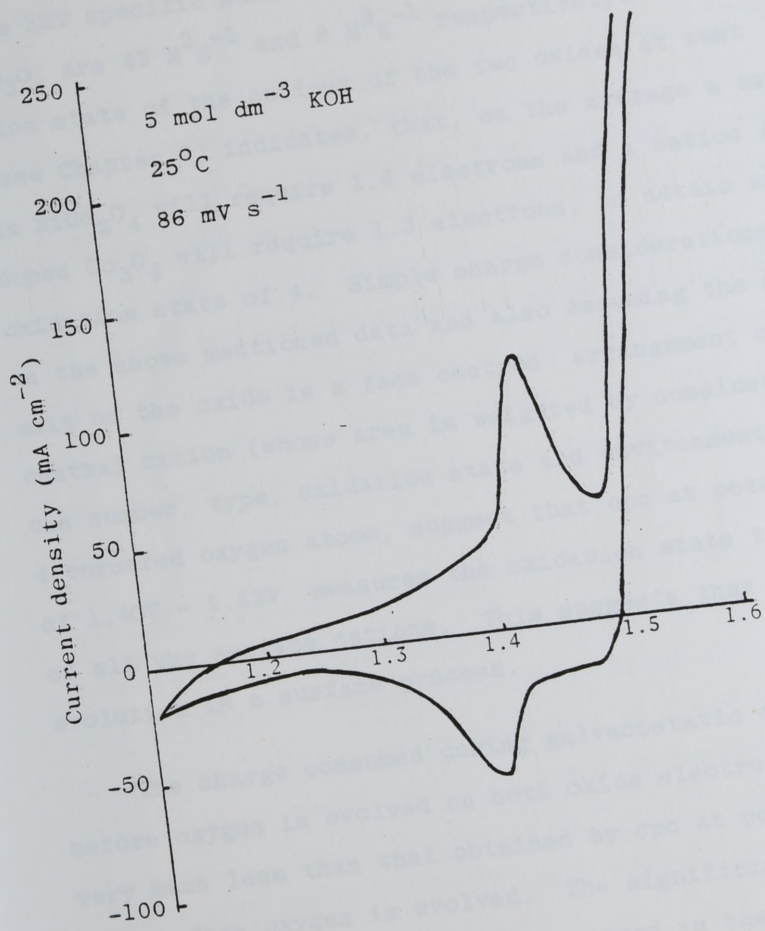

Figure 3.11: Cyclic voltagram on a Teflon bonded 4 at. % Li doped Co_3O_4 electrode.

electrodes are 15.4 mg cm^{-2} and 14.1 mg cm^{-2} respectively. The BET specific surface areas of $NiCo_2O_4$ and Li doped Co_3O_4 are 43 M^2g^{-1} and 8 M^2g^{-1} respectively. The oxidation state of the cations of the two oxides at rest (see Chapter 2) indicates, that, on the average a cation in $NiCo_2O_4$ will require 1.6 electrons and a cation in Li doped Co_3O_4 will require 1.3 electrons, to attain an oxidation state of 4. Simple charge considerations based on the above mentioned data and also assuming the surface unit on the oxide is a face centred arrangement of a central cation (whose area is weighted by considering the number, type, oxidation state and environment) and, 4 cornered oxygen atoms, suggest that cpc at potentials of 1.40V - 1.43V measures the oxidation state transitions of all the surface cations. This suggests that oxygen evolution is a surface process.

The charge consumed during galvanostatic charging before oxygen is evolved on both oxide electrodes are very much less than that obtained by cpc at potentials just before oxygen is evolved. The significance of this apparent discrepancy will be discussed in the next chapter.

However the results obtained from the 3 techniques (cpc, galvanostatic charging and cyclic voltammetry) agree on the number of different types of surface compounds formed and the potentials at which these compounds are formed on both electrodes. On $NiCo_2O_4$ 3 types of surface compounds are formed at potentials of

approximately 1.31V, 1.38V and 1.45V, and on Li doped Co_3O_4, 2 types of surface compounds are formed at potentials of approximately 1.36V and 1.44V. It is to be noted that the three techniques will only identify the oxidation state of the transition metal ion of the surface compounds. The surface compounds are generally hydroxides, oxyhydroxides or dioxides and the exact identification of the compounds are not possible. Furthermore the surface compounds formed electrochemically could form another species chemically before undergoing a second electrochemical step. Such a sequence will not be identified by the experiments carried out.

Comparing the potentials at which electron transitions are complete on the two oxides and taking into account the charge required to bring about these transitions, which are in the ratio of 1:1:2 on $NiCo_2O_4$ and 1:2 on Li doped Co_3O_4, it could be concluded that the oxidation state transition $Ni^{2+} \rightarrow N^{3+}$, $Co^{2+} \rightarrow Co^{3+}$ $Ni^{3+} \rightarrow Ni^{4+}$ and $Co^{3+} \rightarrow Co^{4+}$ takes place at potentials of approximately 1.32V, 1.36 - 1.38V, 1.45V and 1.45 V respectively.

CHAPTER FOUR

OXYGEN EVOLUTION STUDIES ON $NiCo_2O_4$ AND ON THE Li DOPED Co OXIDES.

4.1 Introduction

This chapter describes the oxygen evolution studies carried out on $NiCo_2O_4$ and on Li doped Co_3O_4 electrodes in alkaline medium and the proposed reaction mechanism that was put forward to explain the process of oxygen evolution on the two electrocatalysts. This chapter also includes a survey of the literature on oxygen evolution relevant to the studies described in this chapter.

4.2 Literature Survey On Oxygen Evolution

It is known from thermodynamic[45] and experimental[46] considerations that the overall reaction for oxygen evolution in alkaline medium is

$$4OH^- \rightarrow 2H_2O + O_2 + 4e \qquad 4.1$$

This 4 electron process is complicated by the formation of oxy, hydroxy, peroxy and dioxy compounds as intermediates. Conclusive proof that a surface compound decomposes to give oxygen was obtained by Rosental and Veselovsky[49]. They polarised a clean, oxide free platinum electrode at 1.8 - 1.9V in O^{18} enriched in H_2SO_4 for 5 - 6 hours. The electrode was thoroughly cleaned, free of the O^{18} enriched electrolyte, with distilled water and was then dried in vacuum. The electrode was polarised in "unenriched" IN H_2SO_4, and the first portions of the oxygen evolved was collected in evacuated ampules. The first portions of oxygen, when analysed with a mass spectrometer, showed a high

O^{18} concentration compared to standard oxygen obtained during polarisation of IN H_2SO_4.

The kinetics and the mechanism of oxygen evolution; in 1955 Bockris[47] proposed 5 pathways for the evolution of oxygen in alkaline medium. He derived rate equations by considering each step of the 5 pathways to be rate determining under Langmuir absorption conditions. Damjanovic, Dey and Bockris[48] compiled 14 pathways for the oxygen reaction and calculated the Tafel slopes for the anodic and cathodic processes by taking each step in turn to be rate determining. Their results are shown in Table 4.1. The method of calculation was similar to that of Bockris[47]. The Tafel slopes (Table 4.1) for the anodic and cathodic paths under limitingly low Langmuir absorption conditions can also be obtained using the expression[48,186].

$$b = \frac{\nu}{(n + \beta n^*)} \frac{RT}{F} \qquad 4.2$$

where b is the Tafel slope, n is the number of electrons transfered before the rate controlling step during one act of the overall reaction, n^* is the total number of electrons transfered by the rate controlling step during one act of the overall reaction, β is the symmetry factor and is taken as 0.5, ν is the stoichiometric number, which is the number of times the rate determining step takes place for one act of the overall reaction, R, T

Table 4.1: Paths for the oxygen reaction[48] and the associated values of the Tafel slope.

Path	$\partial V/\partial \ln i$ Anodic Low θ	Anodic High θ	Cathodic
(1) The oxide path[47].			
$S+H_2O \rightarrow SOH+H^+ +e^-$	2RT/F		-2RT/F
$2SOH \rightarrow SO+SH_2O$	RT/2F		∞
$2SO \rightarrow O_2+2S$	RT/4F		∞
(2) The electrochemical oxide path[47].			
$S+H_2O \rightarrow SOH+H^+ +e^-$	2RT/F		-2RT/3F
$SOH+S+H_2O \rightarrow SO+SH_2O+H^+ +e^-$	2RT/3F	2RT/F	-2RT/F
$2SO \rightarrow O_2+2S$	RT/4F		∞
(3) The hydrogen peroxide path[47]			
$4S+4H_2O \rightarrow 4SOH+4H^+ +4e^-$	2RT/F		-2RT/F
$2SOH \rightarrow SH_2O_2+S$	RT/2F		-RT/2F
$SH_2O_2+SOH \rightarrow SOH_2+SO_2H$	RT/3F		-RT/F
$SO_2H+SOH \rightarrow SH_2O+S+O_2$	RT/3F		∞
(4) The metal peroxide path[47]			
$4S+4H_2O_2 4SOH+4H^+ +4e^-$	2RT/F		-2RT/F
$2SOH \rightarrow SO+SH_2O$	RT/2F		-RT/2F
$SO+SOH \rightarrow S+SHO_2$	RT/3F		-RT/F
$SHO_2+SOH \rightarrow O_2+S+SH_2O$	RT/4F		∞

..... Continued

Table 4.1 continued.

Path	$\partial V/\partial \ln i$ Anodic Low θ	Anodic High θ	Cathodic
(5) The electrochemical metal peroxide path[47].			
$3S+3H_2O \rightarrow 3SOH+3H^+ +3e^-$	2RT/F		-6RT/5F
$2SOH \rightarrow SO+SH_2O$	RT/2F	RT/F	-RT/2F
$SO+H_2O \rightarrow SHO_2+H^+ +e^-$	2RT/5F	2RT/F	-2RT/3F
$SHO_2+SOH \rightarrow S+O_2+SH_2O$	RT/4F		∞
(6) The alkaline path[43]			
$S+H_2O \rightarrow SOH+H^+ +e^-$	2RT/F		-2RT/3F
$SOH+H_2O \rightarrow SH_2O_2^- +e^-$	RT/F		-RT/F
$2SH_2O_2^- \rightarrow S+SO_2^{2-}+2H_2O$	RT/2F	RT/F	-RT2F
$SO_2^{2-} \rightarrow S+O_2+2e^-$	RT/3F		-RT/F
(7) Path suggested by Conway and Bourgault[56].			
$3S+3H_2O \rightarrow 3SOH+3H^+ +3e^-$	2RT/F		-6RT/5F
$SOH \rightarrow SO+H^+ +e^-$	2RT/3F	2RT/F	-2RT/5F
$SO+SOH \rightarrow SHO_2$	RT/3F	RT/F	-RT/F
$SHO_2+SOH \rightarrow S+SH_2O+O_2$	RT/4F		∞
(8) Alternative path of Conway and Bourgault[56]			
$2S+2H_2O \rightarrow 2SOH+2H^+ +2e^-$	2RT/F		-2RT/3F
$SOH \rightarrow SO+H^+ +e^-$	2RT/3F	2RT/F	-2RT/5F
$SO+H_2O \rightarrow SHO_2+H^+ +e^-$	2RT/5F		-2RT/3F
$SHO_2+SOH \rightarrow S+SH_2O+O_2$	RT/4F		∞

..... continued

Table 4.1 continued.

Path	$\partial V/\partial \ln i$ Anodic Low θ	Anodic High θ	Cathodic
(9) Path suggested by Riddiford[50]			
$S+H_2O \rightarrow SOH+H^+ +e^-$	2RT/F		-2RT/3F
$2SOH \rightarrow SO+SH_2O$	2RT/3F	2RT/F	-2RT/5F
$SO+H_2O \rightarrow SHO_2+H^+ +e^-$	2RT/5F		-2RT/3F
$SHO_2+H_2O \rightarrow O_2+SH_2O+H^+ +e^-$	RT/4F		∞
(10) Krasilshchikov path[51]			
$S+OH^- \rightarrow SOH+e^-$	2RT/F		-2RT/3F
$SOH+OH^- \rightarrow SO^- +H_2O$	RT/F		-RT/F
$SO^- \rightarrow SO+e^-$	2RT/3F	2RT/F	-2RT/F
$2SO \rightarrow O_2+2S$	RT/4F		∞
(11) Wade and Hackerman's path[52]			
$2S+1H_2O \rightarrow SO+SH_2O+2H^+ +2e^-$	RT/F		-RT/3F
$SO+2SOH^- \rightarrow 2S+SH_2O+O_2+2e^-$	RT/3F		-RT/F
(12)* $S+H_2O \rightarrow SOH+H^+ +e^-$	2RT/F		-2RT/7F
$SOH \rightarrow SO+H^+ +e^-$	2RT/3F	RT/F	-2RT/3F
$SO+H_2O \rightarrow SO_2H+H^+ +e^-$	2RT/5F	2RT/F	-2RT/3F
$SO_2H \rightarrow S+O_2+H^+ +e^-$	2RT/7F		-2RT/F

.....Continued

* Path suggested by Damjanovic, Dey and Bockris[48].

Table 4.1 continued.

	Path	$\partial V/\partial \ln i$ Anodic Low θ	Anodic High θ	Cathodic
(13)*	$S+H_2O \rightarrow SOH+H^+ +e^-$	2RT/F		-2RT/3F
	$SOH+H_2O \rightarrow SO-H-OH^- +H^+$	RT/F		-RT/F
	$SO-H-OH^- \rightarrow SO-H-OH+e^-$	2RT/3F	2RT/F	-2RT/F
	$SO-H-OH \rightarrow SO+H_2O$	RT/2F	RT/F	∞
	$2SO \rightarrow S+O_2$	2RT/F		∞
(14)*	$S+H_2O \rightarrow SOH+H^+ +e^-$	2RT/F		-2RT/7F
	$SOH+H_2O \rightarrow SO-H-OH^-$	RT/F		-RT/3F
	$SO-H-OH^- \rightarrow SO-H-OH+e^-$	2RT/3F	2RT/F	-2RT/5F
	$SO-H-OH \rightarrow SO+H_2O$	RT/2F	RT/F	-RT/2F
	$SO+H_2O \rightarrow SHO_2+e^-$	2RT/5F	2RT/3F	-2RT/3F
	$SHO_2 \rightarrow S+O_2+H^+ +e^-$	2RT/7F		-2RT/F

* paths suggested by Damjanovic, Dey and Bockris[48].

and F have the usual meanings. Of the 14 paths given in Table 4.1 paths 1-5 were proposed by Bockris[47], path 6 is that proposed by Hoar[43] for alkaline solutions, 7 and 8 are due to Conway and Boargault[56], path 9 is by Riddiford[50], 10 is by Krasilshchikov[51], 11 is by Wade and Hackerman[52] and paths 12, 13 and 14 are by the three authors themselves.

The mechanism of oxygen evolution and the rate determining step suggested by the value of the Tafel slope is generally confirmed by reaction order studies with respect to the electroactive species. Conway and Salomon[53] have discussed reaction order in context of oxygen evolution.

It is known that the extent and the type (Langmuir or Temkin) of coverage of the intermediates also determines the kinetics and mechanism[54, 55] of oxygen evolution. The relation between the mechanism and measurable kinetic parameters for oxygen evolution has been discussed by many authors[47, 48, 53, 54] under Langmuir conditions, and by Conway and Bourgault[56, 57] and Conway and Gileadi[73,74] under Temkin conditions.

Oxygen evolution on certain substrates (e.g. Pt[48], PtO_2[63] $NiLa_2O_4$[64]) shows two Tafel regions, the Tafel slope increases in going from low to high overpotentials. This observation can be attributed to[58] 3 possible reasons. They are: (1) change in the reaction mechanism;

(2) the mechanism is the same but absorption concentration of the intermediate changes from limitingly low to limitingly high state; (3) the rate determining step of the mechanism changes. This study proposes another reason to explain the two Tafel regions observed on $NiCo_2O_4$.

The oxygen evolution reaction on metals and metal alloys has been extensively studied and has been reviewed by many authors[58, 59, 60, 61, 62].

Many workers have studied the oxygen evolution reaction on porous oxide electrodes by means of steady state electrochemical techniques. They obtained the Tafel and reaction order parameters experimentally and postulated reaction mechanisms for the oxygen evolution process.

Iwakura, Fukuda and Tamura[63] studied the oxygen evolution reaction on porous PtO_2 electrodes by obtaining current potential measurements in electrolytes of different KOH concentration. The PtO_2 electrode was prepared by thermal decomposition of chloroplatinic acid on titanium plate current collector. They obtained two Tafel regions for oxygen evolution, a slope of 0.059V per decade at low overpotential and a slope of 0.114V per decade at high overpotentials at 25°C: a mechanistic sequence similar to that suggested by Krasilschkikov[51] for oxygen evolution in KOH medium was proposed for PtO_2.

The sequence is

$$S + OH \rightarrow SOH + e \qquad 4.3$$

$$SOH + OH^- \rightarrow SO^- + H_2O \qquad 4.4$$

$$SO^- \rightarrow SO + e \qquad 4.5$$

$$2SO \rightarrow 2S + O_2 \qquad 4.6$$

where S is an active site. They concluded that the rate determining step is step 2 at low overpotentials and step 1 at high overpotentials under low adsorption conditions (i.e. $\theta \rightarrow 0$). The experimentally obtained reaction order parameters confirmed their mechanistic proposals.

Fiori, Formaro, Mari, Scolari and Vago[64] carried out steady state oxygen evolution polarization measurements on perovskite like structured $NiLa_2O_4$ in electrolyte of KOH concentration ranging from 0.1 - 6 mol dm^{-3}. The porous $NiLa_2O_4$ electrodes were prepared by thermal decomposition of a stoichiometric mixture of Ni and La nitrate solution on Pt sheet current collector. They found the oxygen evolution reaction to be governed by two Tafel regions, at low potentials a Tafel region of 0.04V per decade and at high potentials a Tafel region of 0.12V per decade. They proposed a mechanistic sequence:

$$S + OH^- \rightarrow SOH + e \qquad 4.3$$

$$SOH + OH^- \rightarrow SO + H_2O + e \qquad 4.7$$

$$2SO \rightarrow 2S + O_2 \qquad 4.6$$

for oxygen evolution with the second step, i.e. the second electron transfer step to be rate determining. The change in the Tafel slope was attributed to the change in the adsorption concentration of the intermediate SOH. At lower potentials the adsorption is poor tending to zero, i.e. $\theta_{SOH} \rightarrow 0$, and at high potentials the adsorption level tends to a state of completeness, i.e. $\theta_{SOH} \rightarrow 1$. The reaction order parameters obtained with simple treatment of the polarisation data confirms their mechanistic postulations.

Morita, Iwakura and Tamura[65] carried out oxygen evolution polarisation measurements on porous MnO_2 electrodes in KOH electrolyte of varying concentration. The electrodes were prepared by thermal decomposition of manganese nitrate solution on Pt plate substrate. By obtaining the Tafel (0.11V per decade) and reaction order parameters they suggested that the primary hydroxide ion discharge step is rate determining under limitingly low adsorption conditions during oxygen evolution on MnO_2 in alkaline solutions.

Studies on RuO_2 have been carried out extensively[66, 74, 75, 76, 77] in relation to the mechanism and the activity of the oxygen evolution reaction and in relation to the corrosion and the dimensional stability of the electrode. O'Grady, Iwakura, Huang and Yeager[66] carried out oxygen evolution studies on RuO_2 electrodes in alkaline medium. The RuO_2 electrodes were prepared by thermal decomposition of ruthenium chloride on Ti substrate. These workers obtained a Tafel slope of 40 mV per decade and a first order dependence of current density on OH^- concentration, and they explained such results by the following mechanism:

$$S^z + OH^- \rightarrow (SOH)^z + e \qquad 4.8$$

$$(SOH)^z \rightarrow (SOH)^{z+1} + e \qquad 4.9$$

$$2(SOH)^{z+1} + 2OH^- \rightarrow 2S^z + O_2 + 2H_2O \qquad 4.10$$

with step 2 rate determining. The S^z active site was postulated to be a Ru^{4+} ion of the oxide.

Iwakura, Tada and Tamura[67] carried out oxygen evolution studies on IrO_2 Electrodes. They obtained a Tafel slope of 40 mV per decade and a second order dependence of current density on OH^- ion concentration. They proposed a mechanism similar to that proposed by Fiori et al for oxygen evolution on $NiLa_2O_4$ with the second step rate determining under limitingly low absorption conditions.

Oxygen evolution on perovskite structured oxides of Fe, Co and Mn has been studied by Matsumoto and co-workers [68, 69, 70]. The catalytic activity for oxygen evolution on $La_{1-x}Sr_xMnO_3$[68] and $La_{1-x}Sr_xCoO_3$[69] was found to increase with increase of x (up to a value of 0.4). The rate determining step for oxygen evolution on the Mn perovskites in alkaline medium was found to be the primary discharge of the OH^- ion, which was concluded from Tafel slopes of 1.3 to 1.4V per decade and the current density dependence of OH^- ion concentration of 1. However for the Co perovskite oxide, a chemical step

$$CoOH + OH^- \rightarrow CoO^- + H_2O \qquad 4.11$$

which follows an initial OH^- ion absorption step was suggested to be rate determining. This conclusion was based on a Tafel slope and on a OH^- ion dependence of current density of 0.065V per decade and 2 respectively. The same group of workers carried out oxygen evolution studies on $SrFeO_3$ in alkaline medium and obtained similar results to that obtained on $La_{1-x}Sr_xCoO_3$[69] and suggested a similar rate determining step; i.e.

$$FeOH + OH^- \rightarrow FeO^- + H_2O \qquad 4.12$$

The spinel structured $NiCo_2O_4$ was suggested as an active oxygen evolution catalyst by Tseung and Jasem,[78] and since then its long term performance has been evaluated [79, 7]. However, no definite mechanism has yet been put forward to explain the oxygen evolution

activity on $NiCo_2O_4$. The oxygen evolution studies carried out on $NiCo_2O_4$ will be surveyed later in this chapter. Co_3O_4 and $Ni_xFe_{3-x}O_4$ are two other spinel structured oxides on which oxygen evolution studies have been carried out. The Tafel slope for oxygen evolution on Co_3O_4[72] was found to be 0.065V per decade suggesting that a chemical step similar to that postulated to take place on $La_{1-x}Sr_xCoO_3$ is rate determining. Five oxides of the $Ni_xFe_{3-x}O_4$ system[71] with x in the range of 0.49 to 1.68 gave Tafel slopes of approximately 0.04V per decade for oxygen evolution in 30 wt.% KOH at 25°C. The results point to a second electron transfer step as a possible rate determining step.

4.3 Oxygen Evolution on $NiCo_2O4$ Electrodes

4.3.1 Previous Work

Tseung and Jasem[78] put forward guidelines for the choice of semiconducting oxides for the oxygen evolution reaction. They emphasized the role of the metal/metal oxide couple or the lower metal oxide/higher metal oxide couple in determining the minimum potential of oxygen evolution and on the basis of these considerations as well as other essential requirements such as electrical resistivity and corrosion resistance, suggested that $NiCo_2O_4$ should be a good electrocatalyst for oxygen evolution. They confirmed this experimentally; Teflon bonded $NiCo_2O_4$ electrodes gave an oxygen evolution current

density of 1A cm^{-2} at 1.6V vs the dynamic hydrogen electrode (dhe) at 70°C in 5N KOH. Tseung and co-workers workers[7] carried out long term endurance tests by evolving oxygen on Teflon bonded $NiCo_2O_4$ electrodes at a current density of 1A cm^{-2} at 85°C in 45% KOH and found the overvoltage to increase by less than 50 mV after 3000 hours of continuous running. Vandenborre and co-workers[79] reported the performance of $NiCo_2O_4$ to be the best out of four electrocatalysts studied and to have a stable overvoltage for over 200 hours of operation at a current density of 1A cm^{-2} at 85°C in 50 wt.% KOH. The $NiCo_2O_4$ electrodes studied by these workers were prepared by thermal decomposition of Ni and Co nitrate solution on perforated Ni plates. Singh et al[80] prepared $NiCo_2O_4$ by thermal decomposition of Ni and Co salt solution on metal substrate and carried out oxygen evolution studies on it in KOH medium. They found the oxygen evolution reaction on $NiCo_2O_4$ to be governed by one Tafel region of slope 0.04V per decade. However, Efremou and Zhukov[81] reported oxygen evolution on $NiCo_2O_4$ to be controlled by two Tafel slopes, a slope of 0.05V per decade at low potentials increasing to a slope of 0.09V per decade at higher potentials. Jasem and Tseung[82] carried out potentiostatic pulse studies on Teflon bonded $NiCo_2O_4$ electrodes and found the oxygen evolution reaction to be also controlled by two Tafel regions, the value of the slopes depending on the initial pulsing potential.

In the previous chapter[83], the coulometry studies carried out on $NiCo_2O_4$ was reported, which indicated that cation sites (A) on the surface of polycrystaline $NiCo_2O_4$ undergoes oxidation state transitions, $A^{2+} \rightarrow A^{3+} \rightarrow A^{4+}$, thus attaining an oxidation state of 4 before oxygen is evolved. In this section we report the investigation carried out to elucidate the oxygen evolution mechanism of $NiCo_2O_4$ and postulate a role for the different surface sites on $NiCo_2O_4$ during the oxygen evolution process.

4.3.2 Experimental

The $NiCo_2O_4$ for this study was obtained by freeze drying. Teflon bonded electrodes of $NiCo_2O_4$ were fabricated using 100 mesh Ni screen as current collector. Before actual measurements were taken the $NiCo_2O_4$ electrode under study was pre-anodised for $\sim$ 200 hours at a current density of 1A cm^{-2} at 70°C. Oxygen evolution current-potential measurements were obtained on the pre-anodised $NiCo_2O_4$ electrode in KOH solutions of concentration 0.1, 0.2, 0.4, 0.6, 1.2, 2.2, 4 and 5 mol dm^{-3} at 25°C. The experimental details are described in Chapter 2. A dynamic hydrogen electrode (dhe) was used as the reference electrode. The dhe was calibrated against the revesible hydrogen electrode (rhe) in the same electrolyte, for the different electrolytes at 25°C and was found to vary between -18 mV to -21 mV. The interrupter technique[166] was used to measure the ohmic drop between the Luggin capillary and the working electrode.

4.3.3 Results and Discussion

Figure 4.1 shows the current potential oxygen evolution performance on $NiCo_2O_4$ in 5 mol dm^{-3} KOH at 25°C. From Figure 4.1 it is seen that oxygen evolution on $NiCo_2O_4$ is governed by two Tafel regions; at low potentials (< 1.56V) a slope of ∿ 40mV per decade increases to a slope of ∿ 120 mV per decade at high potentials(> 1.56V). The results are reproducible on preanodised electrodes. Table 4.2 shows the values of the slopes obtained by 4 successive runs on one electrode, and on two other electrodes. The polarisation behaviour in 2.2 and 4 mol dm^{-3} KOH were found to be identical to that in 5 mol dm^{-3} KOH.

Figure 4.2 shows the oxygen evolution potential characteristics on preanodised $NiCo_2O_4$ in KOH electrolyte of concentration 0.1, 0.2, 0.4, 0.6 and 1.2 mol dm^{-3}. It is to be noted that oxygen evolution in KOH electrolyte of concentration 0.4 mol dm^{-3} and less did not show a decrease of the slope at low potentials and the two slopes were clearly observable only in KOH electrolyte of concentration 1.2 mol dm^{-3}.

To postulate a mechanistic path for oxygen evolution on $NiCo_2O_4$ it is essential to critically analyse the paths already proposed for oxygen evolution, and the nature and concentration of the active sites in $NiCo_2O_4$.

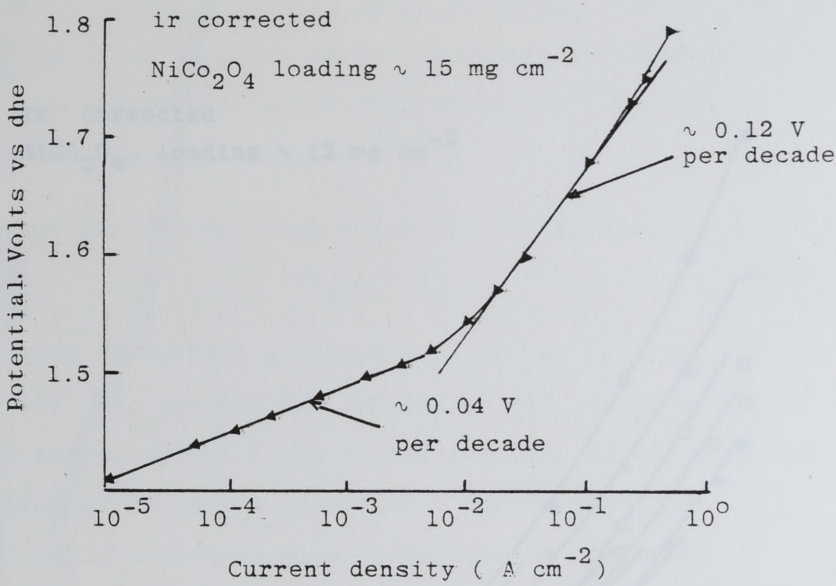

Figure 4.1: Oxygen evolution current - potential characteristics on preanodised Teflon bonded $NiCo_2O_4$ at 25°C in 5 mol dm^{-3} KOH.

Table 4.2: Reproducibility of the Tafel slopes for oxygen evolution on preanodised Teflon bonded $NiCo_2O_4$ at 25°C in 5 mol dm^{-3} KOH.

Electrode	Tafel slope (volts per decade)	
	lower potential	high potential
(1)	0.044	0.105
	0.044	0.117
	0.046	0.120
	0.042	0.106
(2)	0.044	0.099
	0.040	0.110
(3)	0.042	0.123
	0.043	0.110

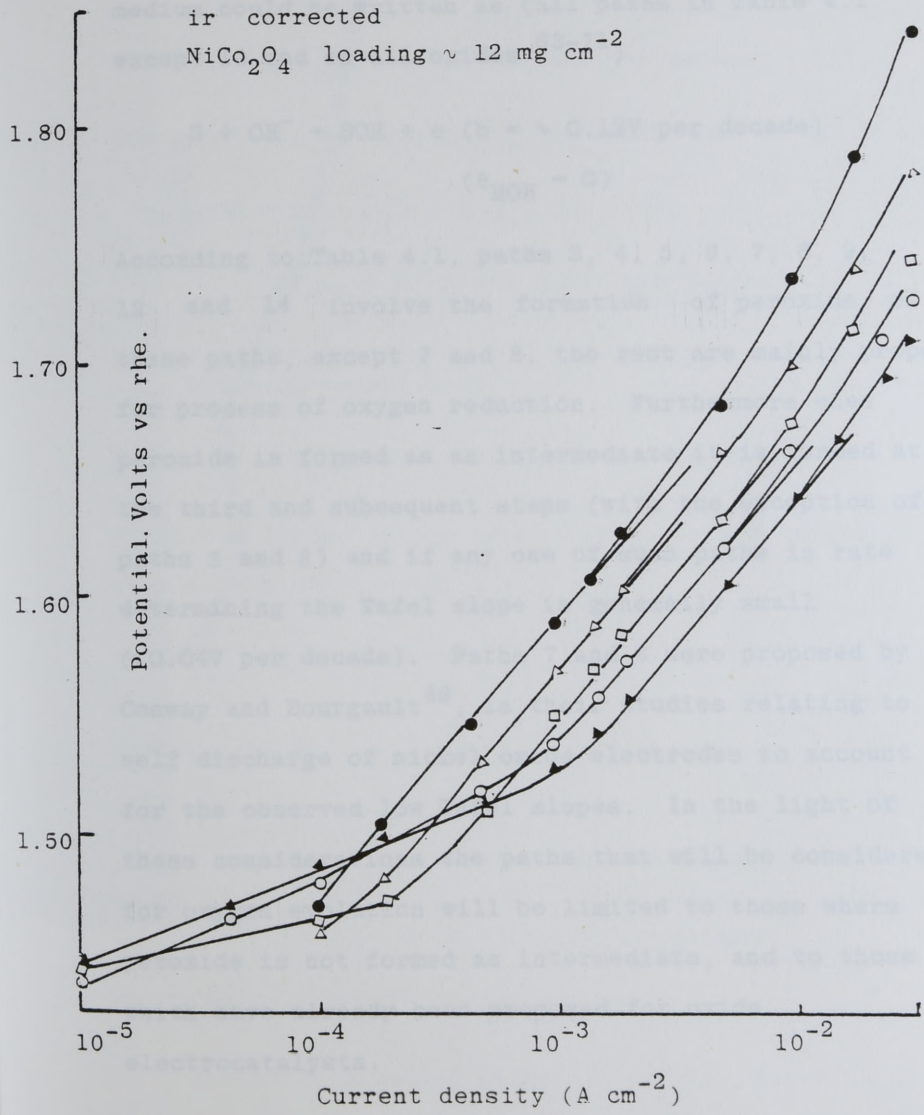

Figure 4.2: Oxygen evolution current potential characteristics on preanodised Teflon bonded $NiCo_2O_4$ in electrolytes of KOH concentration 0.1(●), 0.2(△), 0.4(□), 0.6(○) and 1.2(▲) mol dm^{-3} KOH at 25°C.

4.3.3.1 Oxygen Evolution Paths on Oxides

The first step for oxygen evolution in alkaline medium could be written as (all paths in Table 4.1 except 13 and on all oxides [63-71])

$$S + OH^- \rightarrow SOH + e \quad (b = \sim 0.12V \text{ per decade}) \quad (\theta_{MOH} \rightarrow 0) \qquad 4.3$$

According to Table 4.1, paths 3, 4, 5, 6, 7, 8, 9, 12 and 14 involve the formation of peroxide: of these paths, except 7 and 8, the rest are mainly proposed for process of oxygen reduction. Furthermore when peroxide is formed as an intermediate it is formed at the third and subsequent steps (with the exception of paths 3 and 6) and if any one of such paths is rate determining the Tafel slope is generally small ($\ll$0.04V per decade). Paths 7 and 8 were proposed by Conway and Bourgault[49], in their studies relating to self discharge of nickel oxide electrodes to account for the observed low Tafel slopes. In the light of these considerations the paths that will be considered for oxygen evolution will be limited to those where peroxide is not formed as intermediate, and to those which have already been proposed for oxide electrocatalysts.

The second step during oxygen evolution in alkaline medium is proposed to be either the second electron transfer step or a chemical step. If electron transferring, it is

$$SOH + OH^- \rightarrow SO + H_2O + e \qquad 4.7$$

$$(\theta_{SOH} \rightarrow 0,\ b = \sim 0.04V \text{ per decade})$$

$$(\theta_{SOH} \rightarrow 1,\ b = \sim 0.12V \text{ per decade})$$

The chemical step can be of two kinds, one of which is

$$2SOH \rightarrow SO + H_2O + S \qquad 4.7a$$

$$(\theta_{SOH} \rightarrow 0,\ b = \sim 0.03V \text{ per decade})$$

$$SOH + OH^- \rightarrow SO^- + H_2O \qquad 4.4$$

$$(\theta_{SOH} \rightarrow 0,\ b = \sim 0.06V \text{ per decade})$$

If SO is formed in the second step, oxygen evolution step is the third step, i.e.

$$2SO \rightarrow 2S + O_2 \qquad 4.6$$

However, if SO^- is formed, the third step is

$$SO^- \rightarrow SO + e \qquad 4.5$$

$$(\theta_{SO^-} \rightarrow 0,\ b = \sim 0.04V \text{ per decade})$$

$$(\theta_{SO^-} \rightarrow 0,\ b = \sim 0.12V \text{ per decade})$$

which is followed by oxygen evolution.

The three proposed paths for oxygen evolution on oxides in alkaline medium are given in Table 4.3.

It is to be noted that paths II and III are similar, if steps III(b) and III(c) are considered to be one step.

Table 4.3: Three paths for oxygen evolution on oxides and the associated values of the Tafel slopes at 25°C.

			Tafel slope (Volts per decade)	
			Low θ	High θ
(I)	(a)	$S + OH^- \rightarrow SOH + e$	0.118	
	(b)	$2SOH \rightarrow SO + S + H_2O$	0.030	
	(c)	$2SO \rightarrow 2S + O_2$	0.015	
(II)	(a)	$S + OH^- \rightarrow SOH + e$	0.118	
	(b)	$SOH + OH^- \rightarrow SO + H_2O + e$	0.039	0.118
	(c)	$2SO \rightarrow 2S + O_2$	0.015	
(III)	(a)	$S + OH^- \rightarrow SOH + e$	0.118	
	(b)	$SOH + OH^- \rightarrow SO^- + H_2O$	0.059	
	(c)	$SO^- \rightarrow SO + e$	0.039	0.118
	(d)	$2SO \rightarrow 2S + O_2$	0.015	

4.3.3.2 Active Sites in $NiCo_2O_4$

$NiCo_2O_4$ has been shown to be a mixed spinel of ionic distribution[96],

$$Co^{2+}_{0.9}\ Co^{3+}_{0.1}\ (Ni^{2+}_{0.9}\ Ni^{3+}_{0.1}\ Co^{3+})\ O^{2-}_{3.2}\ O^{-}_{0.8}\ ,$$

where the cations in parenthesis have octahedral coordination and those outside have tetrahedral coordination. Therefore the cations are mixed and differ in concentration, oxidation state and coordination. Since oxygen evolution is a surface process involving an increase in oxidation state and thus a shrinking of ionic volume of the cations, site coordination differences will not be expected to affect the oxygen evolution path. Further, the mixed nature of the cation sites will be expected to affect the oxygen evolution path to a lesser degree than the difference in the oxidation state. This is more emphasized since a divalent site in $NiCo_2O_4$ can increase its oxidation state by 2, whereas the trivalent site can increase by only 1, before oxygen is evolved. The bulk concentration of divalent and trivalent sites are 60% and 40% respectively, and the bulk site concentrations could be taken to represent surface site concentrations.

4.3.3.3 Oxygen Evolution Paths on $NiCo_2O_4$

The Tafel slope of 0.12V per decade on $NiCo_2O_4$ is attributed to the oxygen evolution process taking place on divalent Ni and Co(M) by path II (Table 4.3). The

mechanistic steps are

$$M + OH^- \rightarrow MOH + e \qquad 4.13$$

$$MOH + OH^- \rightarrow MO + H_2O + e \qquad 4.14$$

$$2MO \rightarrow 2M + O_2 \qquad 4.15$$

A Tafel slope of 0.12V per decade could be due to step 1 being rate determining at limitingly low coverage of MOH or step 2 rate determining when the surface coverage of MOH approaches unity.

Experimental reaction order parameters have been obtained by simple analysis of the polarisation data in different KOH concentration. Figure 4.3 shows the KOH concentration dependence of current density for oxygen evolution on $NiCo_2O_4$ at a constant potential of 0.8V at 25°C giving a slope of 1.12. Figure 4.4 shows the KOH concentration dependence of the oxygen evolution potential at a constant current density of 4×10^{-3} A cm^{-2} giving a slope of -0.11V. Figure 4.5 shows the KOH concentration dependence of the current density at a constant overpotential of 0.35V, giving a slope of 0.44.

Rate equations are derived assuming steps 4.13 and 4.14 to be rate determining, to evaluate the theoretically predicted kinetic parameters.

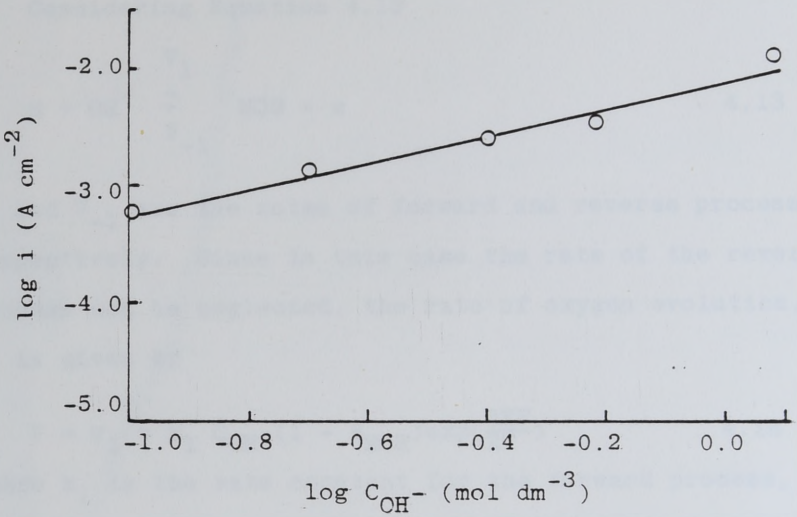

Figure 4.3: KOH concentration dependence of current density for oxygen evolution on $NiCo_2O_4$ at a constant potential of 0.8 V (vs she) at 25°C.

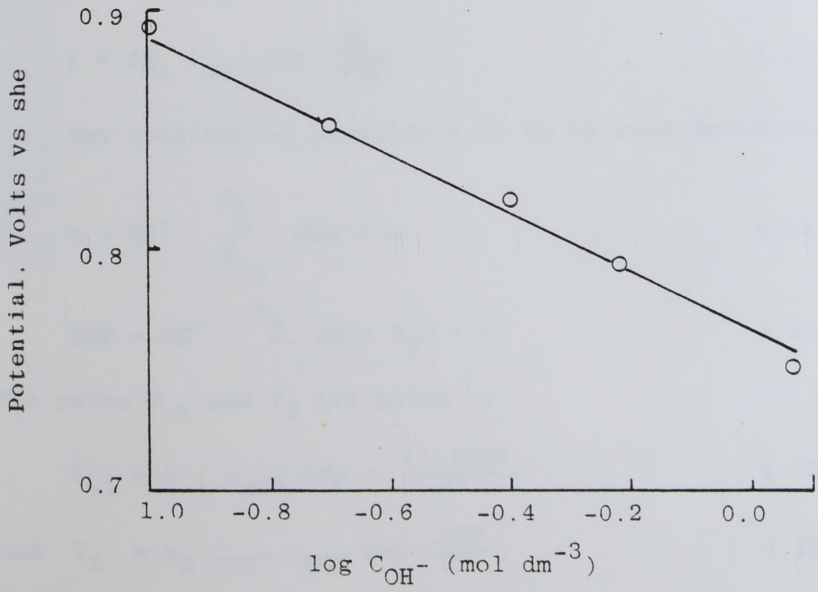

Figure 4.4: KOH concentration dependence of oxygen evolution potential on $NiCo_2O_4$ at a constant current density of 4×10^{-3} A cm^{-2} at 25°C.

Considering Equation 4.13

$$M + OH^- \underset{V_{-1}}{\overset{V_1}{\rightleftarrows}} MOH + e \qquad 4.13$$

V_1 and V_{-1} are the rates of forward and reverse processes respectively. Since in this case the rate of the reverse process can be neglected, the rate of oxygen evolution, V, is given by

$$V = V_1 = k_1 C_{OH^-}(1 - \theta_{MOH})\exp(\frac{\beta EF}{RT}) \qquad 4.16$$

where k_1 is the rate constant for the forward process, θ_{MOH} is the extent of coverage of MOH compared to unit, C_{OH^-} is the activity of the OH^- ion, B, E, F, R and T have the usual meanings. At limitingly low coverage of MOH, $\theta_{MOH} \rightarrow 1$, and taking $\beta = 0.5$, $V = i/nF$, the oxygen evolution current density i is given by

$$i = Fk_1 C_{OH^-} \exp(\frac{EF}{2RT}) \qquad 4.17$$

Now considering Equation 4.14 to be rate determining

$$M + OH^- \underset{V_{-1}}{\overset{V_1}{\rightleftarrows}} MOH + e \qquad 4.13$$

$$MOH + OH^- \overset{V_2}{\rightarrow} MO + H_2O + e \qquad 4.14$$

The rates V_{-1} and V_2 are given by

$$V_{-1} = k_{-1}\, \theta_{MOH} \exp - (\frac{(1-\beta)EF}{RT}) \qquad 4.18$$

and $$V_2 = k_2 C_{OH^-}\, \theta_{MOH} \exp(\frac{\beta EF}{RT}) \qquad 4.19$$

Applying steady state concepts to the coverage of MOH

$$\frac{d\theta_{MOH}}{dt} = V_1 - V_{-1} - V_2 = 0 \qquad 4.20$$

i.e. $k_1 C_{OH^-}(1 - \theta_{MOH})\exp(\frac{\beta EF}{RT}) - k_{-1}\theta_{MOH}\exp-(\frac{(1-\beta)EF}{RT})$

$$- k_2\,\theta_{MOH}\,C_{OH^-}\exp(\frac{\beta EF}{RT}) = 0 \qquad 4.21$$

Rearranging Equation 4.21 and bringing θ_{MOH} to one side, we have

$$\theta_{MOH} = \frac{k_1 C_{OH^-}\exp(\frac{\beta EF}{RT})}{k_1 C_{OH^-}\exp(\frac{\beta EF}{RT}) + k_{-1}\exp-(\frac{(1-\beta)EF}{RT}) + k_1 C_{OH^-}\exp(\frac{\beta EF}{RT})} \qquad 4.23$$

Substituting for θ_{MOH} in Equation 4.19, which determines the rate of oxygen evolution, we have

$$V = \frac{k_2 k_1 C_{OH^-}^2\exp(\frac{2\beta EF}{RT})}{k_1 C_{OH^-}\exp(\frac{\beta EF}{RT}) + k_{-1}\exp-(\frac{(1-\beta)EF}{RT}) + k_2 C_{OH^-}\exp(\frac{\beta EF}{RT})} \qquad 4.24$$

At high potentials, if the coverage of MOH approaches unity, the assumptions, that $k_1 >> k_{-1}$ and $k_1 >> k_2$ is justifiable, thus

$$k_1 C_{OH^-}\exp(\frac{\beta EF}{RT}) >> k_{-1}\exp-(\frac{(1-\beta)EF}{RT})$$

and

$$k_1 C_{OH^-} \exp(\frac{\beta EF}{RT}) >> k_2 C_{OH^-} \exp(\frac{\beta EF}{RT})$$

The rate Equation 4.26 simplifies to

$$V = k_2 C_{OH^-} \exp(\frac{\beta EF}{RT}) \qquad 4.25$$

Equation 4.25, in terms of current density is given by

$$i = 2Fk_2 C_{OH^-} \exp(\frac{EF}{2RT}) \qquad 4.26$$

It is seen from Equations 4.17 and 4.26, that when step 4.13 or 4.14 is rate determining, the Tafel and the reaction order parameters are the same. Therefore the reaction order parameters will not help to identify the rate determining step. However, the preferred rate determining step is the primary discharge of the OH^- ion (step 4.13). The reason for this preference will be given later in this chapter.

From the rate equation the Tafel slope is 2RT/F equal to 0.118V per decade at 25°C. The KOH concentration dependence of current density at constant potential is 1 and the KOH concentration dependence of potential at constant current density is -2RT/F equal -0.118V per decade, at 25°C. The KOH dependence of current density at constant overpotential can be derived from the rate equation. The potential E is related to the equilibrium potential (E_e) and the overpotential (η) by

$$E = E_e + \eta \qquad 4.27$$

The standard equilibrium potential varies with concentration of KOH by

$$E^o = E_e^o - \frac{2.303\ RT}{F} \log C_{OH^-} \qquad 4.28$$

where E_e^o is the standard equilibrium potential. Substitutiong Equation 4.28 into the rate equation (Equation 4.17) and differentiating i with respect to KOH concentration, we obtain

$$\left(\frac{\partial \log i}{\partial \log C_{OH^-}}\right)_\eta = 1 + \frac{\beta F}{2.303\ RT}\left(\frac{\partial E_e}{\partial \log C_{OH^-}}\right) \qquad 4.29$$

Differentiating E_e in Equation 4.28 with respect to concentration of OH^-, we obtain

$$\left(\frac{\partial E_e}{\partial \log C_{OH^-}}\right) = -\frac{2.303\ RT}{F} \qquad 4.30$$

From Equations 4.29 and 4.30

$$\left(\frac{\partial \log i}{\partial \log C_{OH^-}}\right)_\eta = 1 - \beta \qquad 4.31$$

Therefore the current density dependence of KOH concentration at constant overpotential is 0.5.

Table 4.4 compares the experimentally observed and the theoretically predicted values of the kinetic parameters for oxygen evolution on $NiCo_2O_4$ (Tafel slope $\sim$ 0.12V per decade) showing a good agreement.

The Tafel slope of 0.04V per decade obtained for oxygen evolution on $NiCo_2O_4$ at low potentials would be attributed to the second electron transfer step (step

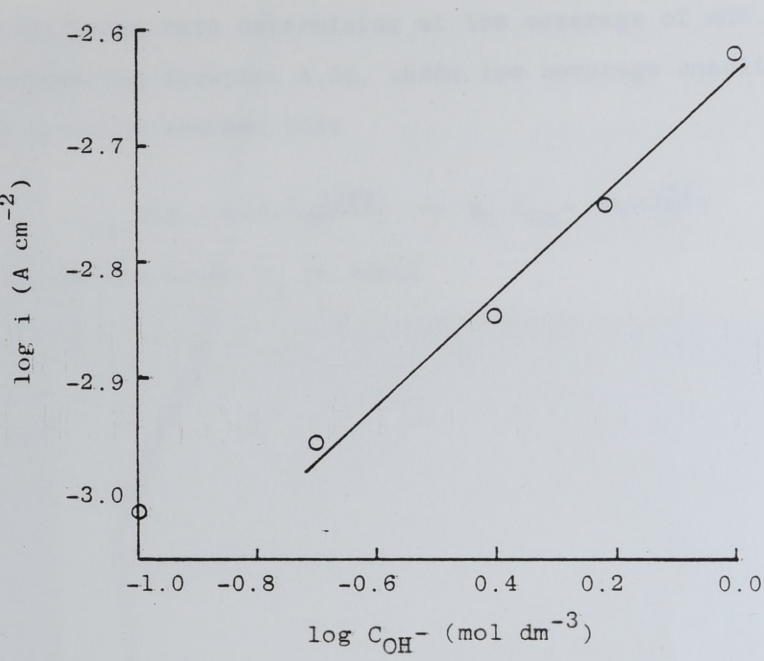

Figure 4.5: KOH concentration dependence of oxygen evolution current density on $NiCo_2O_4$ at a constant overpotential of 0.35 V at 25°C.

Table 4.4: Comparison of the theoretically predicted and the experimentally observed kinetic parameters for oxygen evolution on $NiCo_2O_4$ at higher potentials at 25°C.

Parameter	Theoretical	Experimental
$\left(\frac{\partial E}{\partial \log i}\right)_T$	$\frac{2 \times 2.303\ RT}{F}$	∿ 0.120 V
$\left(\frac{\partial \log i}{\partial \log C_{OH^-}}\right)_{E,T}$	1	1.12
$\left(\frac{\partial E}{\partial \log C_{OH^-}}\right)_{i,T}$	$-\frac{2 \times 2.303\ RT}{F}$	- 0.11 V
$\left(\frac{\partial \log i}{\partial \log C_{OH^-}}\right)_{\eta,T}$	1-β	0.44

4.14) being rate determining at low coverage of MOH. Thus, considering Equation 4.24, under low coverage conditions it could be assumed that

$$k_{-1} \exp - (\frac{(1 - \beta)EF}{RT}) \gg k_1 C_{OH^-} \exp(\frac{\beta EF}{RT})$$

and further since k_s is small

$$k_{-1} \exp - (\frac{(1 - \beta)EF}{RT}) \gg k_2 C_{OH^-} \exp(\frac{\beta EF}{RT})$$

Therefore the simplified rate equation in terms of current density is

$$i = \frac{2F\ k_2 k_1}{k_{-1}} C^2_{OH^-} \exp(-\frac{(1 + \beta)EF}{RT}) \qquad 4.32$$

according to which the Tafel slope is $\sim$ 0.04V per decade at 25°C. It was not possible to calculate reaction order parameters for the Tafel slope of 0.04V per decade from the polarisation data, since, a clear slope of 0.04V per decade was not observed in KOH concentrations of 0.4 mol dm^{-3} and less, and also because in KOH concentrations greater 1.2 mol dm^{-3} the polarisation characteristics changed very little with concentration.

However, a further possibility for the existence of the slope of 0.04V per decade is oxygen evolution taking place on the trivalent sites. If this is the case, then it implies that oxygen evolution takes place at lower potentials on trivalent sites than on divalent sites of Ni and Co. It is difficult if not impossible to prove this hypothesis on $NiCo_2O_4$. However, oxygen evolution studies on an oxide of Ni or Co with a high concentration

of trivalent ions should provide evidence for this hypothesis. A suitable oxide system selected for this purpose is Li doped Co_3O_4. Further discussion on the slope of 0.04V per decade will be left until the oxygen evolution study on the Li doped Co_3O_4 system is described and discussed.

4.4 Oxygen Evolution on Li Doped Co_3O_4

4.4.1 Selection of an Oxide

Co has three well defined oxides[86] CoO (cubic), Co_2O_3(hexagonal and Co_3O_4 (normal spinel). The cation distribution[85] in Co_3O_4 is:

$$Co^{2+}(Co_2^{3+})O_4^{2-}$$

where all the Co^{2+} are in tetrahedral environment and all Co^{3+} are in octahedral environment. The electrical resistivities of CoO and Co_2O_3 are > 10^5 ohm - cm and the electrical resistivity of Co_3O_4 is 4 x 10^3 ohm - cm. However, it is possible to lower the electrical resistivity of CoO and Co_3O_4 by incorporating Li into the lattice. The Co^{3+} concentration could be increased ideally from 0 to 33% of total cations in CoO (i.e. $Li_x^+ Co^{2+} Co_{1-2x}^{2+} Co_x^{3+} O^{2-}$)

and from 67% to 70% in Co_3O_4

(i.e. $Li_x^+ Co_{1-2x}^{2+} Co_x^{3+} (Co_2^{3+}) O_4^{2-}$). A further advantage of studying the spinel system compared to the CoO is that the former requires relatively low sintering temperatures

for spinel formation whereas the CoO phase is formed only above 950°C.

Of the oxides of Ni, Li doped NiO oxide has the same disadvantages as Li doped CoO. Trivalent Ni is known to form hydrated oxides[88] e.g. $Ni_2O_3 . 2H_2O$ and these compounds are not well characterised and Ni oxide does not exist in a spinel structured form. Therefore the Li doped Co_3O_4 system is an ideal choice.

4.4.2 Experimental

Oxygen evolution studies were carried out on Co_3O_4 and Co_3O_4 doped with 4, 7 and 10 at.% Li. The 4 polycrystaline oxide powders were obtained by the method of freeze drying. The electrical resistivities and the BET specific surface areas of the 4 powders are given in Chapter 2. Teflon bonded electrodes of the 4 oxides were made. The electrodes were preanodised before oxygen evolution studies were carried out. The preanodisation conditions for each of the 4 oxide electrode are, 1 A cm^{-2} for ∿ 200 hrs. in 5 mol dm^{-3} KOH at 70°C. The oxygen evolution current-potential characteristics were obtained on the 4 oxide electrodes in 5 mol dm^{-3} KOH at 25°C. The transient current-potential characteristic of the 10 at.% Li doped Co_3O_4 electrode in 5N KOH at 25°C was obtained by the potentiostatic pulse technique. The current-potential characteristics of the same electrode was also obtained in electrolyte of KOH concentration 0.4, 0.6,

1.0 and 1.5 mol dm^{-3}. A dhe was used as the reference electrode. The dhe was calibrated against the rhe in the same electrolyte, for the 4 different electrolytes and was found vary between -19 mV to -23 mV. The interrupter technique[166] was used to measure the ohmic drop between the Luggin capillary and the working electrode. The experimental details are similar to that of $NiCo_2O_4$ and is described in Chapter 2.

4.4.3 Results and Discussion

Figure 4.6 gives the oxygen evolution current-potential characteristics on the 4 oxide electrodes at 25°C in 5N KOH. A point to note is that the oxygen evolution potential increases with increase in Li doping. Two reasons could be attributed for this trend: (a) an increase in electrical conductivity with Li doping (see Table 2.2); (b) an increase in the Co^{3+} ions with Li doping. A consideration based solely on increased electrical conductivity will not explain the trend, especially the difference in performance of the 7 and 10 atomic % Li doped Co_3O_4, both having an electrical resistivity of ∿ 1 ohm-cm. However, if all the Li^+ enters the tetrahedral sites[87], the cationic percentage of Co^{3+} ion in this spinel will be 76, 73, 70 and 66 for 10, 7, 4 and 0 atomic % doping. This trend is more in accordance with the oxygen evolution trends. The tetrahedral site preference of the Li^+ ion in Co_3O_4 spinel lattice can at present only be justified by (a) the ionisation potential[188]

of Co^{3+} (53 eV) being greater than that of Co^{2+} (33.5 eV), (b) Co_2O_3 being resistant to Li doping. The resistivity of Co_2O_3 (10^6 ohm-cm) was not lowered when sintered with 10 atomix % Li in the form of LiOH, at 600°C in N_2 for 10 hours. Therefore, the increased electrical conductivity of the Li doped Co_3O_4 is attributed to an electron hopping process in the Co^{2+} and Co^{3+} ions in the tetrahedral sites[87].

The Tafel slopes for the evolution of oxygen on all 4 oxide systems obtained by steady state technique (Figure 4.6) are ∿ 0.06V per decade. Figure 4.7 gives the current-potential relationship for oxygen evolution on two 10 at.% Li doped Co_3O_4 electrodes obtained by potentiostatic pulse technique in 5N KOH at 25°C showing a slopes of 0.064V per decade, up to a current density of 1A cm^{-2} (∿ 1.7V), therefore confirming that the slope of ∿ 0.06V per decade on the Co oxide electrodes is activation controlled.

Figure 4.8 gives the current-potential plots for oxygen evolution on 10 at.% Li doped Co_3O_4 in KOH concentration of 0.4, 0.6,1.0 and 1.5 mol dm^{-3} at 25°C. The experimental reaction order parameters $(\partial E/\partial \log C_{OH^-})_{i,T}$ and $(\partial \log i/\partial \log C_{OH^-})_{E,T}$ for oxygen evolution on 10 at.% Li doped Co_3O_4 are obtained as shown in Figures 4.9 and 4.10 respectively, and have values of -0.117V are 1.76 respectively.

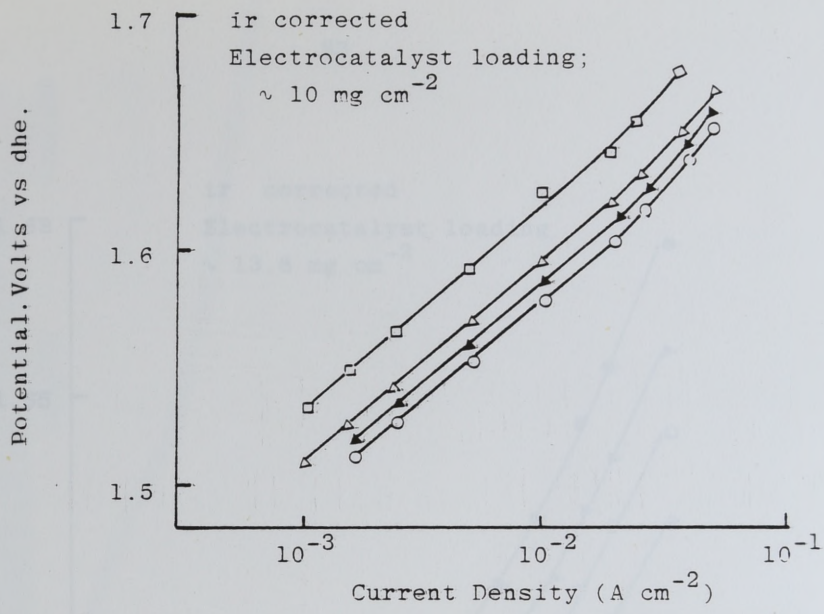

Figure 4.6: Oxygen evolution current potential characteristics on preanodised Teflon bonded Co_3O_4 doped with 0(□), 4(△), 7(▲) and 10(○) at. % Li, at 25°C in 5 mol dm^{-3} KOH.

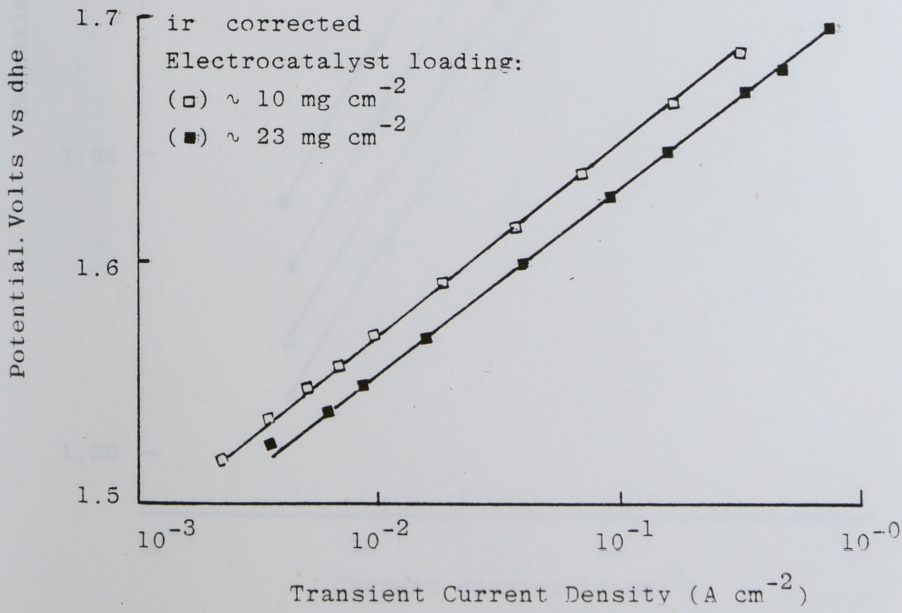

Figure 4.7: Oxygen evolution current potential characteristics on preanodised Teflon bonded 10 at. % Li doped Co_3O_4, obtained by potentiostatic pulse technique, in 5 mol dm^{-3} KOH at 25°C.

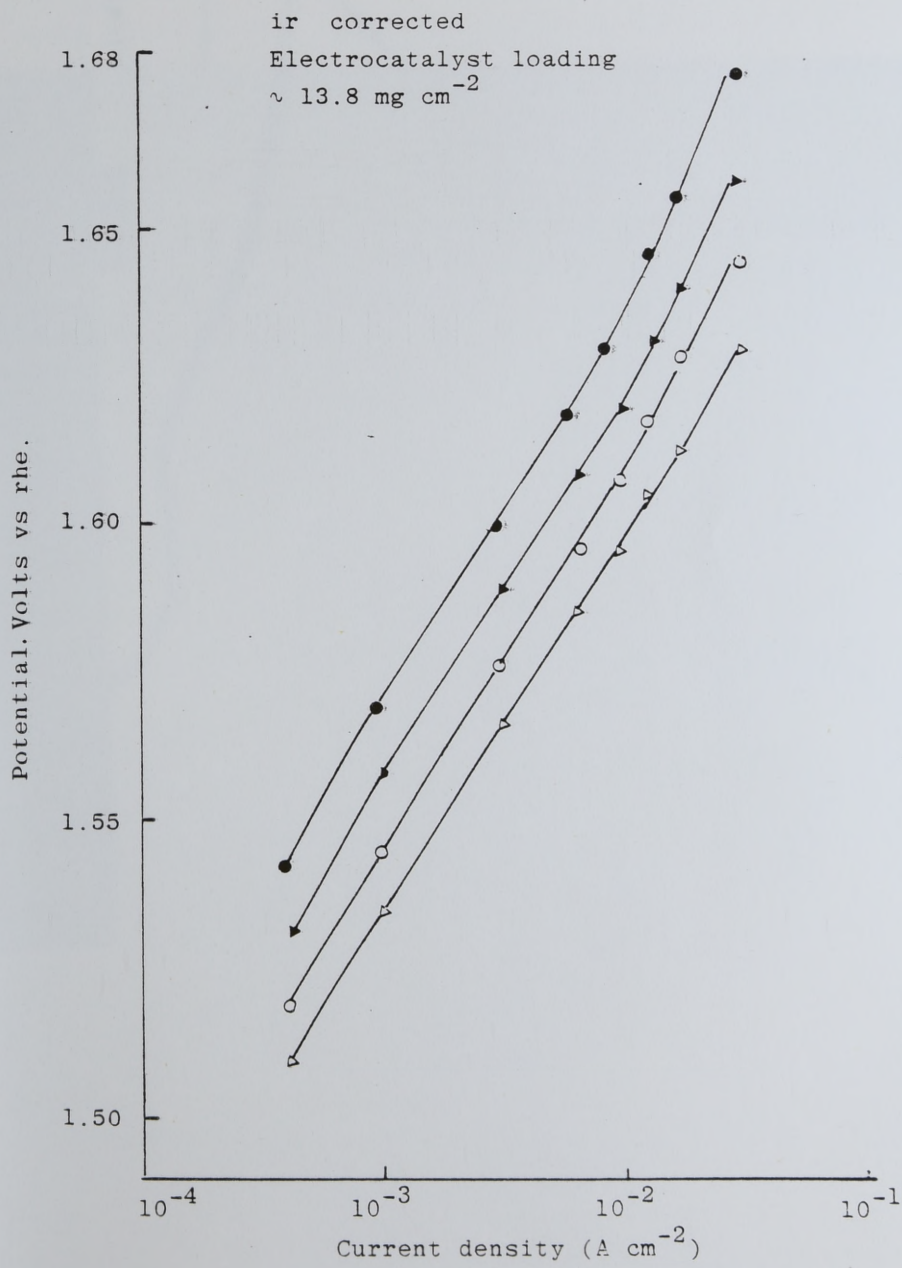

Figure 4.8: Oxygen evolution current potential characteristics on preanodised Teflon bonded 10 at. % Li doped Co_3O_4 in electrolytes of KOH concentration of 1.0(○), 0.4(●), 0.6(▲), and 1.5(△) mol dm^{-3} at 25°C.

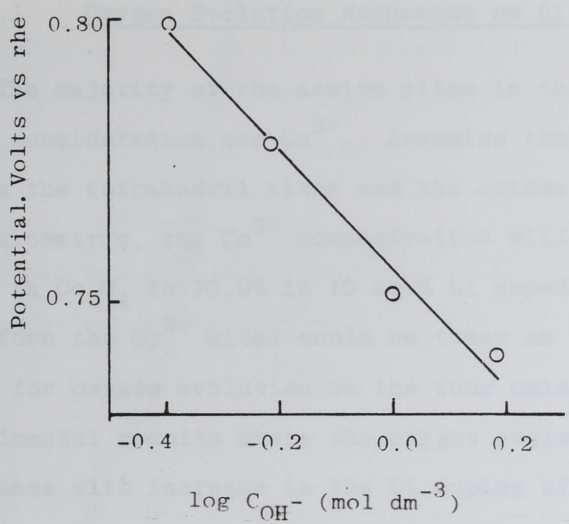

Figure 4.9: KOH concentration dependence of oxygen evolution potential on a 10 at. % Li doped Co_3O_4 at a constant current density of 4 x 10^{-3} A cm^{-2} at 25°C.

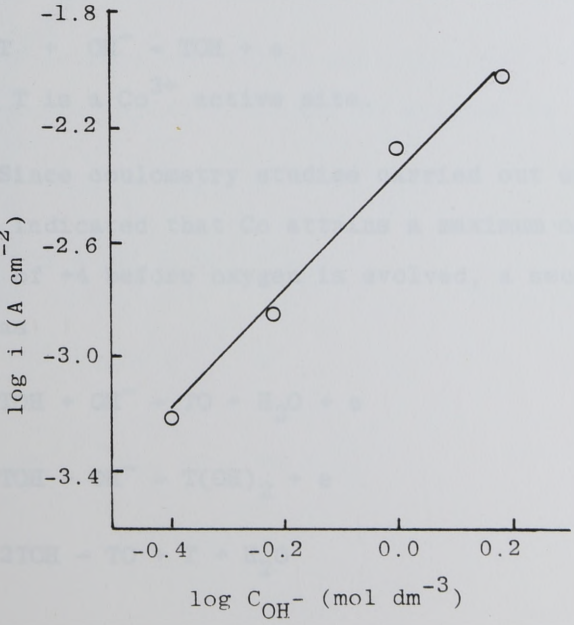

Figure 4.10: KOH dependence of oxygen evolution current density on a 10 at. % Li doped Co_3O_4 electrode at a constant potential of 0.75 V at 25°C.

4.4.3.1 Oxygen Evolution Mechanism on Li Doped Co_3O_4

The majority of the active sites in the 4 oxides of Co under consideration are Co^{3+}. Assuming that all the Li^+ enters the tetrahedral sites and the oxides are completely stoichiometric, the Co^{3+} concentration will increase from 66.7% in Co_3O_4 to 70.0% in 10 at.% Li doped Co_3O_4. Therefore the Co^{3+} sites could be taken as the main active sites for oxygen evolution on the four oxides. The experimental results where the oxygen evolution performance increases with increase in the Li doping of the oxides (Figure 4.6) also supports this hypothesis.

The first mechanistic step during oxygen evolution on the 4 oxides, is forming a tetravalent species of Co. This could be written as

$$T + OH^- \rightarrow TOH + e \qquad 4.33$$

where T is a Co^{3+} active site.

Since coulometry studies carried out on Li doped Co_3O_4 indicated that Co attains a maximum oxidation state of +4 before oxygen is evolved, a second step such as

$$TOH + OH^- \rightarrow TO + H_2O + e \qquad 4.34$$

or $$TOH + OH^- \rightarrow T(OH)_2 + e \qquad 4.35$$

or $$2TOH \rightarrow TO + T + H_2O \qquad 4.36$$

is not possible. Therefore oxygen evolution on spinel oxides of Co cannot take place by paths I and II shown in Table 4.3. A possible second step is

$$TOH + OH^- \rightarrow TO^- + H_2O \qquad 4.37$$

which is similar to step (b) in path III (Table 4.3). Since further steps such as

$$TO^- \rightarrow TO + e \qquad 4.38$$

wil form a pentravalent species of Co, oxygen evolution could take place by

$$TO^- + M \rightarrow T\overset{O}{\diagup\diagdown}M \qquad 4.39$$

and $$2T\overset{O}{\diagup\diagdown}M \rightarrow 2T + 2M + O_2 \qquad 4.40$$

where M is a divalent or trivalent Co.

Therefore the oxygen evolution path on the 4 spinel structured oxides of Co can be written as

$$T + OH^- \rightarrow TOH + e \qquad 4.34$$

$$TOH + OH^- \rightarrow TO^- + H_2O \qquad 4.37$$

$$TO^- + M \rightarrow T\overset{O}{\diagup\diagdown}M \qquad 4.39$$

$$2T\overset{O}{\diagup\diagdown}M \rightarrow 2T + 2M + O_2 \qquad 4.40$$

If step 2 (step 4.37) is assumed to be the rate determining step at limitingly low coverage of TOH, the Tafel slope for oxygen evolution will be 0.059V per decade, which is in accordance with the value of ∿ 0.06V per decade obtained on the 4 oxides by experiment.

The rate equation for oxygen evolution can be derived by considering steady state concepts

$$T + OH^- \underset{V_{-1}}{\overset{V_1}{\rightleftharpoons}} TOH + e \qquad 4.34$$

$$TOH + OH^- \xrightarrow{V_2} TO^- + H_2O \qquad 4.37$$

where V_1 and V_{-1} are rates of the forward and reverse processes of step 1 and V_2 is the rate of the forward process of step 2. Now,

$$V_1 = k_1(1 - \theta_{TOH})C_{OH^-} \exp(\frac{\beta EF}{RT}) \qquad 4.41$$

$$V_{-1} = k_{-1}\, \theta_{TOH} \exp - (\frac{(1 - \beta)EF}{RT}) \qquad 4.42$$

and $V_2 = k_2\, \theta_{TOH}\, C_{OH^-}$ 4.43

The notations used in the above 3 equations were defined in Section 4.3.3.3.

Considering a steady state surface concentration of TOH, we get

$$\frac{d\theta_{TOH}}{dt} = V_1 - V_{-1} - V_2 = 0 \qquad 4.44$$

from which

$$k_1(1 - \theta_{TOH})C_{OH^-} \exp(\frac{\beta EF}{RT}) - k_{-1}\ \theta_{TOH} \exp - (\frac{(1 - \beta)EF}{RT})$$

$$- k_2\ \theta_{TOH} C_{OH^-} = 0 \qquad 4.45$$

from Equation 4.45, θ_{TOH} is given by

$$\theta_{TOH} = \frac{k_1\ C_{OH^-} \exp \frac{\beta EF}{RT}}{k_1\ C_{OH^-} \exp \frac{\beta EF}{RT} + k_{-1} \exp - (\frac{(1-\beta)EF}{RT}) + k_2\ C_{OH^-}} \qquad 4.46$$

At conditions of low coverage of TOH (i.e. when $\theta_{TOH} \rightarrow 0$)

$$k_{-1} >> k_1$$

and

$$k_{-1} >> k_2$$

and Equation 4.46 could be simplified to

$$\theta_{TOH} = \frac{k_1}{k_{-1}} C_{OH^-} \exp (\frac{EF}{RT}) \qquad 4.47$$

Now, the rate of oxygen evolution, V, is given by

$$V = V_2 = k_2\ \theta_{TOH}\ C_{OH^-} \qquad 4.48$$

Substituting for θ_{TOH} in Equation 4.48, and expressing the rate of oxygen evolution in terms of current density, the rate equation for oxygen evolution is

$$i = \frac{Fk_1k_2}{k_{-2}} C_{OH^-}^2 \exp (\frac{EF}{RT}) \qquad 4.49$$

The rate equations predicts that the Tafel slope has a value of 0.059V per decade and the reaction order

parameters $(\partial E/\partial \log C_{OH^-})_i$ and $(\partial \log i/\partial \log C_{OH^-})_E$ have values of -0.118V per decade and 2 respectively.

Table 4.5 compares the experimentally observed and the theoretically predicted values of the kinetic parameters obtained for the 10 at.% Li doped Co_3O_4 showing a good agreement.

4.5 Overall Discussion

Although the extent of surface coverage of intermediates in stepwise consecutive reactions, determines kinetics of the process and therefore the value of the kinetic parameters, in this chapter the discussions were based only on limitingly low coverage of intermediates under Langmuir condition. An attempt is made here to give experimental evidence to support this assumption. Constant potential coulometry (cpc) carried out at 1.45V for $NiCo_2O_4$ and Li doped Co_3O_4 (Chapter 2) suggested that all the cations in both oxides undergo oxidation to the + 4 state. Furthermore, galvanostatic charging on both oxides indicated that the charge consumed before steady state oxygen evolution is very much less than that obtained by cpc. Table 4.6 compares the charge consumed during galvanostatic charging before oxygen evolution and the integrated charge obtained by cpc at 1.45V for preanodised $NiCo_2O_4$ and 4 at.% Li doped Co_3O_4 electrodes. The ratio of the galvanostatic to potentiostatic charge consideration is 0.7% for $NiCo_2O_4$ and 13% for Li doped Co_3O_4. Since the ratio

Table 4.5: Comparison of the experimentally observed and the theoretically predicted kinetic parameters for oxygen evolution on 10 at. % Li doped Co_3O_4 at 25°C.

Kinetic parameter	Theoretical	Experimental
$\left(\frac{\partial E}{\partial \log i}\right)_T$	$\frac{2.3.03\ RT}{F}$	∿ 0.06 V
$\left(\frac{\partial E}{\partial \log C_{OH^-}}\right)_{i,T}$	$-\frac{2 \times 2.303\ RT}{F}$	- 0.117 V
$\left(\frac{\partial \log i}{\partial \log C_{OH^-}}\right)_{E,T}$	2	1.76

Table 4.6: Comparison of the charge measured by constant potential coulometry at 1.41 V and the charge consumed during galvanostatic charging (10^{-4} A cm^{-2}) on preanodised oxide electrodes.

Oxide	Electrocatalyst loading (Mg cm^{-2})	cpc at 1.41 V (coulombs)	Galvanostatic charging (coulombs)
$NiCo_2O_4$	13.8	2.4	0.017
4 at .% Li doped Co_3O_4	14.4	0.31	0.04

values are less than 0.2, and the theoretical kinetic parameters assuming $\theta \rightarrow 0$ is in good agreement with experimentally obtained parameters, a discussion based solely on limitingly low coverage of intermediates was found adequate, and therefore a discussion based on Temkin adsorption conditions ($0.2 < \theta < 0.8$)[89, 90] was found unnecessary. The low adsorption requirements is the reason for prefering

$$M + OH^- \rightarrow MOH + e \qquad 4.13$$

as the rate determining step for oxygen evolution on $NiCo_2O_4$, when governed by a Tafel slope of 0.12V per decade, rather than the subsequent step; i.e.

$$MOH + OH^- \rightarrow MO + H_2O + e \qquad 4.4$$

It is very probable that oxygen evolution on $NiCo_2O_4$ governed by a Tafel slope of $\sim$ 0.04V per decade could take place on trivalent sites by a similar mechanism to that proposed for the Li doped oxides of Co. The proposed mechanism is

$$T + OH^- \rightarrow TOH + e \qquad 4.34$$

$$TOH + OH \rightarrow TO^- + H_2O \qquad 4.37$$

$$TO^- + M \rightarrow T\overset{O}{\diagup\diagdown}M + e \qquad 4.39$$

$$2T\overset{O}{\diagup\diagdown}M \rightarrow 2T + 2M + O_2 \qquad 4.40$$

where T and M are trivalent and divalent cations respectively. If step 3 is assumed to be rate determining, the

Tafel slope at low coverage conditions, evaluated from Equation 4.2 ($\nu = 2$, $n = 2$ and $\eta^* = 2$) is 0.039V per decade at 25°C.

The oxygen evolution studies reported in this chapter suggests that the trivalent ions in $NiCo_2O_4$ and the Li doped spinel structured oxides of Co have good activity for oxygen evolution. Studies based on the 4 Li doped spinel structured oxides of Co showed the oxygen evolution performance to increase with increase in trivalent Co. A direct comparison of the activity for oxygen evolution between $NiCo_2O_4$ and the Li doped oxides of Co is not possible due to the variables such as electrocatalyst loading, specific surface area of electrocatalyst and Teflon loading, which will effect electrode performance. However, it is interesting to note that the performance of optimised electrodes show that the Li doped spinel structured oxides of Co to be better oxygen evolution electrocatalyst than $NiCo_2O_4$. Table 4.7 compares the oxygen evolution performance of 0, 4, 7 and 10 at.% Li doped spinel structured oxides of Co and $NiCo_2O_4$. The performance of a Teflon bonded $NiCo_2O_4$ electrode is 1.60V at a current density of 1A cm^{-2} at 70°C in 5N KOH compared to a performance of 1.52V for a Teflon bonded 10 at.% Li doped Co_3O_4 electrode under the same conditions.

Table 4.7: Oxygen evolution performance on optimized Teflon bonded electrodes of spinel structured oxides of Co and Ni at 1 A cm^{-2} in 5 mol dm^{-3} KOH at $70^{o}C$.

Oxide	Potential Volts vs dhe	Reference
$NiCo_2O_4$	1.60	178
Co_3O_4	1.69	91
4 at. % Li doped Co_3O_4	1.59	91
7 at. % Li doped Co_3O_4	1.535	91
10 at. % Li doped Co_3O_4	1.52	91

CHAPTER FIVE

SOME FACTORS THAT GOVERN OXYGEN EVOLUTION.

5.1 Introduction.

Although oxygen evolution has been studied on numerous metals and oxides, and many mechanisms have been put forward to explain the oxygen evolution reaction on these substrates, no satisfactory explanation has yet been given for the different overvoltage magnitudes on different substrates at a particular current density. It is of great fundamental interest to determine the factors responsible for the different overvoltage values on different anodes. Up to now, only very few investigations[93,94,78] have been directed in ascertaining these factors.

Hickling and Hill[93] carried out oxygen overvoltage measurements on ten different metal anodes, in alkaline solution over a current density range of 10^{-5} to 1 A cm^{-2}, in 1 mol dm^{-3} KOH at $20^{o}C$. They also studied the variation of the oxygen overvoltage on the different metals with time.

Ruetschi and Delhahay[94] carried out a theoretical investigation and concluded that different overvoltages on metals arise because of the difference in magnitude of the M-OH bond energies. They assumed the rate determining step to be the initial discharge of the OH^{-} ion. The M-OH bond energies were estimated in three ways and then plotted against the values of the overpotential for oxygen evolution at 1A cm^{-2} in 1N KOH at room temperture. The slope of the plot was indicating that the difference in

overvoltages and the heats of activation for oxygen evolution may be accounted for by the changes in the M-OH bond energies that occur from metal to metal. The authors did not choose to plot all the bond energy values, since some of them showed marked departures from the correlation. A point to note is that of the ten metals that were correlated, Co metal showed the lowest overpotential and the highest M-OH bond energy.

Tseung and Jasem[78], in a recent investigation of oxygen evolution on semiconducting oxides, emphasized, the role of the metal/metal oxide or the lower metal oxide/higher metal oxide couple in determining the minimum voltage required for oxygen evolution, together with other essential factors such as electrical resistivity, electrode microstructure and corrosion properties. Based on these criteria they suggested that $NiCo_2O_4$ is of interest as an oxygen evolution electrocatalyst.

The work carried out by Vijh, although not directly pertaining to oxygen evolution warrants mention in this section, He found an empirical correlation[95] between two quantities, the metal/metal oxide standard electrode potential and the electronic conductivity, that is postulated to govern oxygen evolution. He also correlated[95] the band gap of oxides to the metal/metal oxide standard electrode potential, thus linking two solid state properties to the electrode potential.

This chapter describes the work that was carried out to determine the factors that govern oxygen evolution and the choice of electrocatalyst for oxygen evolution.

5.2 Relationship of the lower oxide/higher oxide couple and oxygen evolution.

5.2.1 Oxygen evolution study on metals, based on literature data.

Table 5.1 gives the oxygen evolution potentials of ten metals at current densities of 1A cm^{-2}, in 1 mol dm^{-3} KOH at 25°C. This oxygen evolution data are those obtained by Hickling and Hill[93]. Also including in Table 5.1 are the lower metal oxide/higher metal oxide couples of the ten metals. The couples and their values were also obtained from literature[97,78].

Figure 5.1 gives the plot of the oxygen evolution potential at a current desnity of 1A cm^{-2} vs the lower oxide/higher oxide couple, showing a very good correlation. The metal cadmium was not included in the correlation since the lower oxide/higher oxide couple for cadmium was not available in literature. This investigation carried out from literature data suggests that, oxygen evolution potentials at high current densities (e.g., 1A cm^{-2}) on metals is governed by the lower metal oxide/highest metal oxide couple of the metal. Therefore oxygen evolution

Table 5.1: The oxygen evolution potentials at 1 A cm^{-2}, $25^{o}C$ in 1 mol dm^{-3} KOH and the potentials of the lower oxide/higher oxide couple of ten metals.

Metal.	Oxygen evolution potential (volts vs rhe).	Lower oxide/ higher oxide couple.	Potential of lower oxide/higher oxide couple (volts).	Literature reference for couple.
Co	1.84	Co_2O_3/CoO_2	1.477	97
Cu	2.0	Cu_2O/CuO	0.669	97
Au	2.86	Au_2O_3/AuO_2	2.63	97
Pb	2.27	††	1.76	*
Fe	1.86	FeO/Fe_2O_3	0.271**	97
Ni	2.27	Ni_2O_3/NiO_2	1.434	97
Pd	2.51	PdO_2/PdO_3	2.03	97
Pt†	1.14	PtO/PtO_{1+x}	1.7	78
Ag	2.29	AgO/Ag_2O_3	1.569	97
Cd	2.44	-	-	-

* Ascertained from the galvanostatic charging curves on PbO, Pb_3O_4 and PbO_2.

** Value of hydrated oxide used.

† Platinised Pt.

†† Possibly governed by the H_2O/H_2O_2 couple, for which $E^o_e = 1.77$ V.

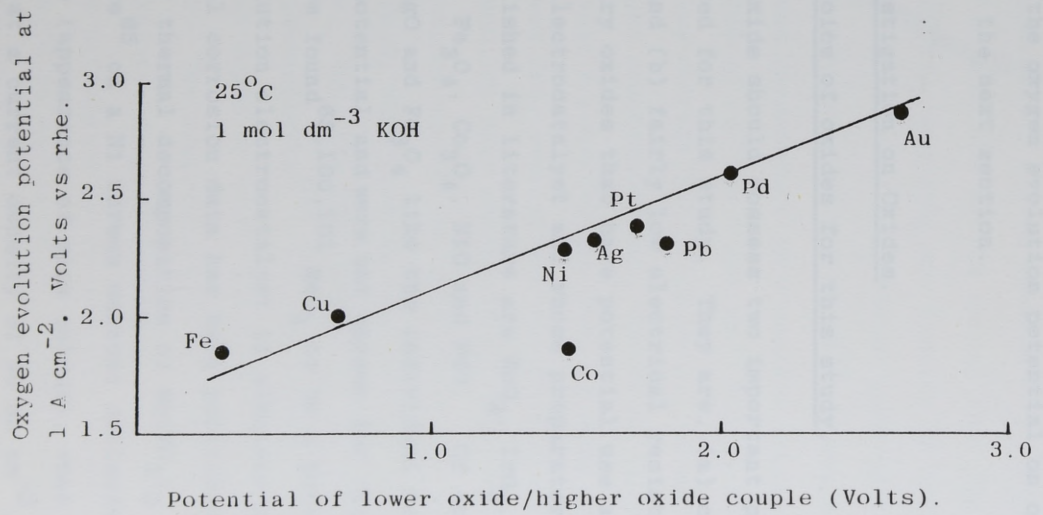

Figure 5.1: Relationship between the lower oxide/higher oxide couple of ten metals and their respective oxygen evolution potentials.

takes place only after the thermodynamically possible highest oxidation state oxide is formed. The experimental work that was carried out to show the relationship between the potential of the lower metal oxide/higher metal oxide couple and the oxygen evolution potential on oxides, is reported in the next section.

5.2.2 Investigation on Oxides.

5.2.2.1 Choice of oxides for this study.

An oxide should possess two important properties to be considered for this study. They are, (a) corrosion stability and (b) fairly low electrical resistivity. The common binary oxides that have potential use as oxygen evolution electrocatalyst and whose preparatory methods are well established in literature are RuO_2, IrO_2, PtO_2, CuO, AgO, PbO_2, MnO_2, Fe_3O_4, Co_3O_4, NiO and PdO. Of these oxides, CuO, PbO_2 AgO and Fe_3O_4 like the individual metals dissolve at anodic potential and were not chosen for this study. Many workers have found[65,100,101] MnO_2 to be a potentially good oxygen evolution electrocatalyst in alkaline medium, but no experimental corrosion data has been published. MnO_2 prepared by thermal decomposition of $Mn(NO_3)_2$ according to reference[65] on a Ni screen current collector was found to dissolve (appearence of pink colour), when polarised anodically at a current density of 50 mA cm^{-2}, in 5 mol dm^{-3} KOH at 25°C for over 125 hours. Oxygen evolution on IrO_2

and RuO_2 have been carried out extensively in acid medium[67, 102,103,104] and both oxides were reported to be very good electrocatalysts. Though IrO_2 has good corrosion stability in acid medium[102], RuO_2 was found to dissolve at potentials above approximately 1.45V vs the rhe[104]. Initial experiments carried out in alkaline medium showed that the corrosion properties of RuO_2 and IrO_2 are similar to that observed in acid medium. FEP bonded IrO_2 showed good corrosion stability upto current densities of 400 mA cm^{-2}, whereas FEP bonded RuO_2 dissolved (appearence of a scarlet colour), at a current density of 200 mA cm^{-2} in 5 mol dm^{-3} KOH at $20^{o}C$ (1 hour), however at low current densities (e.g., 50 mA cm^{-2}) and under the same conditions, RuO_2 was found to be corrosion resistant, over a polarisation time of about 100 hours. Thus, RuO_2 and IrO_2 were chosen for this study, together with the remaining four oxides (PtO_2, PdO, NiO and Co_3O_4). Of the six oxides chosen for this study the resistivities of NiO and Co_3O_4 were lowered (see table 5.2) by doping with lithium. RuO_2 and IrO_2 are known to have metallic electrical conductivity[180,179], the resistivities of PdO and PtO_2 were found to be 25 ohm-cm and 140 ohm-cm respectively. The resistivity of 140 ohm-cm obtained for PtO_2, differs from a literature value[179*] of 10^6 ohm-cm. The difference in preparatory technique in the two cases could be the cause of the difference in resistivities.

5.2.2.2 Experimental.

The preparatory methods of the six oxides were outlined in chapter 2. The electrical resistivities (see table 5.2) and the specific surface areas of the six oxides were measured.

Electrode preparation: since this investigation involves a comparative study of six oxides, it is required to have a normalised oxide loading of the electrodes. Furthermore, the electrode preparation has to be carried out under uniform conditions. The electrocatalyst loading of each of the six oxide electrodes were controlled as far as possible to contain approximately 1 M^2 of BET specific surface area of oxide per cm^2 of electrode. The oxide loading was kept at such high values, so that oxygen evolution potentials will be the lowest possible for all six electrodes, so that a comparative study is possible. Initial speculatory work based on oxide loading confirmed this. For example, a preanodised FEP bonded Li doped Co_3O_4 electrode of electrocatalyst loading 27.8 mg cm^{-2} gave an oxygen evolution performance of 1.562V vs the dhe in mol dm^{-3} KOH at 25^oC at a current density of 5 mA cm^{-2}. Changing the electrocatalyst loading from 27.8 mg cm^{-2} to 32.1 mg cm^{-2} gave approximately the same oxygen evolution potential under similar conditions. Similar observations were made for PtO_2, preanodised PtO_2 electrodes consisting of ∿44 and ∿63 mg of PtO_2 per cm^2 gave oxgyen evolution

Table 5.2: BET specific surface areas and the electrical resistivities of six oxides.

Oxide	BET specific surface area ($m^2\ g^{-1}$)	Electrical resistivity (ohm - cm) Experimental	Literature*
PtO_2	14	140	10^6 (179)
IrO_2	14	<0.1	6×10^{-7} (179)
RuO_2	17	<0.1	5×10^{-5} (180)
10 at. % Li doped† Co_3O_4	38	<5	
10 at. % Li doped NiO	47	60	
PdO	9	25	10-1000 (181)

* literature reference in parenthesis.

† heat treatment conditions; 400°C, 10 hours in air.

potentials of 1.771V and 1.774V for a current density of 5 mA cm^{-2}, under similar conditions. Furthermore, for each oxide, initial optimisation studies were carried out by preparing electrodes containing different FEP to oxide ratio and evolving oxygen, to determine the ratio that will give the best performance and good electrode stability. All the electrodes that were prepared were preanodised to obtain a stable electrocatalytic surface and to reduce the oxygen bubble size. Electrodes of different oxides required different preanodisation conditions. Table 5.3 gives the BET specific surface areas of the six oxides and the oxide loading, FEP to oxide ratio and the preanodisation conditions of the electrodes of the oxides.

Electrochemical evaluation; oxygen evolution current potential characteristics were obtained on the six oxide electrodes by the steady state technique in 5 mol dm^{-3} KOH at 25°C. Potentials were measured against the dhe. The pseudo exchange current densities for oxygen evolution on the six oxides were evaluated.

5.2.2.3 Results and Discussion.

Figure 5.2 gives the V-logi plots for oxygen evolution on preanodised FEP bonded RuO_2, IrO_2, PtO_2, PdO, Li doped NiO and Li doped Co_3O_4 electrodes, at 25°C in 5 mol dm^{-3} KOH.

Table 5.3: Characteristics of the six oxide electrodes under study.

Oxide	BET specific Surface area ($M^2\ g^{-1}$)	Oxide loading* ($mg\ cm^{-2}$)	FEP solids oxide ratio (W/W)	Preanodisation conditions 5 mol dm^{-3} KOH
PtO_2	12	80	1.3 : 3	0.5 A cm^{-2}, ∿100 hrs, 20°C
IrO_2	12	76	1.3 : 3	0.2 A cm^{-2}, " "
RuO_2	14	70	1.1 : 3	0.05 A cm^{-2}, " "
PdO	8	110	1 : 2	0.2 A cm^{-2}, " "
10 at. % Li doped Co_3O_4	27	34	0.9 : 3	1 A cm^2, ∿ 75 hrs, 70°C
10 at. % Li doped NiO	32	35	0.9 : 3	1 A cm^{-2}, ∿ 75 hrs, 70°C

* Oxide loadings are approximate values due to some electroctalyst shedding during preanodisation.

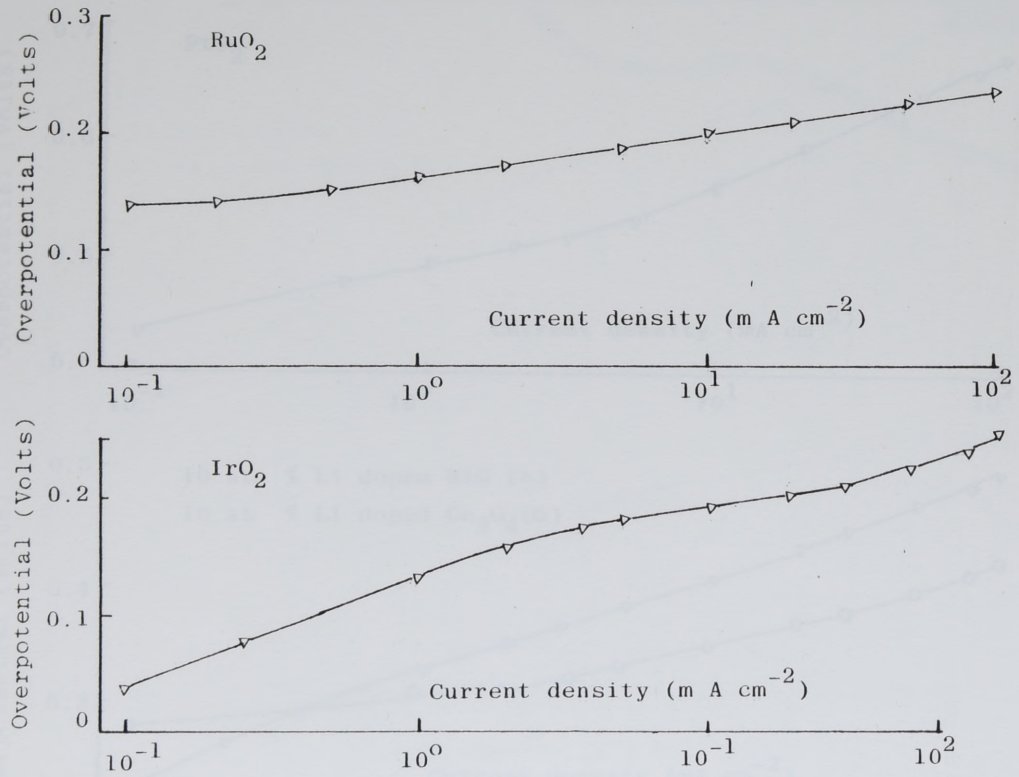

Figure 5.2: Oxygen evolution current potential characteristics on FEP bonded preanodised electrodes (of maximised electrocatalyst loading) of six oxides in 5 mol dm^{-3} KOH at $25^{o}C$.

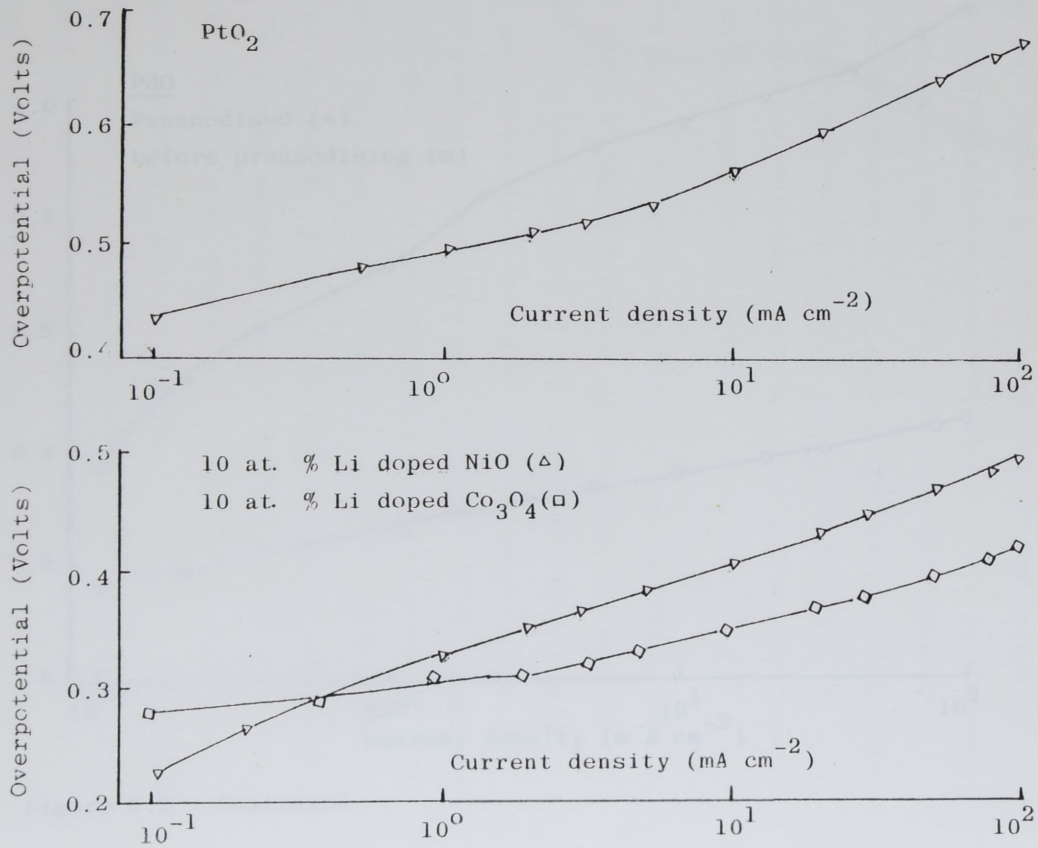

Figure 5.2 continued.

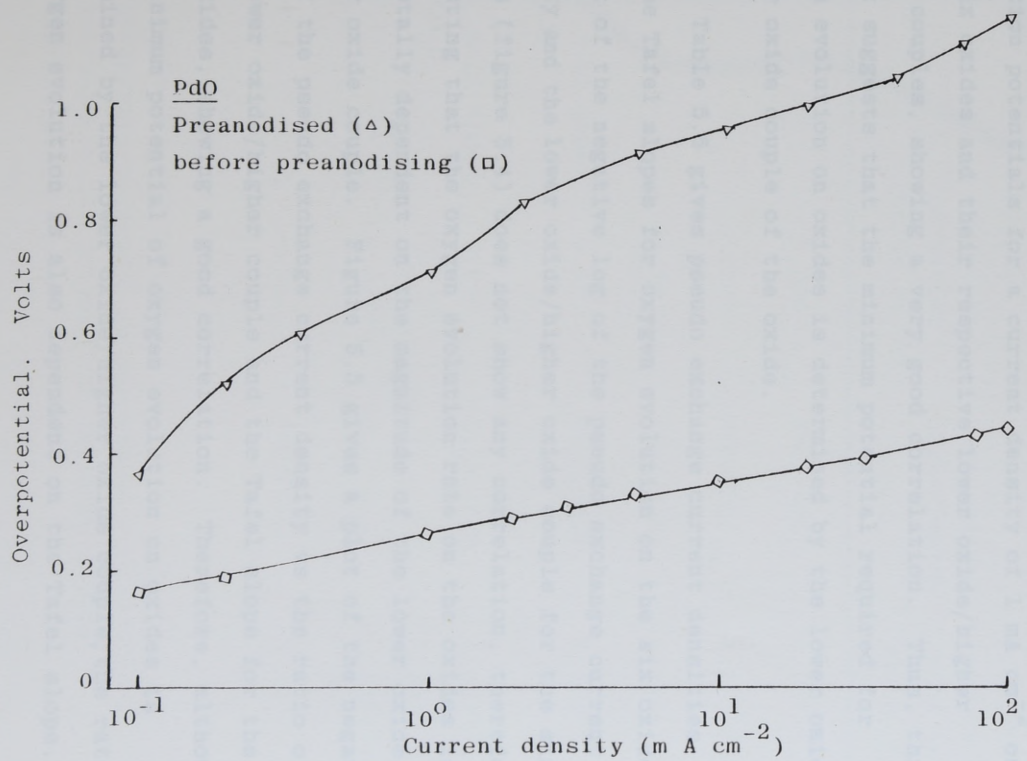

Figure 5.2 - Continued.

Table 5.4 gives the oxygen evolution potentials for a current density of 1 mA cm^{-2} together with the lower oxide/higher oxide couples of the oxides that are expected to govern oxygen evolution and the potential values of the couples. Figure 5.3 gives the plot of the oxygen evolution potentials for a current density of 1 mA cm^{-2} on the six oxides and their respective lower oxide/higher oxide couples, showing a very good correlation. Thus, this result suggests that the minimum potential required for oxygen evolution on oxides is determined by the lower oxide/ higher oxide couple of the oxide.

Table 5.5 gives pseudo exchange current densities and the Tafel slopes for oxygen evolution on the six oxides. A plot of the negative log of the pseudo exchange current density and the lower oxide/higher oxide couple for the six oxides (figure 5.4) does not show any correlation, therefore suggesting that the oxygen evolution rate on the oxides is not totally dependent on the magnitude of the lower oxide/ higher oxide couple. Figure 5.5 gives a plot of the negative log of the pseudo exchange current density vs the ratio of the lower oxide/higher couple and the Tafel slope for the six oxides, showing a good correlation. Therefore, although the minimum potential of oxygen evolution on oxides is determined by the lower oxide/higher oxide couple, the rate of oxygen evolution is also dependent on the Tafel slope.

Table 5.4: Oxygen evolution potentials for a current density of 1 mA cm^{-2} in 5 mol dm^{-3} KOH at $25^{o}C$ and the potentials of the lower oxide/higher oxide couples for six oxides.

	Oxygen evolution potential (Volts vs rhe)	Lower oxide/ higher oxide	Potental† of Lower oxide/ higher oxide Couple, E' (Volts)
RuO_2	1.394	RuO_2/RuO_4	1.387(97)
PtO_2	1.725	PtO/PtO_{1+x}	1.7(78)
IrO_2	1.36	IrO_2/IrO_3	1.35**
10 at. % Li doped NiO	1.55	Ni_2O_3/NiO_2	1.434(97)
10 at. % Li doped Co_3O_4	1.53	Co_2O_3/CoO_2	1.447(97)
PdO	2.05††	PdO_2/PdO_3	2.03(97)
*PdO	1.51	PdO/PdO_2	1.45(105,106)

* before preanodisation.

† Literature reference in parenthesis

** evaluated by the author from charging curves.

†† extrapolated value.

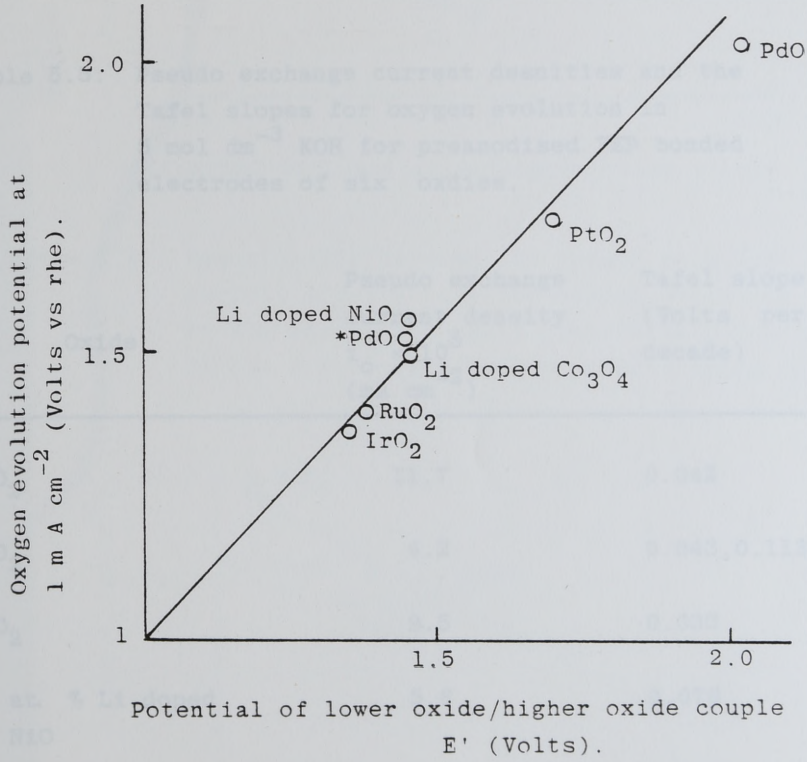

Figure 5.3: Relationship between the minimum potential of oxygen evolution and the potential of the lower oxide/higher oxide couple of oxides.

* before preanodisation.

Table 5.5: Pseudo exchange current desnities and the Tafel slopes for oxygen evolution in 5 mol dm^{-3} KOH for preanodised FEP bonded electrodes of six oxdies.

Oxide	Pseudo exchange current density $i_o \times 10^5$ ($mA\ cm^{-2}$)	Tafel slope (Volts per decade)
RuO_2	11.7	0.042
PtO_2	4.2	0.043,0.113
IrO_2	9.5	0.033
10 at. % Li doped NiO	5.6	0.076
10 at. % Li doped Co_3O_4	5.8	0.063
PdO		0.130
*PdO	6.0	0.064

* before preanodisation.

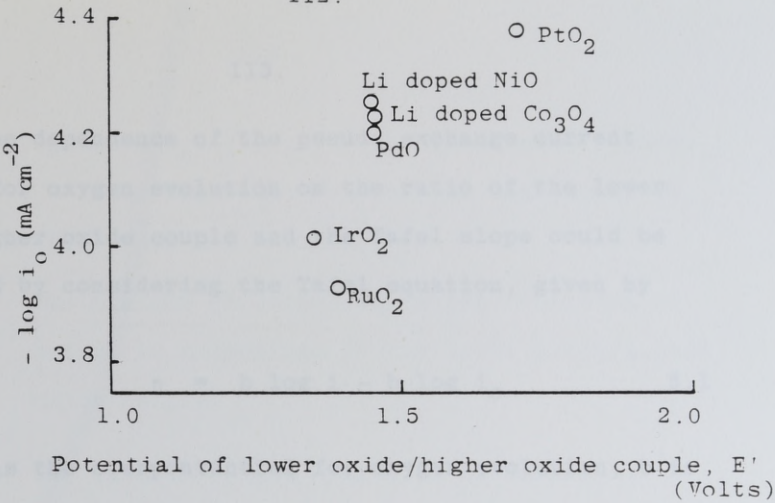

Figure 5.4: Relationship between the pseudo exchange current density (i_o) for oxygen evolution on six oxides and their respective potentials of the lower oxide/higher oxide couples (E').

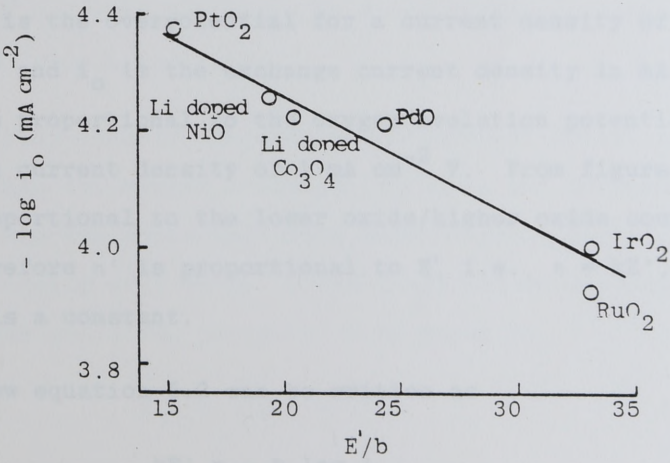

Figure 5.5: Relationship between the pseudo exchange current density (i_o) & the Tafel slope (b) for oxygen evolution on oxides and the potentials of their respective lower oxide/higher oxide couples (E').

The dependence of the pseudo exchange current density for oxygen evolution on the ratio of the lower oxide/higher oxide couple and the Tafel slope could be explained by considering the Tafel equation, given by

$$\eta = b \log i - b \log i_o \qquad 5.1$$

where η is the overpontential for oxygen evolution, b is the Tafel slope, i is the current density and i_o is the exchange current density. When considering a current density of 1 mA/cm^{-2}, the Tafel equation can be written as

$$\eta' = b \log i_o \qquad 5.2$$

where η' is the overpotential for a current density of 1 mA cm^{-2} and i_o is the exchange current density in mA cm^{-2}. Now η' is proportional to the oxygen evolution potential (V') at a current density of 1 mA cm^{-2} V. From figure 5.3, V' is proportional to the lower oxide/higher oxide couple E'. Therefore η' is proportional to E', i.e., $\eta = kE'$, where k is a constant.

Now equation 5.2 can be written as

$$kE' = - b \log i_o \qquad 5.3$$

from which

$$\frac{E'}{b} = \frac{1}{k} (- \log i_o) \qquad 5.4$$

Therefore, equation 5.4 justifies the relationship shown in Figure 5.5. Two important conclusions that could be drawn from this study are

a) The minimum potential of oxygen evolution on oxides is determined by the lower oxide/higher oxide couple.

b) The rate of oxygen evolution on oxides is dependent on the magnitude of the lower oxide/ higher oxide couple (E') and the Tafel slope (b). Therefore the factors that determine the magnitude of the Tafel slope such as the type and nature of the sites, extent of site converage, etc., are also important in determining the rate of oxygen evolution.

A relationship predicting the current potential relationship for oxygen evolution could be put forward based on the two above mentioned conclusions. For a current density of 1 mA cm^{-2}, the ohmic and mass transfer free oxygen evolution potential E is given by

$$E = b \log i + V' \qquad 5.5$$

where V' is the oxygen evolution potential for a current density of 1 mA cm^{-2}. From figure 5.3 the relationship between V' and the lower oxide/higher oxide couple is E' is, V' = 1.05 E'. Therefore equation 5.4 will become

$$E = b \log \dot{i} + 1.05\ E' \qquad 5.6$$

predicting current-potential relationship for oxygen evolution as a function of the Tafel slope and the lower oxide/higher oxide couple. For oxygen evolution to be governed by equation 5.6 the following characteristics of the oxide are essential

(1) The oxide should have a fairly low electrical resistivity. (preferably less than 100 ohm-cm).

(2) The oxide should not dissolve at anodic potentials ($E' > 1.4$, see section 5.3).

(3) Oxygen evolution on the oxide should be governed by only one Tafel region.

In this discussion, the minimum potential of oxygen evolution was taken to be the potential at a current density of 1 mA cm^{-2}, although, potentials for current densities less than 1 mA cm^{-2} can be obtained (see figure 5.2). However, at lower current densities the current potential characteristics did not obey the Tafel relationship that was obtained at higher current densities. This behaviour is attributed to the anodic reactions leading to oxidation state changes before the highest oxidation state oxide in formed.

5.3 Corrosion Stability.

Although there are numerous metal oxides (30 transition metal oxides, oxides of Pb and Sn) that have potential use as oxygen evolution electrocatalysts in alkaline medium, only few could be used in practice, the usefulness of the others are limited by their corrosion property. Pourbaix[97,108] studied the thermodynamic stability of the metals and their respective oxides at a pH range of -2 to 16 and at a potential range of -1.8 to 2.2. He put forward three domains of stability for the metals. They are

(1) Immunity, where the metal is stable and does not dissolve.

(2) Passivation, where the metal oxide is stable and does not dissolve.

(3) Corrosion, where the metal oxide is unstable and dissolves.

Therefore from the thermodynamic studies carried out by Pourbaix, one is able to predict the corrosion stability of the oxides of the metals. Table 5.6 gives the following data:

(1) The lower oxide/higher oxide couples of 23 metals and the potential values of the couples in descending order.

(2) The thermodynamic corrosion stability of the

oxides of the metals in alkaline medium from the work of Pourbaix.

(3) The experimentally observed corrosion stability of the metals and oxides at rest, and at anodic potentials in alkaline medium. This data was obtained from literature and in instances where literature data were not available, the corrosion stability was verified experimentally.

The data presented in Table 5.6 shows that most oxides having a lower oxide/higher oxide couples less than 1.40 V have very poor corrosion stability in alkaline medium according to the thermodynamic predictions of Pourbaix. The exceptions being the oxides of Ti, Nb, and Ta i.e., TiO_2, Nb_2O_5 and Ta_2O_5 respectively. The extreme passivation brought about by these oxides is related to the very high resistivites of the oxides (see Table 5.2). On anodisation, these metals or oxides form thick insulating films. These films have high dielectric strength and high heats of formation which favour film growth rather than oxygen evolution, and can sustain voltages greater than 200 V[109]. For example when an anodic current density of 5 mA cm^{-2} is passed on FEP bonded TiO_2 electrodes, the potential increases rapidly from 0.8 V to greater than 70 V in ten minutes. Therefore these three oxides have no practical use as oxygen evolution electrocatalysts in alkaline medium. However, these three oxides are used as inactive

Table 5.6: Survey of the corrosion properties of oxides (or metals, or metal oxide films) in alkaline medium.

Higher oxide/lower oxide couple and potential** (volts)		Corrosion property	Reference for corrosion property.
Au_2O_3/AuO_2	2.63	C*,N	97,E
PdO_2/PdO_3	2.03	N*,N	97,E
PtO_2/PtO_3	2.0	N*,N	97,E
PtO/PtO_{1+x}	1.7	N*,N	97,E
Rh_2O_3/RhO_2	1.73	N*	97
AgO/Ag_2O_3	1.569	C	93,E
Co_2O_3/CoO_2	1.477	N*,N	97,E
Ni_2O_3/Ni_2O_3	1.434	N*,N	97,E
RuO_2/RuO_4	1.387	C*,C	97,E
†IrO_2/IrO_3	1.35	C*,N	97,E
Cr_2O_3/CrO_3	1.284	C*	97
Pb_2O_3/PbO_2	1.093	C*,C	97,93,E
Mn_2O_3/MnO_2	1.014	C	E

Continued .....

Table 5.6 continued ...

OsO_2/OsO_4	1.005	C*	97
TcO_2/TcO_3	0.757	C*	97
Cu_2O/CuO	0.669	C*	97,93,E
V_2O_4/V_2O_5	0.666	S	203
ReO_2/ReO_3	0.399	S	203
W_2O_5/WO_3	-0.029	S	203
FeO/Fe_2O_3	-0.057	C*,C	97,E
NbO_2/Nb_2O_5	-0.289	P*	97
Ti_2O_3/TiO_2	-0.556	P*,P	97,E
Ta/Ta_2O_5	-0.750	P*	97
MoO_2/MoO_3	-1.091	S	203

KEY: N oxide does not dissolve at anodic potentials.
C oxide dissolves at anodic potentials.
S oxide soluable at rest potentials.
P forms passive film.
E experimental.
N*,C* and P* are Pourbaix's thermodynamic predictions.

** potentials of the lower oxide/higher oxide couples are from the work of Pourbaix (Ref.97) except for the IrO_2/IrO_4 couple which was obtained from the charging curve on IrO_2.

supports with highly conducting (electrically) and active but expensive electrocatalysts such as IrO_2 and RuO_2[110,111,112] in the evolution of chlorine from brine solutions and in the evolution of oxygen from acidic solutions. When these oxides (TiO_2, Ta_2O_5 and Nb_2O_5) are incorporated into such composite electrodes their electrical resistivities do not affect the electrode performance.

The metals whose lower oxide/higher oxide couples are greater than 1.4 V are Ni, Co, Ag, Rh, Pt, Pd and Au. With the exception of Ag, these metals or their oxides have good corrosion stability at anodic potentials in alkaline medium.

The only oxide that could find use as an oxygen evolution electrocatalyst, and whose lower oxide/higher oxide couple is less than 1.40 V is IrO_2. However, IrO_2 is very expensive and furthermore only very limited studies under mild conditions (200 mA cm^{-2}, 25°C, 100 hours) have been carried out to ascertain its corrosion properties.

From the investigations reported in section 5.2 and 5.3 it could be concluded that only the oxides of Ni and Co have suitable properties to find extensive use as oxygen evolution electrocatalysts in alkaline medium. Metal oxides of Pt, Pd, Rh, Au and Ir are not only expensive,

but with the exception of IrO_2 have high overvoltages. Unfortunately cheaper oxides that have low, lower oxide/ higher oxide couple potentials such as the oxide of Mn and Fe cannot be used due to their poor corrosion stability.

5.4 Electrode Characteristics

5.4.1 Introduction.

In the preceeding sections of this Chapter, the electrocatalyst properties relating to oxygen evolution were discussed. The electrocatalysts with suitable properties have to be produced in a high surface area powder form. Some useful techniques for the preparation of high surface area oxide powders are freeze drying[113,114,115], coprecipitation[116,117,118] and thermal decomposition of suitable salt solutions of the metal.

It has been a practice at the electrochemistry laboratory at The City University to fabricate Teflon bonded (hydrophobic) electrodes using high surface area electrocatalyst powders, for the purpose of gas evolution[78,92,119]. Oxide electrodes for gas evolution purposes can also be prepared by forming the electrocatalyst directly on the current collector by thermal decomposition of the appropriate salt solutions. Srinivasen et al[80], and Vandenborre et al[79] prepared $NiCo_2O_4$ electrodes for oxygen evolution

studies by thermal decomposition of Ni and Co nitrate solutions on Ni mesh current collector and subsequent sintering at 400°C for 10 hours. Co_3O_4 electrodes have been prepared for oxygen and chlorine evolution by thermal decomposition of $Co(No_3)_2$ solution on Ni and Ti current collectors respectively, and subsequent heat treatment. Porous Teflon bonded electrodes have been shown to have numerous advantages over the electrodes prepared by the thermal decomposition method (Porous, non Teflon bonded) when used for gas evolution purposes. Vassie and Tseung[119], studied gas pressures generated inside the pores of gas evolving porous electrodes and concluded that in a 100Å diameter catalyst pore the pressure is of the order of 100 atmospheres. Therefore it has been suggested[119], that the incorporation of sintered Teflon into electrodes has an advantage of binding the catalyst particles together so that mechanical strength of the electrode is improved. This aids in withstanding high pressures caused during gas evolution at high current densities. Tseung, Jasem and Mahmood [92], carried out oxygen evolution on porous non hydrophobic and porous hydrophobic $NiCo_2O_4$ electrodes of different electrocatalyst loading. The porous non Teflon bonded electrodes were prepared by the thermal decomposition of Ni and Co nitrates on Ni screen current collector and Teflon bonded electrodes were made from freeze dried $NiCo_2O_4$ powder. They found the oxygen evolution performance of Teflon bonded electrodes to increase linearly with $NiCo_2O_4$

loading up to 20 mg cm^{-2} and the performance of non Teflon bonded electrodes to increase up to a loading of 6 mg cm^{-2} and to decrease with further loading. The performance of the the Teflon bonded electrodes were found to be very much higher than the non Teflon bonded ones. For example the maximum performance of a Teflon bonded electrode (loading ∿ 20 mg cm^{-2}) at 172 mV vs the dhe at 25°C in 5 mol dm^{-3} KOH was ∿ 2500 mA cm^{-2} compared to a maximum performance of 400 mA cm^{-2} for a non Teflon bonded electrode (loading ∿ 6 mg cm^{-2}) under the same conditions. Therefore, they found a greater utilisation of electrocatalyst surface in Teflon bonded electrodes compared to the non Teflon bonded ones. The above mentioned behaviour was explained as follows; Teflon bonded electrodes are composed of a hydrophobic, porous, Teflon phase intertwined with a porous, hydrophillic catalyst phase. When gas is evolved due to electrochemical reaction, the gas can escape through the dry Teflon channels and therefore the interior of the electrode is not completely denuded of electrolyte. On the other hand, non Teflon bonded porous electrodes do not have dry channels and only the top surface of the electrode is electrochemically active, since the interior is depleted of electrolyte.

Since the work carried out be Tseung, Jasem and Mahmood have shown that Teflon bonded electrodes are more efficient than non Teflon bonded electrodes for gas evolution, it is necessary to know the effectiveness factor

of Teflon bonded electrodes for gas evolution. The effectiveness factor S,[120], of an electrode at constant temperature T, at constant potential E and at constant activity of electroactive species C_i is given by

$$S = \left(\frac{i_{ss}}{i_t}\right)_{T,\ C_i,\ E}$$

where i_{ss} and i_t are the steady state and transient current densities. For an ideally efficient electrode i_{ss} should be equal to i_t. In gas evolution electrodes, in practice i_{ss} is lower than i_t due to two reasons. They are:

(1) i_{ss} being at least partially controlled by mass transfer effects.

(2) Loss of electrochemically active surface area due to gas bubble formation. The gas bubbles formed within the pores and on the surface of the electrode will mask some of the active sites from the electrolyte. These sites will be inactive until the gas gubbles are evolved from the electrode.

A knowledge of the effectiveness factor will help in electrode optimisation studies, to enable the maximum electrode performance to be achieved. This section describes the investigation carried out to determine the effectiveness factor of hydrophobic $NiCo_2O_4$ electrodes

and $NiCo_2O_4$ electrodes prepared by thermal decomposition of Ni and Co nitrate solution on Ni screen current collector, for oxygen evolution.

5.4.2 Experimental.

Electrode preparation; non hydrophobic $NiCo_2O_4$ electrodes of loading 6.4 mg cm^{-2} and 13.6 mg cm^{-2} were prepared from a Ni and Co nitrate solution (1 molar $Ni(No_3)_2 \cdot 6H_2O$ and 2 molar $Co(No_3)_2 \cdot 6H_2O$) by repeated dipping and decomposing at 300°C, on 100 mesh Ni screen current collector and finally heating in air at 400°C for 5 hours to form the spinel phase. To fabricate the hydrophobic electrodes, $NiCo_2O_4$ powder was prepared by decomposing a solution of Ni and Co nitrates (1 molar $Ni(No_3)_2 \cdot 6H_2O$ and 2 molar $Co(NO_3)_2 6H_2O$) and heating in air at 400°C for 5 hours. The formation of the spinel phase was confirmed by X-ray analysis. The BET specific surface area of the powder was found to be 29 m^2 g^{-1}. Hydrophobic electrodes were fabricated using FEP particulate polymer. The $NiCo_2O_4$ to FEP ratio was 2.5:1 by weight. FEP bonded electrodes having $NiCo_2O_4$ loadings of 6.5 mg cm^{-2} and 13.8 mg cm^{-2} were used for this study. Both the FEP bonded electrodes were preanodised. The preanodisation conditions are, 500 mA cm^{-2} for $\sim$ 10 hours in 5 mol dm^{-3} KOH at 70°C.

5.4.3 Results and Discussion.

Figure 5.6 gives the transient and steady state E - i plots for oxygen evolution obtained on FEP bonded and non FEP bonded $NiCo_2O_4$ electrodes of loading of approximately 13.5 mg cm^{-2} in 5 mol dm^{-3} KOH at 25^oC.

Figure 5.7 gives the transient and steady state E - i plots for oxygen evolution obtained on FEP bonded and non FEP bonded electrodes of loading of approximately 6.5 mg cm^{-2} in 5 mol dm^{-3} KOH at 25^oC.

The effectiveness factor[120], was calculated for the 4 electrodes that were investigated. Figure 5.8 shows the plot of the effectiveness factor vs the steady state current density for the four electrodes. At practical current densities (200 - 700 mA cm^{-2}) the effectiveness factor of the two FEP bonded electrodes were higher than the non FEP bonded ones. Of the two FEP bonded electrodes the one with the lower $NiCo_2O_4$ loading had a higher effectiveness factor up to a current density of 700 mA cm^{-2}. However, the steady state current density of the FEP bonded electrode of higher loading is very much greater than that of the lower loading at any particular potential that was studied (see figures 5.7 and 5.8). The effectiveness factor of the non FEP bonded electrode of lower loading was relatively high and that of the higher loading was very low (< 10%). These results confirm that the hydrophobic electrodes have higher

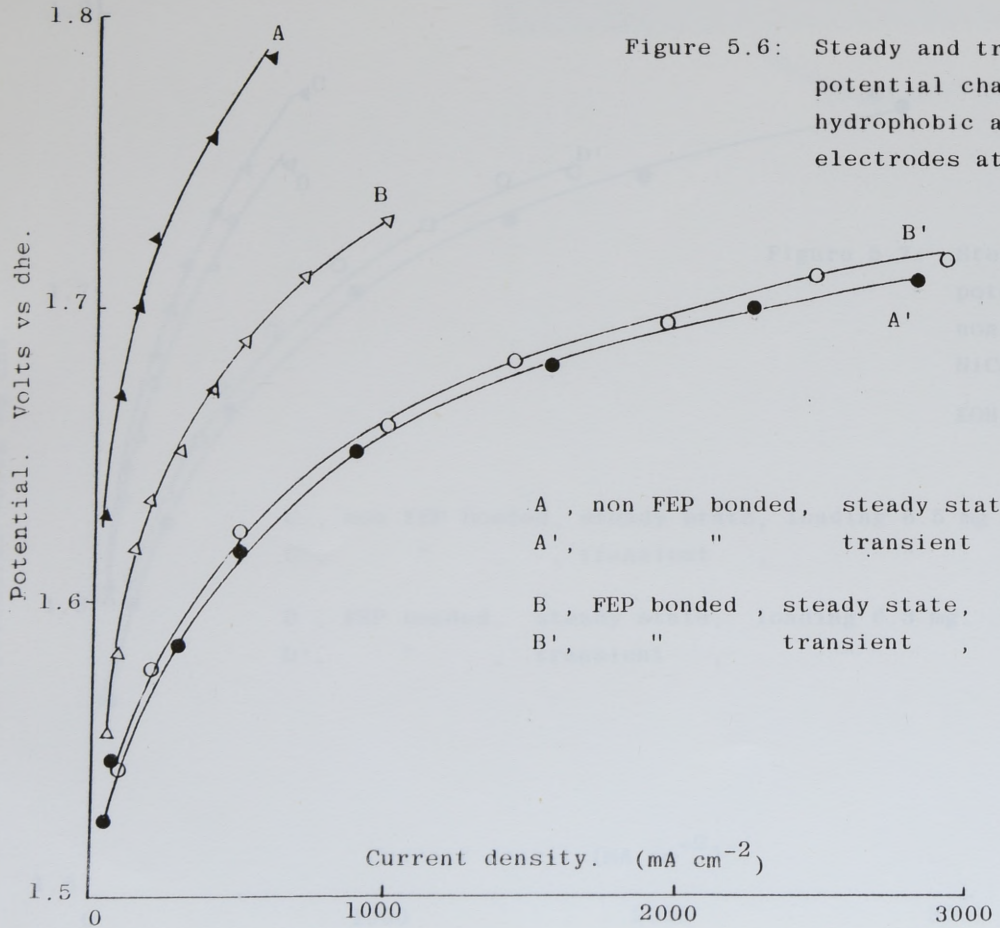

Figure 5.6: Steady and transient oxygen evalution current potential characteristics on porous non hydrophobic and porous hydrophobic $NiCo_2O_4$ electrodes at 25°C in 5 mol dm^{-3} KOH.

A , non FEP bonded, steady state, loading 13.6 mg.
A', " transient , "

B , FEP bonded , steady state, loading 13.8 mg.
B', " transient , "

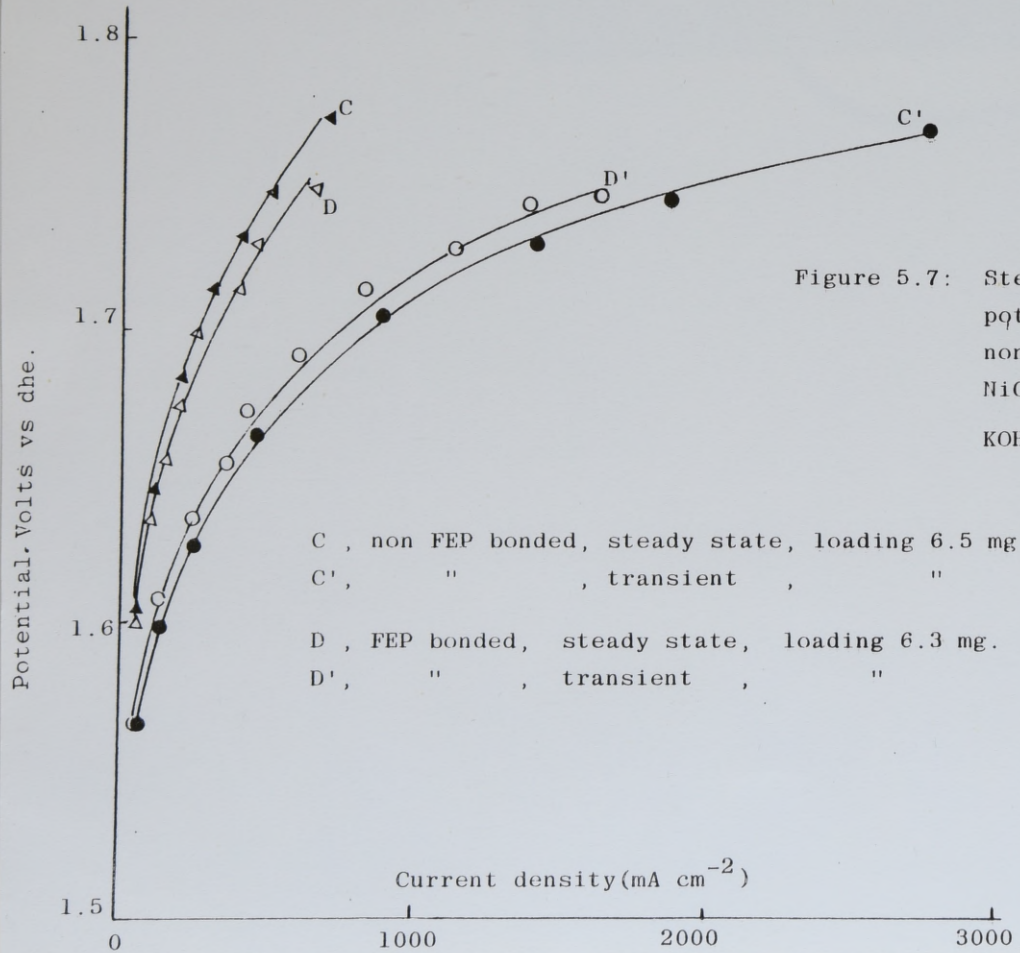

Figure 5.7: Steady state and transient current potential characteristics on porous non hydrophobic and porous hydrophobic $NiCo_2O_4$ electrodes at 25°C in 5 mol dm^{-3} KOH.

Figure 5.8: Oxygen evolution efficiencies on porous non hydrophobic and porous hydrophobic $NiCo_2O_4$ electrodes at 25°C in 5 mol dm^{-3} KOH.

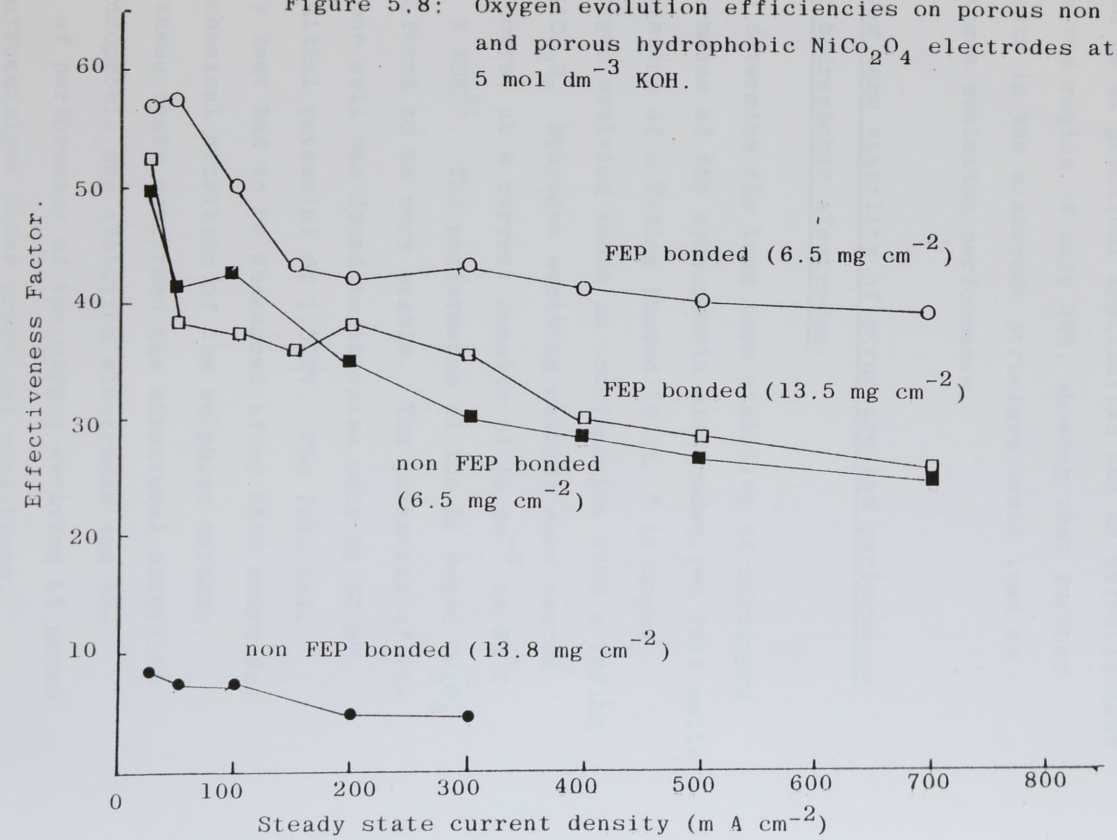

efficiency for oxygen evolution than the non hydrophobic electrodes. Furthermore, the effectiveness factor of the FEP bonded electrode that gave the steady state currents that could be of practical application had an effectiveness factor in the region of only 30%, showing that further improvements in the electrode structure could lead to higher oxygen evolution performance.

5.4.4 Long term stability of structure and performance of hydrophobic electrodes.

To determine the long term stability of structure and performance of the hydrophobic electrodes, two full cells each consisting of a Teflon bonded 10 at. % Li doped Co_3O_4, oxygen evolving anode in conjunction with a Teflon bonded $NiCo_2S_4$ hydrogen evolving cathode were tested for 5800 hours, at a current density of 1A cm^{-2} at 85^oC in 45 wt. % KOH[91]. The performance of the Li doped Co_3O_4 anode was found to be very stable. The potential of the anode of one cell was found to increase only by 60 mV from an initial potential of 1.522V. The full cell durability test had to be abandoned after 5800 hours due to the mechanical attrition of the sulphide cathode. However, these tests confirmed the structural stability of the hydrophobic gas evolution electrodes and the stability of performance of the oxygen evolving Li doped Co_3O_4 electrocatalyst under practical conditions.

CHAPTER SIX

OXYGEN REDUCTION STUDIES ON $NiCo_2O_4$ BY POTENTIOSTATIC PULSE TECHNIQUE.

6.1 Introduction

Oxygen, either in a pure form supplied directly from containers or from air, is important to electrochemical energy conversion as it is to chemical combustion and life. Thus, practically all earth based fuel cells use oxygen as the cathodic reactant. The advantages of air as compared to Cl_2 and F_2 stored in tanks are (a) saving in material cost and (b) an increase in the energy weight ratio. Therefore the oxygen reduction reaction is an important reaction in electrochemical energy conversion. However, oxygen reduction is generally not reversible and hence requires large overpotentials to obtain practical currents.

The oxygen reduction electrochemistry is controlled by three reactions. The reversible thermodynamic potentials of the three reactions in acid and alkali media are given in table 6.1. The reversible potential for the four electron reaction:

$$O_2 + 2H_2O + 4e \qquad 4OH^- \tag{6.1}$$

has been obtained by a few workers[46,48,121,122], but most oxygen electrode potentials are well below the reversible value of 1.23V. On most electrocatalysts oxygen reduction does not go through a direct four electron process, but takes place via the HO_2^- intermediate as follows:

$$H_2O + O_2 + 2e \rightarrow OH^- + HO_2^- \tag{6.2}$$

Table 6.1: Three important reactions of the oxygen electrochemistry and their potentials.

Reaction	Potential (Volts vs she) Alkaline medium	Acid medium
$O_2 + 4H^+ + 4e \rightleftarrows 2H_2O$		1.229
$O_2 + 2H_2O + 4e \rightleftarrows 4OH^-$	0.401	
$O_2 + 2H^+ + 2e \rightleftarrows H_2O_2$		0.682
$O_2 + H_2O + 2e \rightleftarrows HO_2^- + OH^-$	-0.076	
$H_2O_2 + 2H^+ + 2e \rightleftarrows 2H_2O$		1.77
$HO_2^- + H_2O + 2e \rightleftarrows 3OH^-$	0.880	

thus, causing a reduction of the open circuit potential. However, on a good number of catalysts, other than certain types of carbon, the HO_2^- can be further reduced either electrochemically by:

$$HO_2^- + H_2O + 2e \rightarrow 3OH^- \qquad (6.3)$$

or by chemical decomposition by:

$$2HO_2^- \rightarrow O_2 + 2OH^- \qquad (6.4)$$

6.2 Attainment of Reversible Behaviour

Hoar[46] in 1933 was the first to demonstrate the existence of the reversible potential (1.229V vs she at 25°C). He extrapolated the anodic and cathodic Tafel lines in the lower current region on platinum in acid medium, and found the two lines to intersect at a potential of 1.23V.

In 1956, Bockris and Huj[121] were the first to obtain this potential on open circuit on platinum by rigorous purification involving anodic and cathodic pre-electrolysis extending over a period of weeks. The reversible value was steady for over one hour. In 1966, Damjanovic, Dey and Bockris[48] obtained a perfect Tafel line for currents as low as 10^{-10} A on preanodised Pt after prolonged anodic pre-electrolysis of the perchloric acid electrolyte for 60-80 hours. The perfect Tafel line was found to become asymptotic to the log i axis close to a potential of 1.23V.

At zero current densities a potential of 1.23V was established and was found to be steady for a few hours.

Workers were only successful in obtaining the thermodynamic reversible potential of the oxygen electrode at rest. However, platinum cannot be said to behave reversibly because, when, after polarisation anodically or cathodically, it does not revert back to the reversible potential of oxygen.

Various concepts have been put forward for the poor attainment of the equilibrium potential. They are (a) oxide theory; according to this the rest potential is governed by the potential of the oxide on the surface of the metal electrode at rest. (b) a mixed potential concept; according to which the rest potential is governed by two or more potentials. For example, Hoar[123] observed a steady-state rest potential of 1.06V on platinum instead of 1.23V and concluded that the observed lower potential is a mixed potential involving reactions 6.2, 6.3 and a Pt/Pt-O reaction such as:

$$Pt\text{-}O + 2H^+ + 2e = Pt + H_2O, \quad E^o = 0.88V \qquad (6.5)$$

The contribution of reaction (6.2) to the rest potential as pointed out by Hoar is the main cause for anomolous rest potentials in oxygen electrochemistry and brings about irreversibility and inefficiency in the

cathodic reduction of oxygen.

The Nernst equation for reaction (6.2) at 25°C is given by[12,189]:

$$E = 0.68 + 0.03 \log \frac{[O_2][H_2O]}{[HO_2^-][OH^-]} \qquad (6.6)$$

where E is the potential of the electrode measured against the rhe in the same solution.

For unit activity of O_2, H_2O and OH^-, the potential E increase as $[HO_2^-]$ becomes less than 1, and tends to a value of 1.23V. For example, if the HO_2^- is 10^{-2} M then the potential loss is 0.49V, i.e. 1.23 - (0.68 + 0.06). A low value of $[HO_2^-]$ would result if the electrocatalyst were markedly active for peroxide decomposition. If $[HO_2^-]$ could be maintained at concentrations as low as 10^{-16} M, E would then equal the potential of 1.23V. Therefore, an oxygen electrode catalyst is also qualitatively identified as a good peroxide decomposition catalyst and in particular as one which depresses the peroxide concentration to very low concentrations.

The reversible behaviour of oxygen has been attained on certain semiconducting oxide electrodes, where the oxygen bond is ruptured and the HO_2^- ion is not formed. These oxides possess electrical and magnetic properties that enables the oxygen molecule to be chemisorbed side-on.

The oxygen molecule is paramagnetic as it has two unpaired electrons with parallel spins in antibonding $\pi(\pi^*)$ orbitals. Therefore if the electrons are arranged in the transition metal oxide with spin unpaired, then the oxygen molecule could be adsorbed side-on on the transition metal oxide surface. This suggests the use of paramagnetic or ferromagnetic oxides for oxygen reduction. On the other hand, anti-ferromagnetic compounds in which cations are arranged with unpaired spins aligned on allernate (111) planes, will not be able to satisfy the above requirement.

NiO in its normal macroscopic state is anti-ferromagnetic. It becomes paramagnetic at the Neel point, T_N, at 523 K[124]. The magnetic transition is associated with a crystallographic transition from rhombohedral to cubic structure. Winter[125] suggested that the change in mechanism of oxygen chemisorption was attributable to the magnetic transition at the Neel point. He assumed that chemisorption took place predominently at exposed edges of magnetic domains. Below T_N magnetostriction prevents the formation of two Ni^{3+} as adjacent nearest neighbours and hence chemisorption occurs as O_2^-. Above T_N, the restriction is removed and oxygen can be adsorbed as $2O^-$. Tseung, Hobbs and Tantram[15] studied the electrochemical reduction of oxygen on lithiated NiO at 150°C and 220°C, and found that there was a six-fold improvement

in performance at 220°C. The open circuit potential changed from 1.10V to 1.16V, very close to the theoretical open circuit potential of 1.17V at the experimental conditions. Doping with Li is known to lower the T_N by about 20°C. They therefore suggested that oxygen is being dissociatively chemisorbed above the Neel point, thus by-passing the formation of peroxide intermediate, leading to reversible behaviour and improved performance.

Tseung and Bevan[14] carried out oxygen reduction studies on Sr doped $LaCoO_3$. This compound is paramagnetic at room temperature. They confirmed that complete reversibility can be obtained at room temperature and that the electrochemical performance increased linearly with temperature, surpassing that of Pt black at 170°C. However, its performance below 100°C was too low to be of practical interest (only 5 mA cm^{-2} at 900 mV vs DHE at 80°C in 5N KOH). Tseung and Yeung[126] correlated the low oxygen reduction performance of Sr doped $LaCoO_3$ to a low oxygen coverage of 1% and the coverage was found to be independent of temperature in the range 25°C - 80°C. By studying the series $La_{1-x}Sr_xCoO_3$ they attributed the reversible behaviour to the Co^{3+}/Co^{4+} couple which satisfy important conditions for the splitting of the 0 = 0 bond.

6.3 Mode of Oxygen Chemisorption and Oxygen Reduction.

The oxygen reduction path on a catalyst depends on

the mode of interaction of oxygen with the catalyst surface. Figure (6.1) gives three modes of interaction[127] of oxygen with the catalyst surface and the respective reaction paths. Of the three modes of oxygen reduction, paths A and C involves breaking of the O-O bond whereas in the path B the O-O bond is intact forming the superoxide which may form free peroxide in solution or will undergo bond rupture to form OH^- ions.

The electron distribution in d orbitals and the availability of suitable d orbitals of the transition metal ions for interaction with the orbitals of the oxygen molecule is one of the main factors that governs the type of interaction. Path A requires[128] a lateral interaction of the orbitals of oxygen with the empty d_{z^2} orbital of the transition metal ion with back bonding from at least partially filled d_{xy} or d_{yz} orbitals of the transition metal ion to the π^* orbital of oxygen. For path C to take place an interaction of the partially filled d orbitals of transition metal with the π^* orbital of the oxygen molecule is necessary. A further requirement for the occurrance of path B is a proper spacing of the transition metal ions in the electrocatalyst. Materials that are paramagnetic or ferromagnetic bring about oxygen reduction by this path. Path B[129] is essentially on diamagnetic materials and will require interactions of filled or partially filled d orbitals of the transition metal ions with the π^* or σ^* (2p) orbitals of the oxygen molecule.

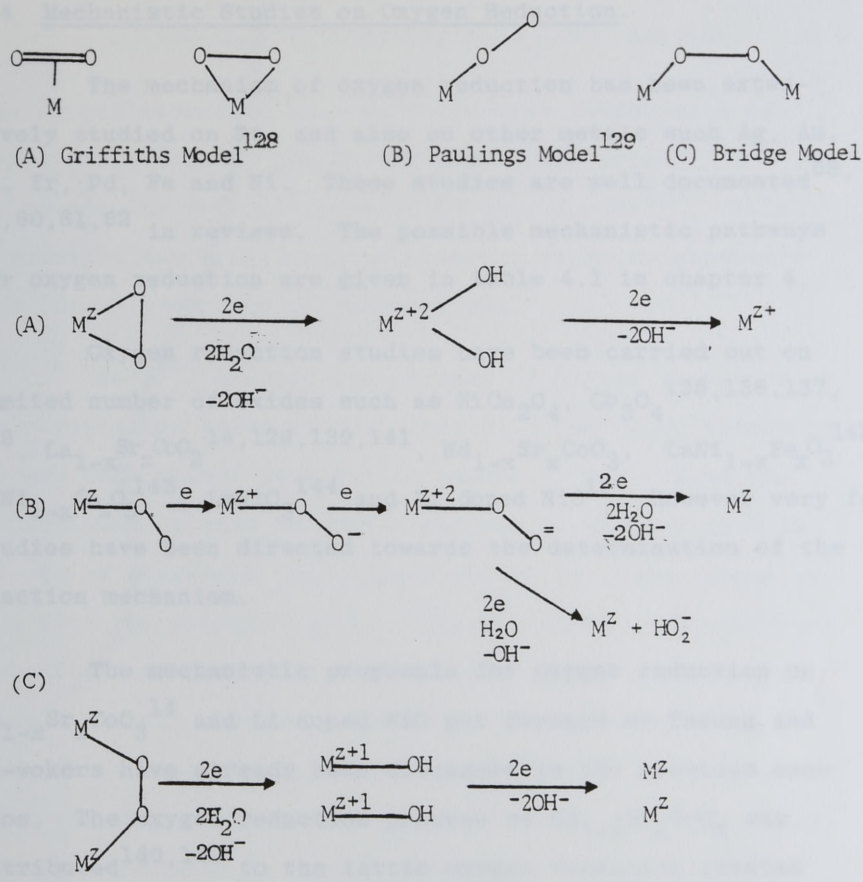

Figure 6.1: Three modes of interaction of O_2 with the catalyst surface and the respective reaction paths [127] for oxygen reduction in alkaline medium.

6.4 Mechanistic Studies on Oxygen Reduction.

The mechanism of oxygen reduction has been extensively studied on Pt. and also on other metals such Ag, Au, Rh, Ir, Pd, Fe and Ni. These studies are well documented[58,59,60,61,62] in reviews. The possible mechanistic pathways for oxygen reduction are given in table 4.1 in chapter 4.

Oxygen reduction studies have been carried out on limited number of oxides such as $NiCo_2O_4$, Co_3O_4[135,136,137,138], $La_{1-x}Sr_xCoO_3$[14,126,139,141], $Nd_{1-x}Sr_xCoO_3$, $LaNi_{1-x}Fe_xO_3$[143], $LaNi_{1-x}Co_xO_3$[143], $LaNiO_3$[144] and Li doped NiO[15]. However very few studies have been directed towards the determination of the reaction mechanism.

The mechanistic proposals for oxygen reduction on $La_{1-x}Sr_xCoO_3$[14] and Li doped NiO put forward by Tseung and co-wokers have already been discussed in the previous section. The oxygen reduction process on $Nd_{1-x}Sr_xCoO_3$ was attributed[140,142] to the lattic oxygen vacancies created by cathodic polarisation. It was proposed that the lattice oxygen is formed at the electrode/electrolyte interface by;

$$O^{2-}(\text{lattice})+2Co^{4+}+H_2O+2e \rightleftarrows V_o(\text{lattice})+2Co^{3+}+2OH^- \qquad 6.7$$

The lattice vacancies formed at the surface in contact with the electrolyte diffuses to the gas phase side to combine with the oxygen. Thus,

$$1/2\ O_2 + V_o(\text{llatice}) + 2e \rightleftarrows O2^- \text{ lattice} \qquad 6.8$$

The oxygen reduction path on perovskite oxides such as $LaNi_{1-x}Fe_xO_3$, $LaNi_{1-x}Co_xO_3$ and $LaNiO_3$ was found[143, 144] to be similar to that proposed by Hoar for Pt[145]. This suggestion was based on the observed kinetic parameters for oxygen reduction on these oxides.

Savy[136] studied the process of oxygen reduction on polycrystaline films of Co_3O_4 and Li doped Co_3O_4 formed on Co and CoLi alloy, in alkaline medium. They found the performance to pass through a maximum Li content of 0.15 at. % and suggested that oxygen reduction takes place by a 2 electron process and the limiting factor is a surface-potential barrier which inhibits the oxygen chemisorption step. However, oxygen reduction studies carried out by ring (Pt)- disc (Co_3O_4) measurements[135,137,138] suggest that the reaction proceeds directly to OH^- and very little desorbed peroxide is formed. One group of workers[137,138] also claimed that oxygen is dissociatively chemisorbed on Co_3O_4 and that peroxide is not formed as an intermediate when oxygen is reduced to water. This claim was supported by isotopic exchange studies.

Oxygen reduction studies carried out on $NiCo_2O_4$ will be described in the next section.

6.5 Oxygen Reduction on $NiCo_2O_4$.

The oxygen reduction performance on $NiCo_2O_4$ prepared by freeze drying, was evaluated by King and Tseung[130] and was found to be very high. An optimised teflon bonded $NiCo_2O_4$ was found to give an oxygen reduction current of $\sim$ 0.2A cm^{-2} at 0.75V vs the dhe, in 5 mol dm^{-3} KOH in oxygen at room temperature. However at lower potentials (e.g. 0.65V) the performance decreased rapidly reaching a value of 2 mA cm^{-2} in 2-3 hours. Tseung and Yeung[131] carried out cyclic voltammetry studies on $NiCo_2O_4$ and found the spinel to be stable only at potentials above 0.75V vs the dhe, and attributed the deterioration in performance below 0.75V to the beakdown of the spinel structure to a mixture of Co_2O_3, CoO, CoO $.H_2O$ and NiOOH. Singh et al[80] carried out oxygen reduction studies on Teflon bonded, $NiCo_2O_4$ and obtained a Tafel slope of 0.06V per decade at 80°C in alkaline medium. A group of wokers from Russia studied the oxygen reduction mechanism on $NiCo_2O_4$[133,134]. They prepared $NiCo_2O_4$ by coprecipitation and correlated the physical characteristic of the oxide to its electrochemical characteristics[133]. They also carried out ring disc experiments and the $NiCo_2O_4$ electrode consisted of a thermally formed film on a $NiCo_2$ alloy disc. They suggested that there is practically no effect of the semiconducting properties on the reaction kinetics and the electrode behaves like a metal. Further, they suggested

that the octahedrally coordinated Co^{3+} sites are active for oxygen reduction by a donor - acceptor mechanism. There is also evidence from Russian literature that the reduction of oxygen on $NiCo_2O_4$ is a parallel process and the main (97 - 99% [135], 97 - 98% [134]) pathway of oxygen reduction leads to the formation of OH^-, and an insignificant part of the process forms peroxide which could be detected in solution. It should be pointed out here that the peroxide detected in solution could also arise at least in part, due to desorption of the peroxide intermediate formed by the main route leading to the formation of OH^-.

To understand the mechanism further, it is essential to study the variation of the oxygen reduction performance with the partial pressure of oxygen, P_{O_2} and KOH concentration. Kinetic parameters derived from these studies will help to ascertain important characteristics which will help to postulate a mechanism. Thus, the variation of current density or potential with P_{O_2} will help to postulate whether oxygen adsorption is end-on or side-on leading to dissociation. The variation of performance with KOH concentration will help to predict the number of water molecules taking part before the rate determing step. These parameters and the Tafel slope together with site features of $NiCo_2O_4$ will help to understand the process of oxygen reduction on it.

6.5.1 Experimental.

Oxygen reduction current - potential characteristics on Teflon bonded $NiCo_2O_4$ were obtained with the electrode in the floating mode, in air and in 100% oxygen, in 5N KOH at 25°C. The experimental setup is described in chapter 2. The potentials were measured against the dhe. The current potential characteristics were also obtained by potentiostatic pulse technique under the same conditions.

The current potential characteristics were also obtained by potentiostatic pulse technique in electrolytes of KOH concentration 0.2, 0.4, 0.8 and 1.0 mol dm^{-3}, in air at 25°C, and also in oxygen partial pressures of 0.21 (air), 0.58, 0.74 and 1 (oxygen gas from cylinder) in 5 mol dm^{-3} KOH at 25°C. The intermediate pressures were obtained by diluting the oxygen with nitrogen. The partial pressures were measured by means of an oxygen sensor supplied by the Wolfsun Unit at The City University. The dhe was calibrated against the rhe in the same electrolyte for the 4 solutions and was found to be -17 ± 3 mV.

6.5.2 Results and Discussion.

Figure 6.2 gives the E-log i plots (A and B) for oxygen reduction on $NiCo_2O_4$ in air and in oxygen at 25°C in 5N KOH. Both plots shows 3 slopes. Intially the slope is ∿ 0.06V per decade, increasing thereafter with potential.

However, Singh et al[80] obtained only one slope of value 0.06V per decade for oxygen reduction on $NiCo_2O_4$. To ascertain that the 3 slopes are activation controlled, E-log i_t (i_t = transient current density) relationship was obtained by potentiostatic pulse technique under the same conditions. These plots (C and D) are also included in figure 6.2. Transient measurements indicate the presence of one slope, 0.064V per decade in air and 0.066V per decade in oxygen, therefore confirming that the slopes of value greater than ∿ 0.06 V per decade obtained by steady state measurement are at least partly mass transfer controlled. Therefore, all subsequent current potential measurements for this study were obtained by potentiostatic pulsing.

Figure 6.3 gives the E-log i_t plots for oxygen reduction on $NiCo_2O_4$ in electrolytes of KOH concentration of 0.2, 0.4, 0.8 and 1.0 mol dm^{-3}, at 25^oC in air. The Tafel slopes evaluated for the 4 plots varied between 0.060 and 0.064V per decade. The E-logi plots varied very little KOH concentration.

Figure 6.4 gives the E-log i_t plots for oxygen reduction on $NiCo_2O_4$ in oxygen partial pressures of 0.21, 0.58, 0.74 and 1.0 atmospheres. The Tafels slope for the 4 plots were in the region of 0.060 to 0.065V per decade and as expected the transient current densities increased with increase in oxygen partial pressure.

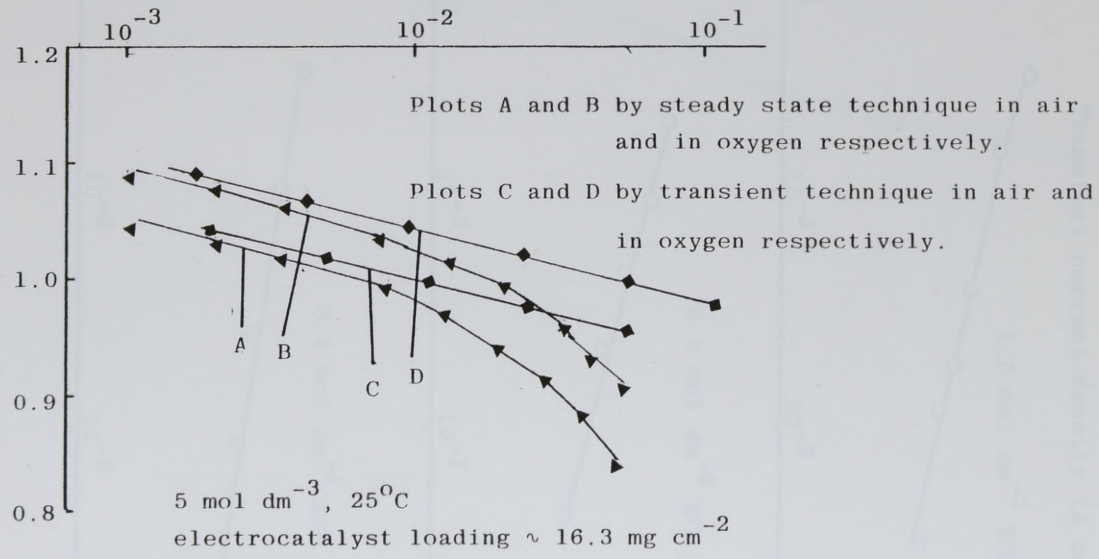

Figure 6.2: Oxygen reduction current potential characteristics on a Taflon bonded $NiCo_2O_4$ electrode in air and in oxygen obtained by steady state and transient techniques.

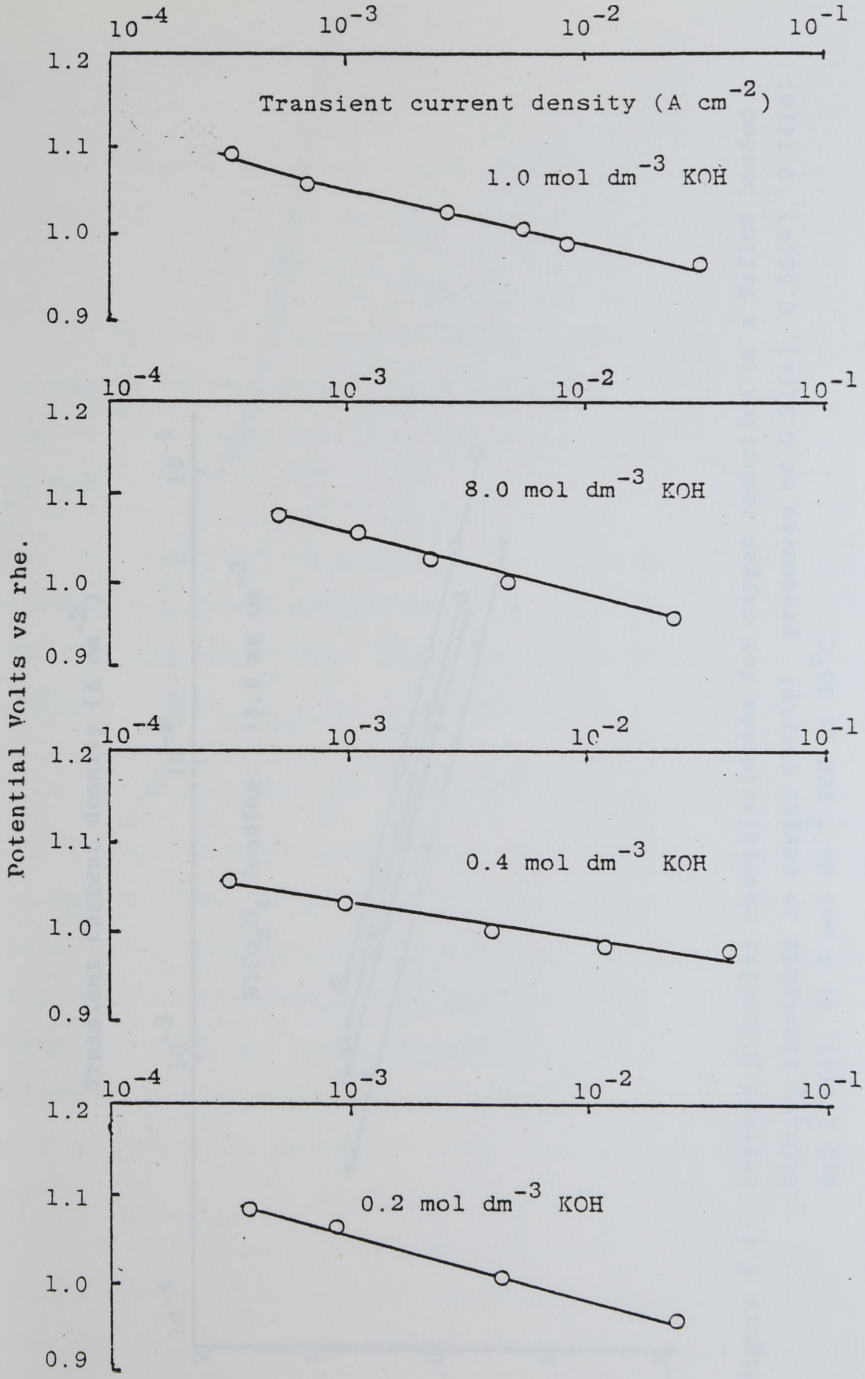

Figure 6.3: Oxygen reduction E-log i_t plots on a Teflon bonded $NiCo_2O_4$ electrode in air at 25°C in KOH electrolyte of different concentration. ($NiCo_2O_4$ loading: 13.4 mg cm^{-2}).

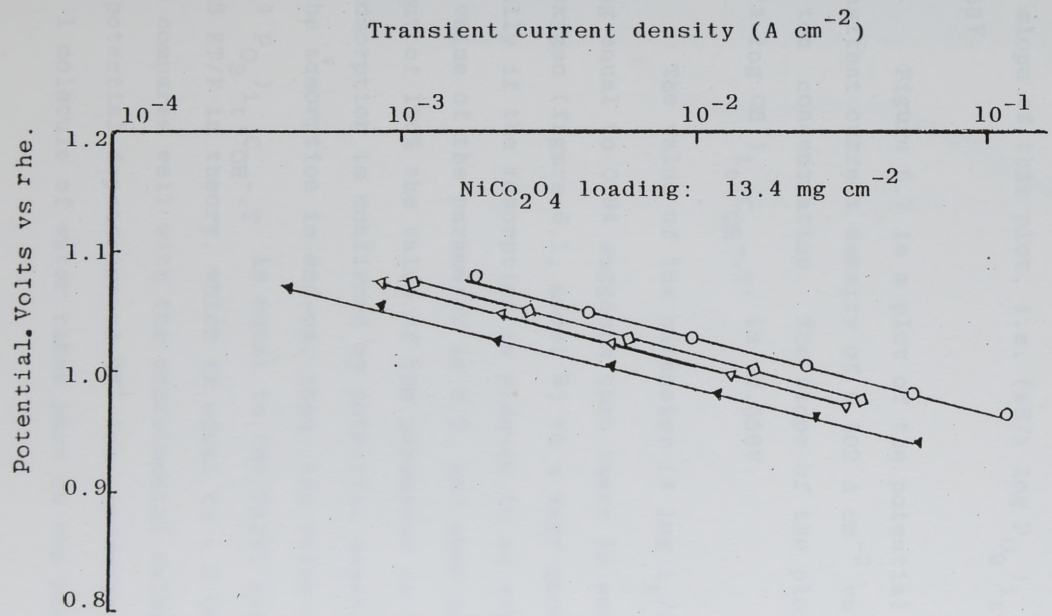

Figure 6.4: Current potential characteristics for oxygen reduction on a Teflon bonded $NiCo_2O_4$ electrode in oxygen partial pressures of 0.21(▲), 0.58(♤), 0.74(□) and 1.0(o), in 5 mol dm^{-3} KOH at 25°C.

Figure 6.5 shows a plot of log i_t at a constant potential of 1.05V vs log P_{O_2}. The slope of this plot, i.e. $(\partial \log i_t/\partial \log P_{O_2})_{E,C_{OH^-},T}$, is 0.94.

Figure 6.6 is a plot of the potential at a constant transient current density of 0.01 A cm^{-2} vs the log P_{O_2}. The slope of this plot, i.e. $(\partial E/\partial \log P_{O_2})_{i_t,C_{OH^-},T}$, is 0.058V.

Figure 6.7 is a plot of the potential at a constant transitent current density of 0.002 A cm^{-2} vs the log of OH^- ion concentration. The slope of the plot, $(\partial E/\partial \log OH^-)_{i_t,C_{OH^-},T}$, is -0.058V.

The value of the parameter $(\partial \log i_t/\partial \log P_{O_2})_{E,C_{OH^-},T}$ being equal to 0.94 suggests that there is end-on adsorption of oxygen (figure 6.1, model B) to a very good extent. Ideally if the adsorption is side-on to an extent of 100% the value of the parameter is 0.5, and when end-on to an extent of 100% the value of the parameter is 1. This mode of adsorption is confirmed by potential dependence of P_{O_2}. If the adsorption is end-on, then, the value of the parameter $(\partial E/\partial P_{O_2})_{i_t,C_{OH^-},T}$ is equal to the Tafel slope, i.e. 2.303 RT/F in theory, which is equal to $\sim$ 0.06V per decade. This compares well with the experimental value of 0.058V. The potential dependence of OH^- ion concentration suggests that 1 molecule of water takes part in the mechanistic steps

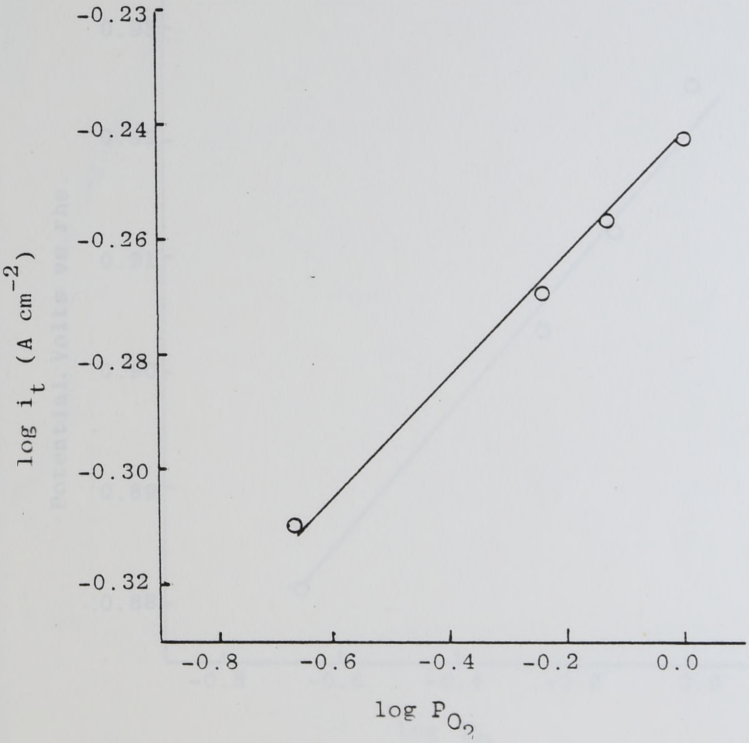

Figure 6.5: Oxygen partical pressure dependence of the transient oxygen reduction current density on a Teflon bonded $NiCo_2O_4$ electrode at a constant potential of 1.05V at 25°C in 5 mol dm^{-3} KOH.

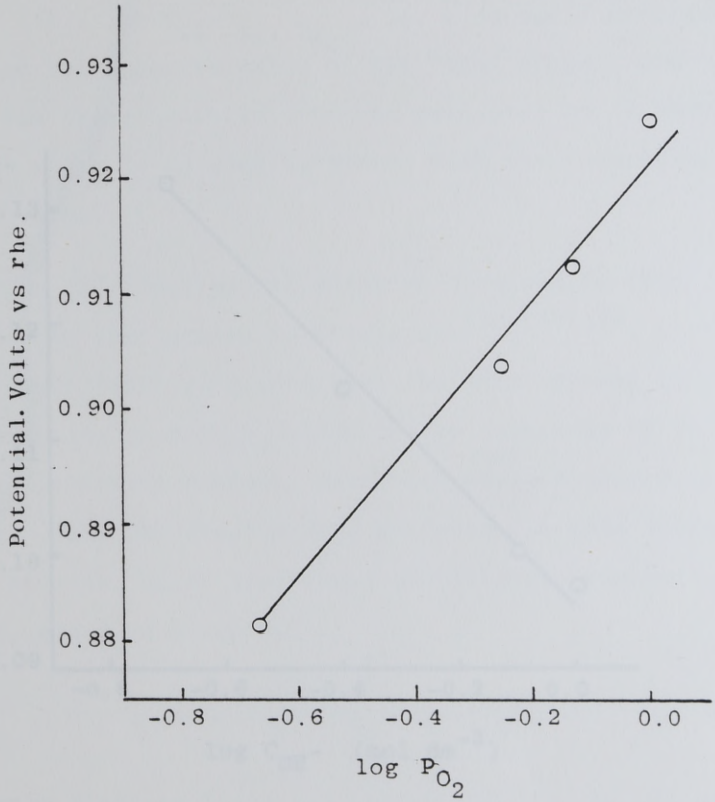

Figure 6.6: Oxygen partial pressure dependence of the oxygen reduction potential on a Teflon bonded $NiCo_2O_4$ electrode at a constant transient current density of 10^{-2} A cm^2, in 5 mol dm^{-3} KOH at 25^oC.

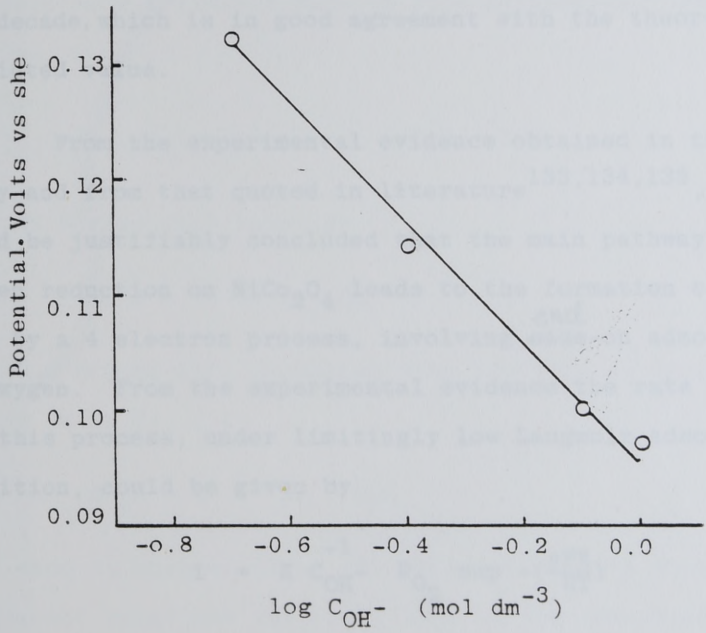

Figure 6.7: KOH concentration dependence of oxygen reduction potential on Teflon bonded $NiCo_2O_4$ electrode at a constant transient current density of 0.002 A cm^{-2} in air at 25°C.

previous to the rate determining step. Therefore the OH^- ion concentration term in the rate equation is raised to the power -1. If this is so, the theoretical value of the parameter $(\partial E/\partial \log C_{OH^-})_{i_t, P_{O_2}, T}$ for a cathodic process is equal to the negative value of the Tafel slope. The value of the experimentally obtained parameter is -0.058V per decade, which is in good agreement with the theoretically predicted value.

From the experimental evidence obtained in this study and from that quoted in literature[133,134,135], it could be justifiably concluded that the main pathway of oxygen reduction on $NiCo_2O_4$ leads to the formation of OH^- ions by a 4 electron process, involving ~~side~~ end-on adsorption of oxygen. From the experimental evidence the rate equation for this process, under limitingly low Laugmuir adsorption condition, could be given by

$$i = K\, C_{OH^-}^{-1}\, P_{O_2} \exp -\left(\frac{\beta FE}{RT}\right) \qquad 6.9$$

Of the paths given in Table 4.1, paths (3), (4) or (7) will satisfy the kinetic parameters obtained for oxygen reduction on $NiCo_2O_4$. Further due to the mixed site nature of $NiCo_2O_4$, the path will be expected to take place on more than one site. The 3 proposed paths also satisfy this requirement.

The first step will involve a weak end-on interaction of an active site (M) on $NiCo_2O_4$ with the oxygen

molecule;

$$M + O_2 \rightarrow M \ldots . O_2 \qquad 6.10$$

The M site is most probably divalent, this assumption will become apparent later in the discussion. The M .... O_2 species could accept a proton from a water molecule with the help of a trivalent site to form an adsorbed peroxide species, i.e.

$$M \ldots . O_2 + H_2O + T \rightarrow MO_2H + TOH \qquad 6.11$$

The TOH formed will react by

$$TOH + e \rightarrow T + OH^- \qquad 6.12$$

The MO_2H formed will decompose with the help of another cation (M or T), i.e.

$$MO_2H + M \rightarrow MO + MOH \qquad 6.13$$

This step is assumed to be the rate determining step. The subsequent reactions that will lead to the formation of OH^-, are

$$e + MO + H_2O \rightarrow MOH + OH^- \qquad 6.14$$

$$2e + 2MOH \rightarrow 2M + OH^- \qquad 6.15$$

Therefore the proposed path for $NiCo_2O_4$ is similar to path 7 given in table 4.1, which, in alkaline medium is

$$S + O_2 + SH_2O \rightarrow SOH + SHO_2 \qquad 6.16$$

$$SO_2H + S \rightarrow SO + SOH \qquad 6.17$$

$$e + SO + H_2O \rightarrow SOH + OH^- \qquad 6.18$$

$$3e + 3SOH \rightarrow 3S + 3OH^- \qquad 6.19$$

Therefore, in the mechanism proposed for $NiCo_2O_4$, oxygen is reduced to OH^- ions with the formation of adsorbed HO_2^- ion as an intermediate. The Tafel slope calculated using equation 4.2 ($v = 1$, $n = 1$ and $n^* = 0$) is 2.303 RT/F volts per decade, having a value of 0.059V per decade at 25°C.

A rate equation is derived assuming step 6.13 to be rate determining

$$M + O_2 \underset{V_{-1}}{\overset{V_1}{\rightleftharpoons}} M \ldots O_2 \qquad 6.10$$

$$M \ldots O_2 + T + H_2O \underset{V_{-2}}{\overset{V_2}{\rightleftharpoons}} MO_2H + TOH \qquad 6.11$$

$$TOH + e \underset{V_{-3}}{\overset{V_3}{\rightleftharpoons}} T + OH^- \qquad 6.12$$

$$MO_2H + M \xrightarrow{V} MO + MOH \qquad 6.13$$

where V_1, V_2, V_3 and V are rates of the forward processes of steps 6.10, 6.11, 6.12 and 6.13 respectively and V_{-1}, V_{-2} and V_{-3} are the rates of the reverse processes of step 6.10, 7.11 and 6.12 respectively. The seven rates

can be expressed as follows

$$V_1 = k_1(1 - \theta_{M\ldots O_2})\, P_{O_2} \qquad 6.20$$

$$V_{-1} = k_{-1}\theta_{M\ldots O_2}\, \theta_T \qquad 6.21$$

$$V_2 = k_2\, \theta_{M\ldots O_2}\, \theta_T \qquad 6.22$$

$$V_{-2} = k_{-2}\, \theta_{MO_2H}\, \theta_{TOH} \qquad 6.23$$

$$V_3 = k_2\, \theta_{TOH} \exp-\left(\frac{EF}{2RT}\right) \quad (\beta = 0.5) \qquad 6.24$$

$$V_{-3} = k_{-3}\, C_{OH^-}\, \theta_T \exp\left(\frac{EF}{2RT}\right) \quad (\beta = 0.5) \qquad 6.25$$

$$V = k_4(1 - \theta_{MO_2H})\, \theta_{MO_2H} \qquad 6.26$$

Considering the kinetics under quasi equilibrium concepts

$$V_1 = V_{-1} \qquad 6.27$$

$$V_2 = V_{-2} \qquad 6.28$$

$$V_3 = V_{-3} \qquad 6.29$$

From equation 6.28

$$\theta_{MO_2H} = \frac{K_2\, \theta_{M\ldots O_2}\, \theta_T}{k_{-2}\, \theta_{TOH}} \qquad 6.30$$

From equation 6.27, assuming $\theta_{M...O_2} \rightarrow 0$ 6.31

$$\theta_{M...O_2} = \frac{k_1 P_{O_2}}{k_{-1}}$$

From equation 6.29

$$\frac{\theta_T}{\theta_{TOH}} = \frac{k_3 \exp-(\frac{FE}{RT})}{k_{-3}\ C_{OH^-}} \qquad 6.32$$

From equations 6.30, 6.31, and 6.32, we get 6.32

$$\theta_{MO_2H} = k\ P_{O_2}\ C_{OH}^{-1} \exp-(\frac{FE}{RT}) \qquad 6.31$$

where k is a constant. The rate of oxygen reduction is given by equation 6.26. Considering $\theta_{MO_2H} \rightarrow 0$, the rate of oxygen reduction in terms of current density is

$$i = K\ P_{O_2} C_{OH}^{-1} \exp-(\frac{FE}{RT}) \qquad 6.32$$

where K is a constant.

Table 6.2 compares the experimentally observed and theoretically predicted kinetic parameters for oxygen reduction on $NiCo_2O_4$ showing a good agreement.

Table 6.2: Comparison of the theoretically predicted and experimentally observed kinetic parameters for oxygen reduction on Teflon bonded $NiCo_2O_4$ at 25°C.

Parameter	Theoretical	Experimental
$\left(\frac{\partial E}{\partial \log i_t}\right)_E$	$-\frac{2.303\ RT}{F}$	0.06V - 0.065V
$\left(\frac{\partial \log i_t}{\partial \log Po_2}\right)_{E,T,C_{OH^-}}$	1	0.94
$\left(\frac{\partial E}{\partial \log Po_2}\right)_{i,T,C_{OH^-}}$	$\frac{2.303\ RT}{F}$	0.058V
$\left(\frac{\partial E}{\partial \log C_{OH^-}}\right)_{i,T}$	$-\frac{2.303\ RT}{F}$	- 0.058V

6.5.2.1 Speculative Discussion on the Active Sites.

$NiCo_2O_4$ is a mixed spinel and has been shown to have an ionic distribution[96] of

$$Co^{2+}_{0.9}\ Co^{3+}_{0.1}(Ni^{2+}_{0.9}\ Ni^{3+}_{0.1}\ Co^{3+})\ O^{2-}_{3.2}\ O^{-}_{0.8}$$

where the cations outside the parenthesis are in tetrahedral sites and those inside are in octahedral sites. Figure 6.8 gives the concentration, environment and electron distribution (high spin or low spin) for the cations in $NiCo_2O_4$ complied from literature[96,146-150]. If the oxygen molecule overlaps via the t_{2g} orbital of the cations in the octahedral sites and via the e orbitals of the cations in the tetrahedral sites, both divalent ions (M) in $NiCo_2O_4$ i.e. Ni^{2+} (octahedral) and Co^{2+} (tetralhedral) have suitable filled orbitals to interact with the vacant orbitals (σ^* (2p)) of oxygen. Further, in the intermediates MO_2H, MOH and MO formed during the process of oxygen reduction, the divalent cation M becomes either trivalent or tetravalent. These oxidation state transitions take place with a gain in crystal field stabilisation energy[151] and thus the formation of the intermediates are energetically feasible. The trivalent sites however have no vacant orbitals that are favourably positioned to interact with a lone pair of electrons of

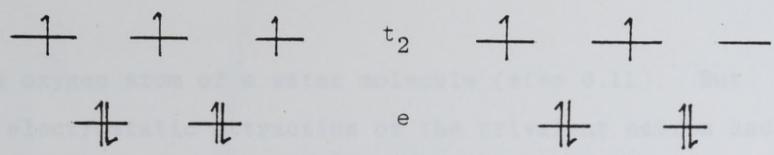

Co^{2+} (d^7), tetrahedral site 30%.

Co^{3+} (d^6), tetrahedral site, 3.3%.

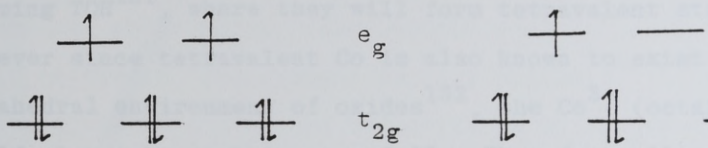

Ni^{2+} (d^8), octahedral site, 30%, low spin.

Ni^{3+} (d^7), octahedral site, 3.3%, low spin.

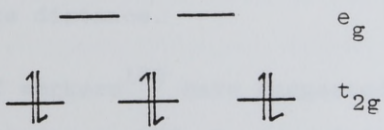

Co^{3+} (d^6), octahedral site 33.3%, low spin.

Figure (6.8). d Electron distribution in the cations in $NiCo_2O_4$.

the oxygen atom of a water molecule (step 6.11). But an electrostatic attraction of the trivalent cation and the oxygen atom of water could facilitate proton transfer to $M....O_2$. Further of the T sites, the Co^{3+} (tetrahedral) and Ni^{3+} (octahedral) will definitely be stabilised when forming TOH[151], where they will form tetravalent states. However since tetravalent Co is also known to exist in octahedral environment of oxides[152], the Co^{3+} (octahedral) could also take part in step 6.15. Therefore all cations on the surface of $NiCo_2O_4$ could take part in oxygen reduction as either T or M sites. However, the activity of certain sites will be limited due to the requirement of a critical inter-site distance.

One group of workers[133] have suggested that the oxygen reduction activity on $NiCo_2O_4$ is related to the electron hopping mechanism of electrical conduction of the cations in the octahedral environment, i.e.

$$\underset{t_{2g}^{6}\ e_{g}^{o}}{Co^{3+}} \rightarrow (\underset{t_{2g}^{5}\ e_{g}^{1}}{C_{o}^{3+}} + \square) \qquad 6.33$$

$$(\underset{t_{2g}^{5}\ e_{g}^{1}}{Co^{3+}} + \square) + \underset{t_{2g}^{6}\ e_{g}^{2}}{Ni^{2+}} \rightleftharpoons [\underset{t_{2g}^{6}\ e_{g}^{1}}{Co^{3+}} + e + \underset{t_{2g}^{5}\ e_{g}^{2}}{Ni^{3+}} + \square] \qquad 6.34$$

and oxygen reduction takes place by an electron donor-acceptor mechanism of the Co ions in the octahedral

environment;

$$[Co^{3+} + e] + O_2 + H_2O \rightarrow [Co^{3+} + \square][H_2O.O_2]^- \qquad 6.35$$

However, electrical conduction and oxygen reduction by this process involves the formation of Co^{2+} in the octahedral environment. The occurance of Co^{2+} in high field octahedral environment is very unlikely[96,153]. A more probable conduction mechanism is by electron hopping in the nickel cations in the octahedral environment;

$$Ni_*^{2+} + Ni^{3+} \rightleftarrows Ni_*^{3+} + Ni^{2+} \qquad 6.36$$

and the Ni^{2+} and Ni^{3+} sites could also be the most probable active sites in the divalent-trivalent oxygen reduction mechanism proposed in this study.

Finally, it has been suggested[134,135] that oxygen reduction on $NiCo_2O_4$ is by a parallel process. The main process reduces oxygen to OH^- ions and an insignificant process reduces oxygen to OH_2^- ions which are detected in the electrolyte. Although the mixed sites found on $NiCo_2O_4$ could bring about both processes, another possibility for the occurence of HO_2^- ions in the electrotyte is by the desorption of HO_2^- formed during step 6.11, by;

$$MO_2H + e \rightarrow M + HO_2^- \qquad 6.37$$

Since the MO_2H intermediate is formed before the rate determining step, there is a likelihood of MO_2H contributing to the HO_2^- detected in the electrolyte.

CHAPTER SEVEN

OXYGEN REDUCTION STUDIES ON COMPOSITE $NiCo_2O_4$/GRAPHITE ELECTRODES.

During the Ph.D. oral examination, [redacted] pointed out that the quantity of (HO_2^-) expressed as (HO_2^-) is in fact the flux of HO_2^- of dimension Mole cm^{-2} sec^{-1}.

7.1 INTRODUCTION

Graphite which could be produced in high surface area form (400 - 500 m^2g^{-1}), is a good electrocatalyst for the cathodic reduction of oxygen in alkali medium. Davis, Clark, Yeager and Horvorka[13] have shown conclusively that during the reduction of oxygen on graphite the oxygen-oxygen bond is not broken, and the product is essentially HO_2^-. Since, graphite decomposes peroxide very poorly it is essential that the peroxide be removed. The removal of peroxide is imperative for the long term stability and efficiency of the cathode. Previous work carried out by Goldstein and Tseung[12] on cobalt iron oxide/graphite system showed that the peroxide formed electrochemically on the graphite by

$$O_2 + H_2O + 2e \rightarrow HO_2^- + HO^- \qquad 7.1$$

can be decomposed chemically by the iron cobalt oxide,

i.e. $$2HO_2^- \rightarrow O_2 + 2OH^- \qquad 7.2$$

when the iron cobalt oxide is incorporated into the graphite cathode. They carried out an extensive kinetic study on the basis of oxygen recycling and concluded that the maximum possible enhancement of performance for a cobalt iron oxide/graphite electrode is the doubling of the exchange current density of the graphite electrode of similar loading. Although cobalt iron oxide has a good peroxide decomposition activity, its activity to reduce oxygen is very poor[12]. However, $NiCo_2O_4$ in addition to

having a good activity for peroxide decomposition is also active for the reduction of oxygen[130]. Therefore, when $NiCo_2O_4$ is incorporated into a graphite cathode it should bring about an enhancement of activity for the reduction of oxygen. Yeung and Tseung[131] found the performance of 10 wt % $NiCo_2O_4$/graphite electrode (electrocatalyst loading $\sim$ 6 mg cm^{-2}) to be 180 mA cm^{-2} at 0.75V vs the dhe at 20°C in air. The performances of $NiCo_2O_4$ and graphite when tested separately under similar conditions were 16 mA cm^{-2} and 110 mA cm^{-2} respectively. This chapter describes the theoretical and experimental work carried out to study oxygen reduction on the composite $NiCo_2O_4$/graphite system. It is hoped that this study will enhance the understanding of the kinetics of formation and decomposition of peroxide and the factors that govern the efficiency of the composite electrode.

7.2 Experimental

To optimise the $NiCo_2O_4$/graphite system for oxygen reduction it is necessary to find the oxygen reduction performance of graphite electrodes having different quantities of $NiCo_2O_4$. Further, it is also essential for the $NiCo_2O_4$ aggregates to be uniformly dispersed among the graphite aggregates in the composite electrodes. Also, since the oxygen reduction performance varies with electrocatalyst loading up to a maximum of approximately 20 mg cm^{-2}, the electrocatalyst loading of the $NiCo_2O_4$/graphite electrodes were kept at approximately 20 mg cm^{-2}.

FEP hydrophobic particulate polymer was used in this study in the fabrication of all electrodes, as the graphite electrode preparation was very much easier. Graphite tends to coagulate when mixed with FLUON GP2. The graphite to FEP ratio is critical for gas dissolution electrodes, since it determines compromise between the electrode stability and electrode activity by maximising the three phase (electrocatalyst, electrolyte and gas) interphase. The graphite to FEP ratio was found to be 3:1.5 by weight.

The electrode preparation is as follows: $NiCo_2O_4$/graphite electrodes of electrocatalyst loading of approximately 20 mg cm^{-2} were made consisting of 10, 20, 30, 40, 50 and 60 weight % $NiCo_2O_4$. In each case 100 mg of the electrocatalyst and the appropriate quantity of FEP were weighed into a small sample bottle. This mixture was ultrasonically dispersed with 3 cm^3 of absolute alcohol. The ultrasonic dispersion was continued until alcohol evaporated to approximately $\frac{1}{3}$ its original volume so that the electrocatalyst, and FEP suspension in alcohol were sufficiently thick to be painted onto the 1 cm^2, 100 mesh Ni screen current collector. To prevent the denser particles (e.g. $NiCo_2O_4$ particles) from settling to the bottom of the container, the suspension was kept stirring by means of a magnetic stirrer until the painting was complete. This process of electrode preparation was carried out to obtain intimate and uniform mixing of the graphite and $NiCo_2O_4$ aggregates and FEP particles as far as possible. The electrodes were dried by means of a hot

air blower and heated at 300°C for 1 hour in a N_2 atmosphere.

The electrochemical performance of these composite electrodes were determined in air, 5N KOH at 25°C in the floating mode. The experimental set up for this determination was described in Chapter 2.

To estimate the enhancement in performance due to synergism of the $NiCo_2O_4$/graphite system it is also necessary to know the performance of the $NiCo_2O_4$ and graphite individually. Therefore oxygen reduction performance was carried out on $NiCo_2O_4$ and graphite electrodes of electrocatalyst loading of approximately 2, 4, 6, 8, 10, 12, 14 and 20 mg cm^{-2}. The electrode fabrication and the oxygen reduction performance evaluation for these electrodes were the same as that for the $NiCo_2O_4$/graphite electrodes.

It was necessary to evaluate an electrochemical parameter to compare the performance of the electrodes that were fabricated. A suitable parameter is the pseudo-exchange current density (i_o), having units of mA cm^{-2}, the area being based on the geometric area of the electrode. This parameter will be expected to increase with increase in electrocatalyst loading. Furthermore, it is necessary for the pseudo-exchange current density to be a representative of activation overpotential only, and to be devoid of ohmic and mass transfer influences. The activation controlled E - log i slopes for $NiCo_2O_4$ and graphite were established initially by potentiostatic pulse technique.

For $NiCo_2O_4$ the Tafel slope was found to be approximately 0.06V per decade for oxygen reduction at 25°C (Chapter 6). Figure 7.1 gives the E-log i_t plot for the cathodic reduction of oxygen on graphite at 25°C, indicating a Tafel slope of 0.04V per decade. The steady state measurements on $NiCo_2O_4$ and graphite were activation controlled at lower current densities (see Figures 7.2 and 7.3), and the psuedo-exchange current densities that were evaluated were a function of these slopes. At higher current densities the slopes increased, possibly due to mass transfer effects. In evaluating the pseudo-exchange current density, complications arose in choosing a suitable reversible potential appropriate to the system under study. Graphite which is known to reduce oxygen according to Equation 7.1 to form HO_2^- has a rest potential greater than 0.682V, which is the reversible potential for Equation 7.1. $NiCo_2O_4$, which reduces oxygen to OH^- and HO_2^- is active at lower overpotentials, compared to graphite. This complication is magnified further when considering the mechanism of composite $NiCo_2O_4$/graphite electrodes. Electrodes having a higher percentage of $NiCo_2O_4$ will be expected to reduce oxygen to form OH^-, whereas, those having a higher percentage of graphite will form mainly HO_2^- as the product. Pseudo-exchange current density evaluations based on a reversible potential value of 1.23V gave rather meaningless results when the three systems were compared. Therefore, it was necessary to use the experimental rest potentials to calculate the overpotentials during the evaluation of the

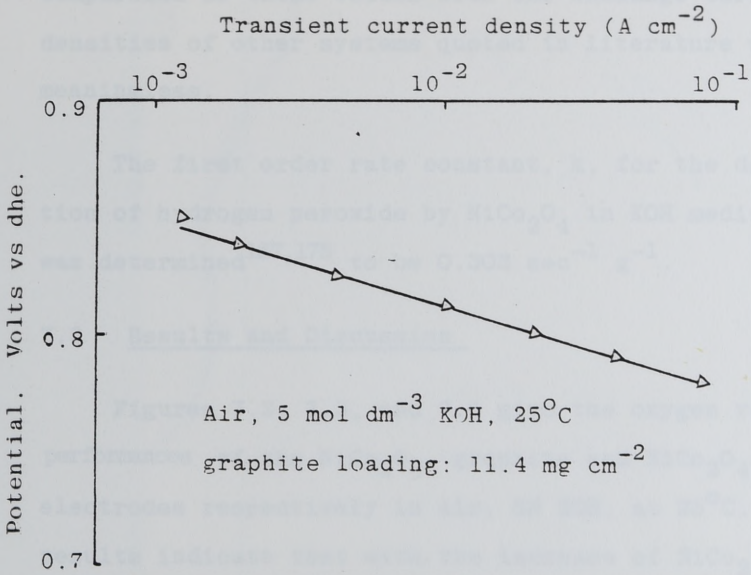

Figure 7.1: Oxygen reduction current potential characteristics on FEP bonded graphite electrodes by potentiostatic pulse technique.

pseudo-exchange current densities. Therefore, the overpotentials quoted in this chapter are also pseudo values. Furthermore, the pseudo-exchange current densities should only be used for comparative purposes within the framework of the kinetic considerations in this chapter. Any comparison of these values with the exchange current densities of other systems quoted in literature will prove meaningless.

The first order rate constant, k, for the decomposition of hydrogen peroxide by $NiCo_2O_4$ in KOH medium at 25°C was determined[157,175] to be 0.303 sec^{-1} g^{-1}.

7.3 Results and Discussion

Figures 7.2, 7.3, and 7.4 give the oxygen reduction performances of the $NiCo_2O_4$, graphite and $NiCo_2O_4$/graphite electrodes respectively in air, 5N KOH, at 25°C. The results indicate that with the increase of $NiCo_2O_4$ content in the graphite electrodes, the performance increases to a maximum and then decreases. The maximum performance is obtained for the electrode having 40 weight % $NiCo_2O_4$.

The study of the electrode activity of the three systems, i.e. $NiCo_2O_4$, graphite and $NiCo_2O_4$/graphite, each having different mechanisms could be carried out by calculating the pseudo-exchange current density i_o. For $NiCo_2O_4$ and graphite the pseudo-exchange current density will vary with electrocatalyst loading, but for the $NiCo_2O_4$/graphite system, it is based on an electrocatalyst loading of 20 mg cm^{-2} Figure 7.5 gives the i_o values for the three systems.

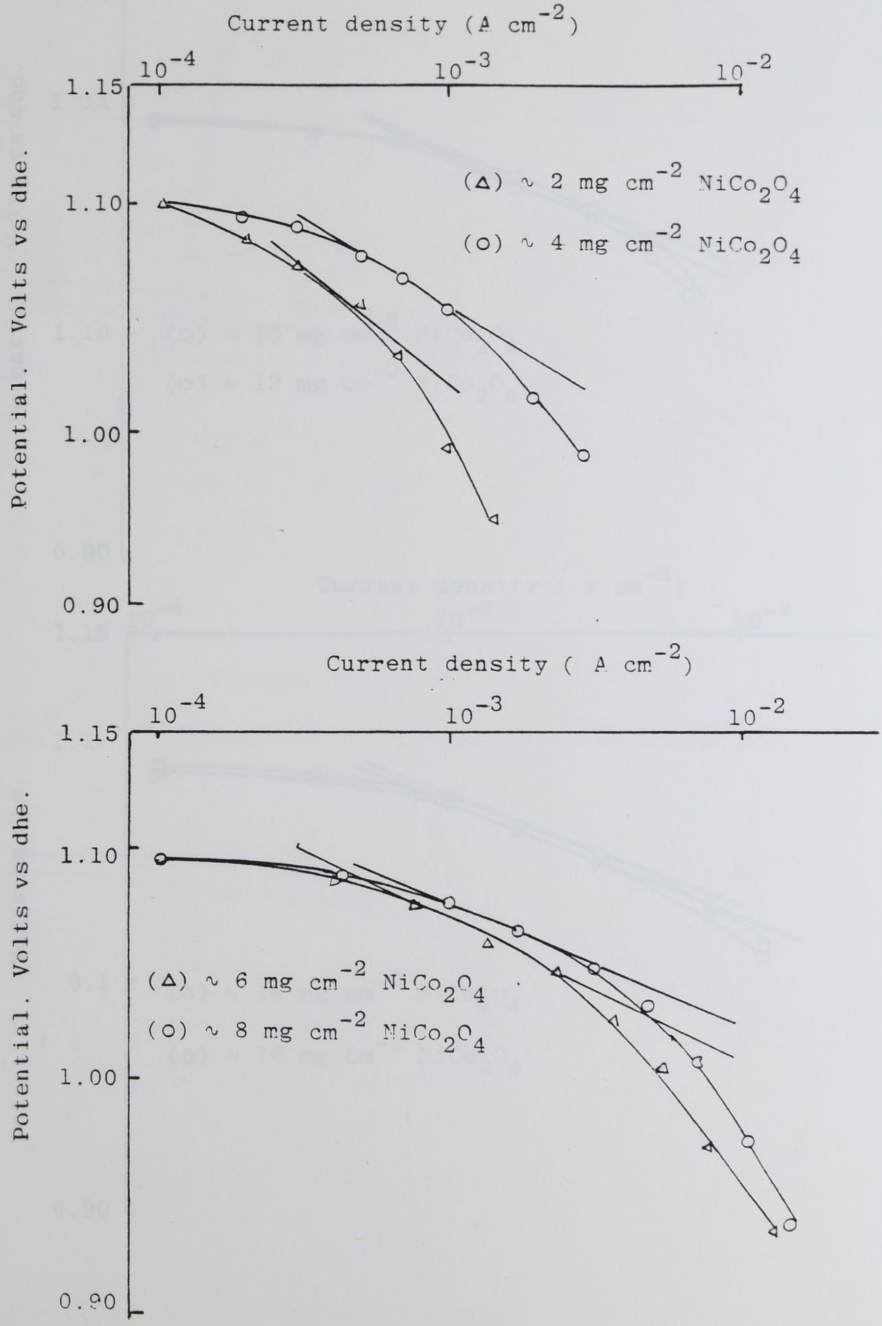

Figure 7.2: Oxygen reduction current potential characteristics on FEP bonded $NiCo_2O_4$ electrodes in 5 mol dm^{-3} KOH, in air at 25°C.

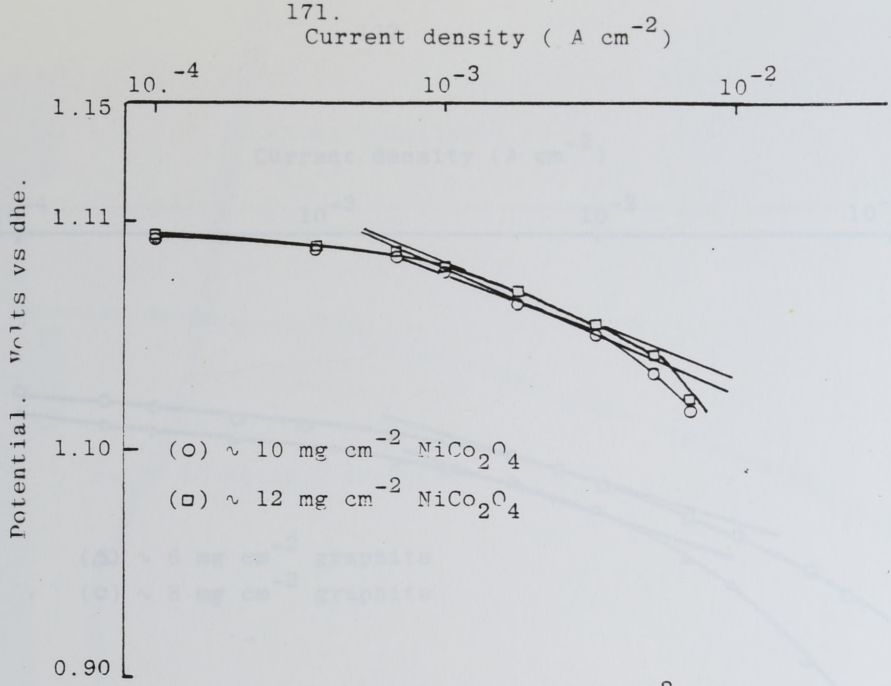

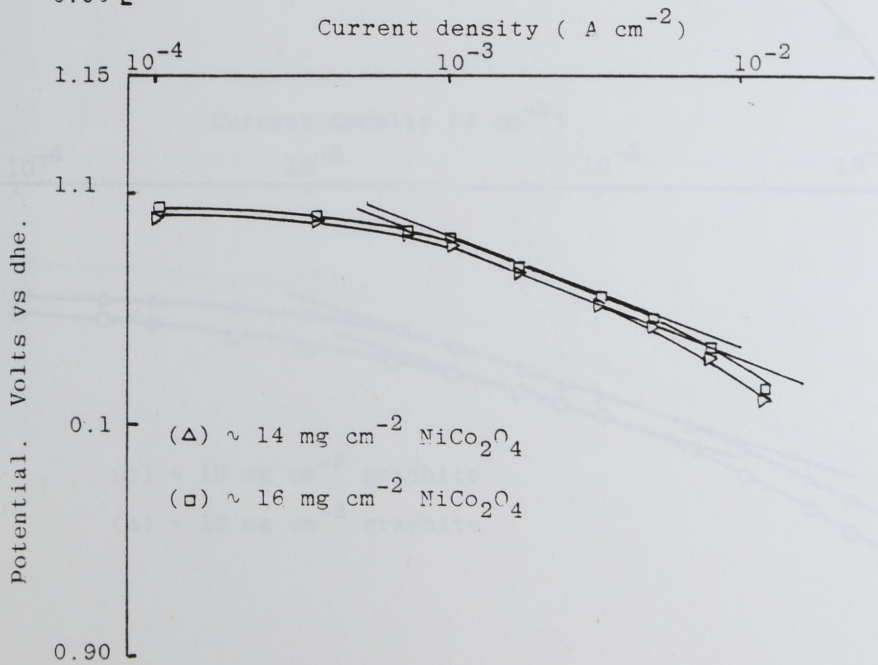

Figure 7.3 .... continued.

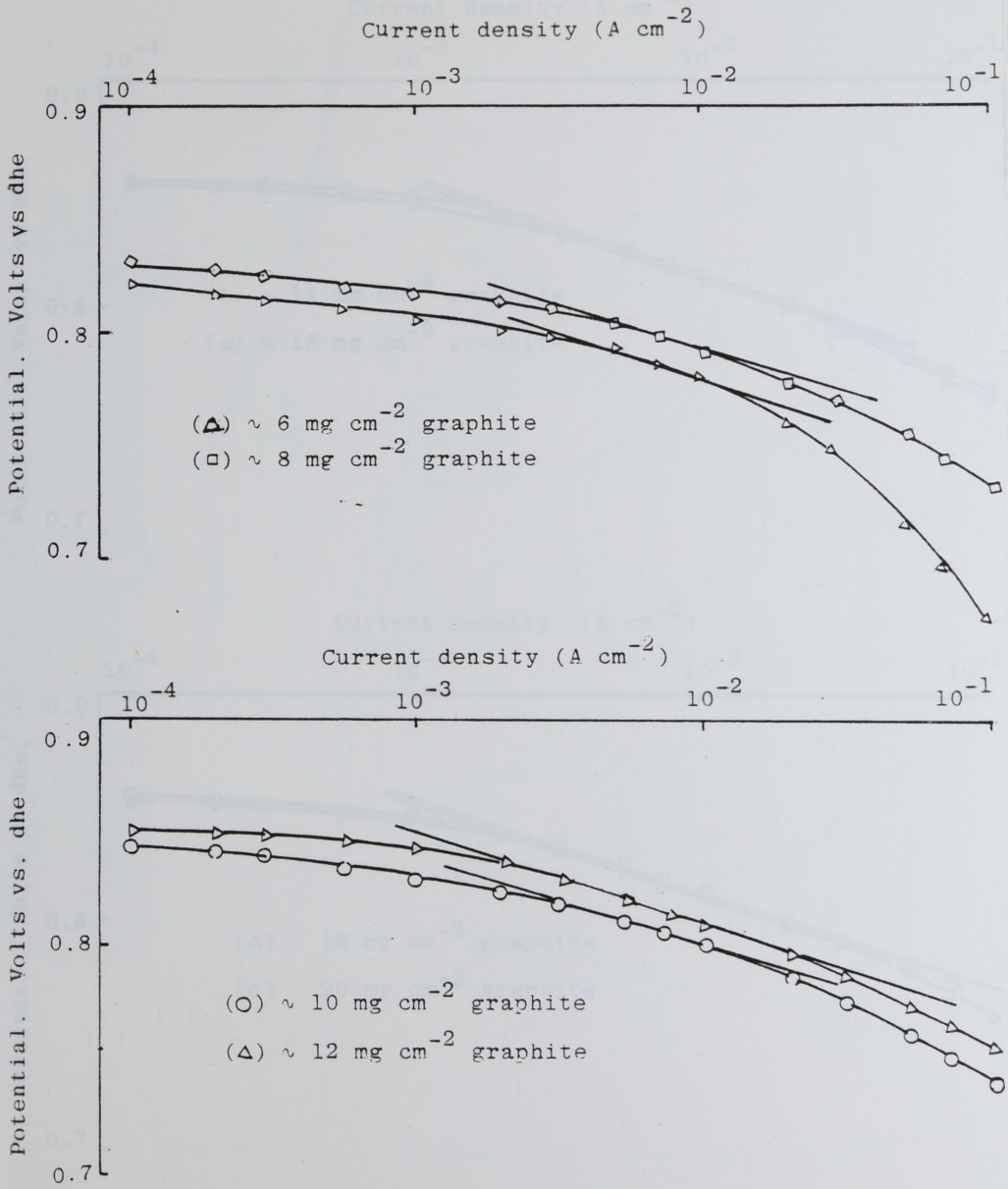

Figure 7.3: Oxygen reduction current potential characteristics on FEP bonded graphite electrodes in 5 mol dm^{-3}, in air at 25°C.

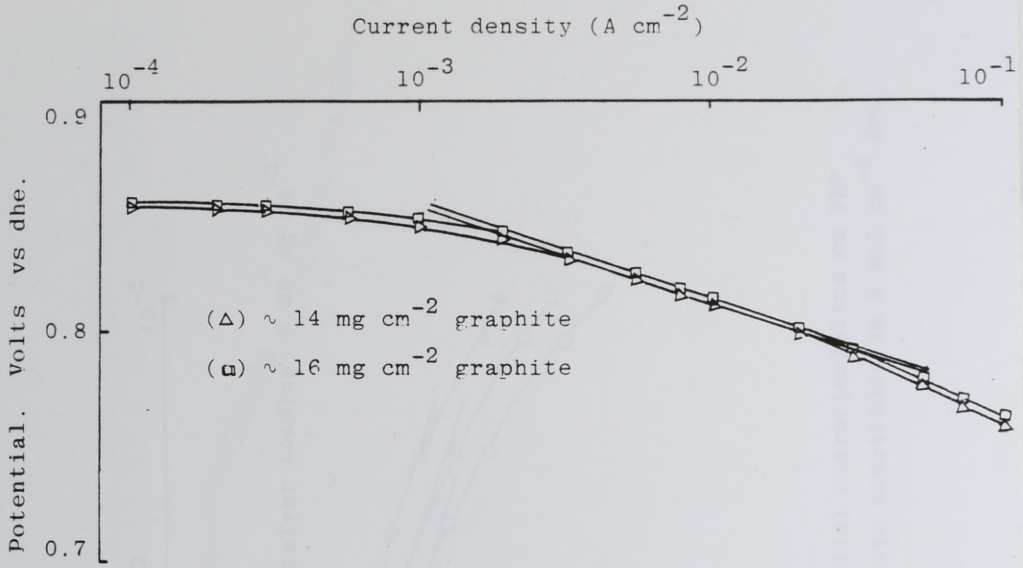

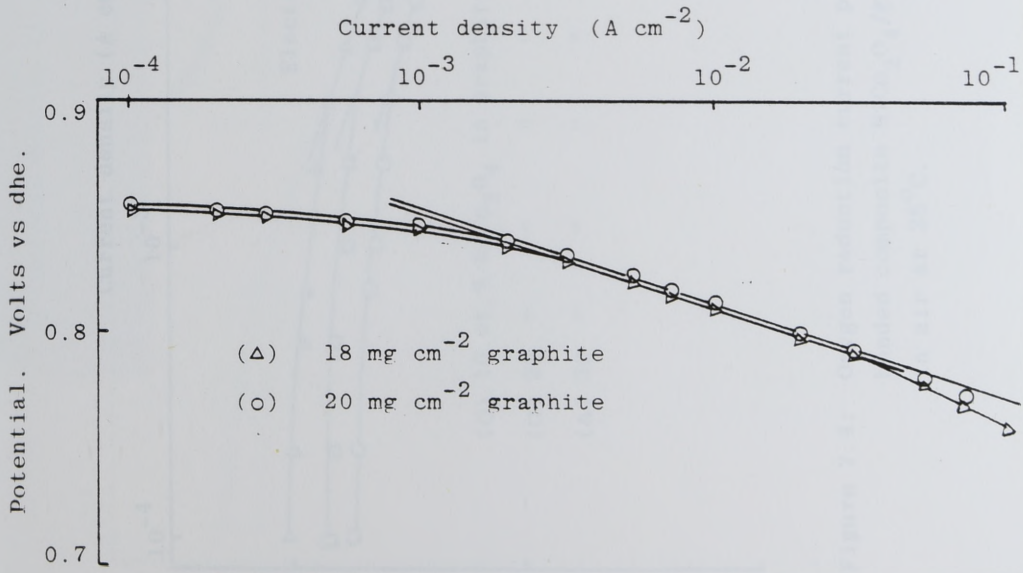

Figure 7.3 continued ....

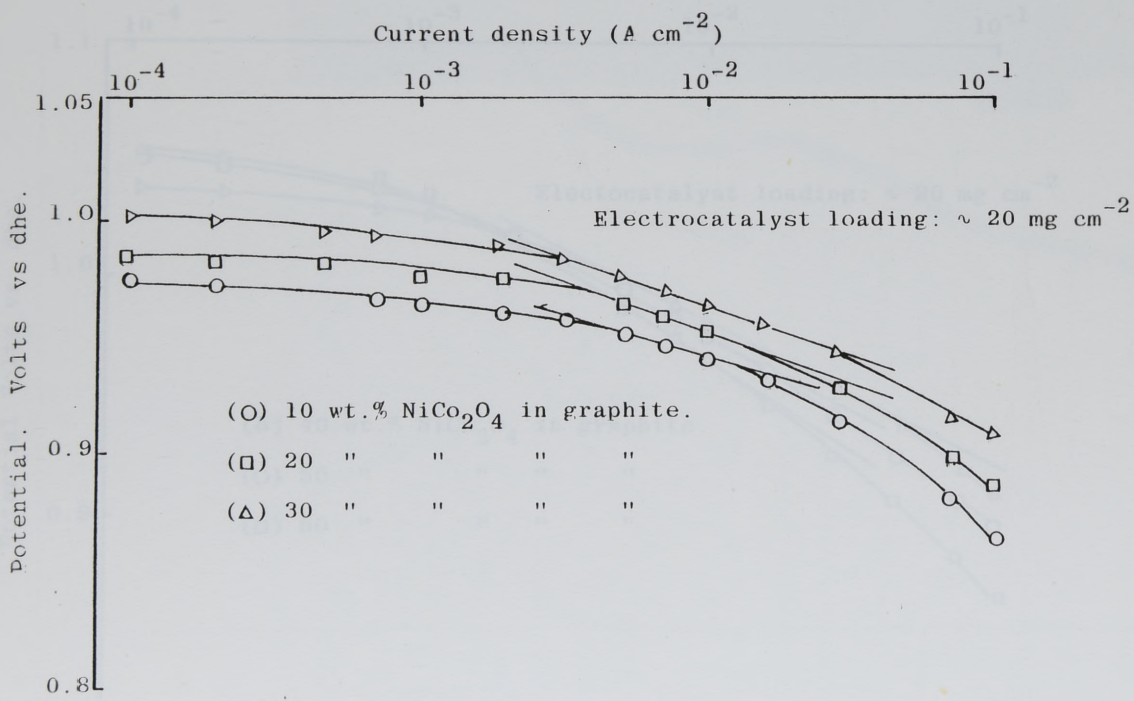

Figure 7.4: Oxygen reduction current potential characteristics on FEP bonded composite $NiCo_2O_4$/graphite electrodes in 5 mol dm^{-3} KOH, in air at 25°C.

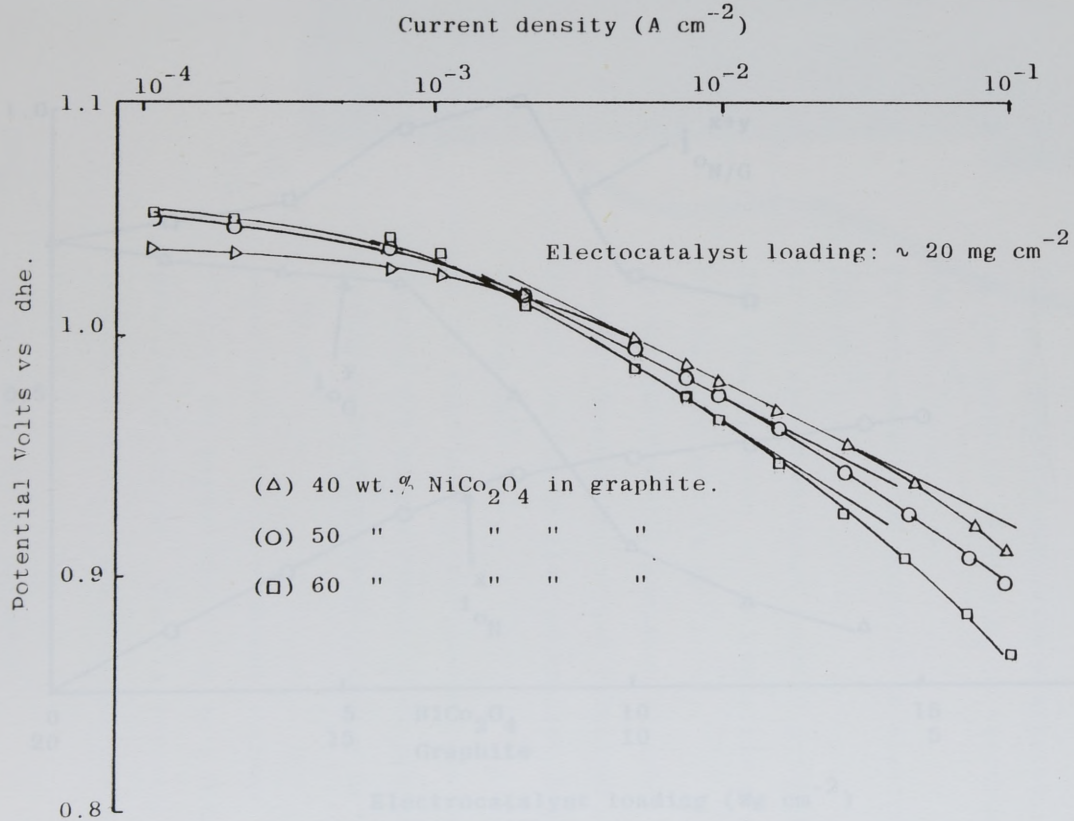

Figure 7.4 continued ...

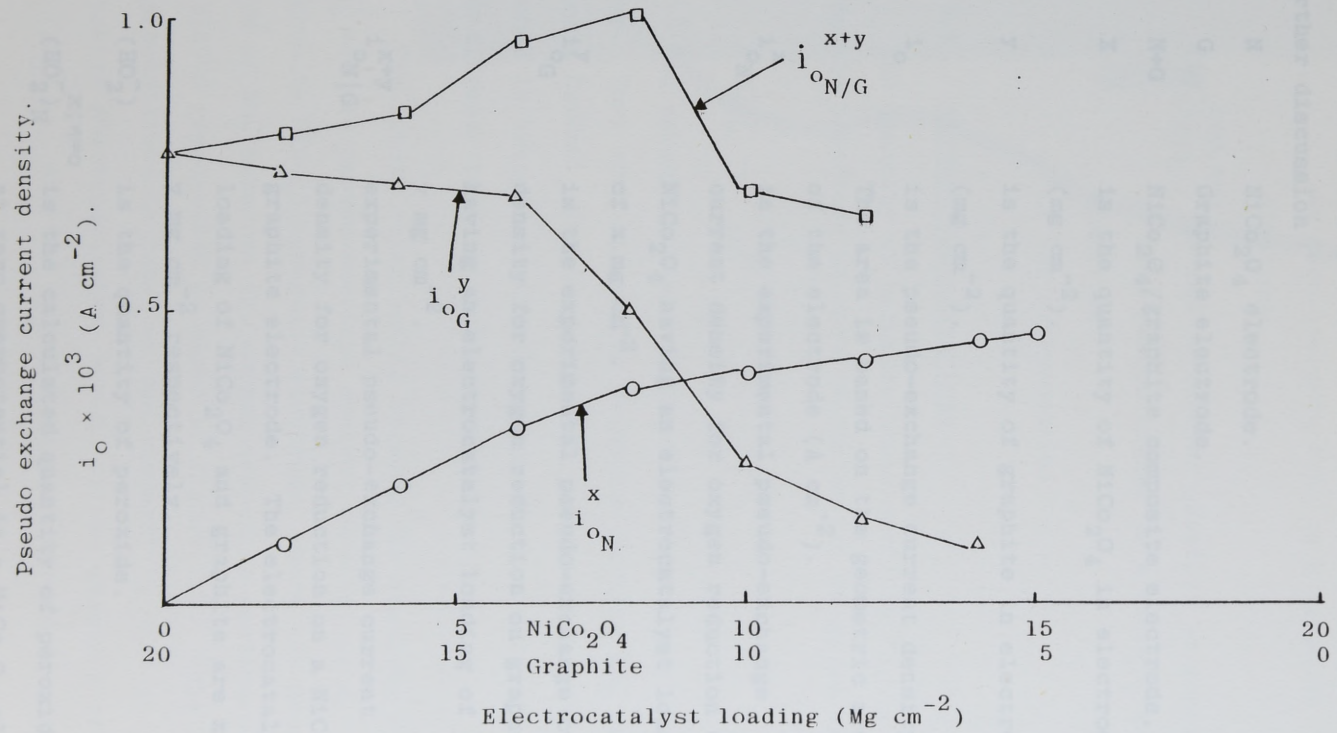

Figure 7.5: Pseudo exchange current densities for oxygen reduction on $NiCo_2O_4$(O), graphite (△) and composite $NiCo_2O_4$/graphite (□) electrodes at 25°C in 5 mol dm^{-3} KOH.

The following quantities are defined to assist further discussion

N	$NiCo_2O_4$ electrode.
G	Graphite electrode.
N+G	$NiCo_2O_4$/graphite composite electrode.
X	is the quantity of $NiCo_2O_4$ in electrode (mg cm^{-2}).
y	is the quantity of graphite in electrode (mg cm^{-2}).
i_o	is the pseudo-exchange current density. The area is based on the geometric area of the electrode (A cm^{-2}).
$i^x_{o_N}$	is the experimental pseudo-exchange current density for oxygen reduction on $NiCo_2O_4$ having an electrocatalyst loading of x mg cm^{-2}.
$i^y_{o_G}$	is the experimental pseudo-exchange current density for oxygen reduction on graphite having an electrocatalyst loading of y mg cm^{-2}.
$i^{x+y}_{o_{N\|G}}$	experimental pseudo-exchange current density for oxygen reduction on a $NiCo_2O_4$/graphite electrode. The electrocatalyst loading of $NiCo_2O_4$ and graphite are x and y mg cm^{-2} respectively.
(HO_2^-)	is the quantity of peroxide.
$(HO_2^-)_N^{x;\eta=o}$	is the calculated quantity of peroxide at zero overpotential in a $NiCo_2O_4$ electrode.

$(HO_2^-)_G^{y,\eta=o}$ is the calculated quantity of peroxide at zero overpotential in a graphite electrode.

$(HO_2^-)_{N|G}^{x+y,\eta=o}$ is the calculated quantity of peroxide at zero overpotential in a $NiCo_2O_4$/graphite electrode.

η is the overpotential.

7.3.1 Kinetic Considerations

The quantity of peroxide (mole sec^{-1} cm^{-2}), in a graphite electrode at zero overpotential is given by

$$(HO_2^-)_G^y = \frac{i_{o_G}^y}{2F} \qquad 7.3$$

Two assumptions are required for Equation 7.3 to be true. They are, (a) oxygen reduction forming HO_2^- should have a faradaic efficiency of 100%. (b) All the HO_2^- formed is trapped inside the pores of the electrode and none diffuses into the bulk electrolyte.

The linear relationship between the quantity of HO_2^- and the pseudo-exchange current density, in a composite $NiCo_2O_4$/graphite electrode, where the decomposition of HO_2^- enhances the oxygen reduction performance, could be represented as shown in Figure 7.6. This representation is based on the concept[12], that in a graphite electrode, when $\eta = 0$, if the quantity of HO_2^- is $(HO_2^-)_G^{y,\eta=o}$ and the pseudo-exchange current density is

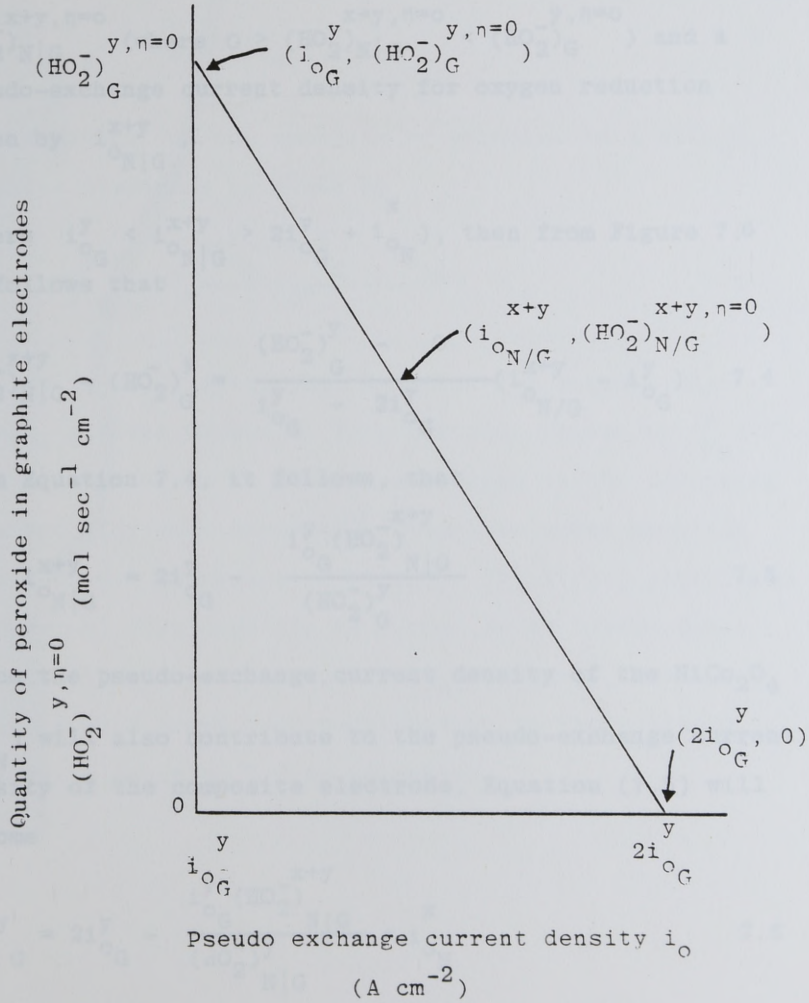

Figure 7.6: Graphical respresentation of the relationship between the quanity of peroxide and the pseudo exchange current density for oxygen reduction on graphite, in composite $NiCo_2O_4$/graphite electrodes.

$i^{y}_{o_G}$, then, when $(HO_2^-)^{y,\eta=o}_G \rightarrow 0$, $i^{y}_{o_G} \rightarrow 2i^{y}_{o_G}$. For a $NiCo_2O_4$/graphite electrode having a quantity of HO_2^-, $(HO_2^-)^{x+y,\eta=o}_{N|G}$ (where $0 > (HO_2^-)^{x+y,\eta=o}_{N|G} < (HO_2^-)^{y,\eta=o}_G$) and a pseudo-exchange current density for oxygen reduction given by $i^{x+y}_{o_{N|G}}$,

(where $i^{y}_{o_G} < i^{x+y}_{o_{N|G}} > 2i^{y}_{o_G} + i^{x}_{o_N}$), then from Figure 7.6 it follows that

$$(HO_2^-)^{x+y}_{N|G} - (HO_2^-)^{y}_G = \frac{(HO_2^-)^{y}_G - 0}{i^{y}_{o_G} - 2i^{y}_{o_G}}(i^{x+y}_{o_{N/G}} - i^{y}_{o_G}) \qquad 7.4$$

From Equation 7.4, it follows, that

$$i^{x+y}_{o_{N|G}} = 2i^{y}_{o_G} - \frac{i^{y}_{o_G}(HO_2^-)^{x+y}_{N|G}}{(HO_2^-)^{y}_G} \qquad 7.5$$

Since the pseudo-exchange current density of the $NiCo_2O_4$ ($i^{x}_{o_N}$) will also contribute to the pseudo-exchange current density of the composite electrode, Equation (7.5) will become

$$i^{x+y}_{o_{N\,G}} = 2i^{y}_{o_G} - \frac{i^{y}_{o_G}(HO_2^-)^{x+y}_{N|G}}{(HO_2^-)^{y}_{N|G}} + i^{x}_{o_N} \qquad 7.6$$

From Equations 7. 6 and 7. 3 it follows that

$$i^{x+y}_{o_{N|G}} = 2i^{y}_{o_G} - 2F(HO_2^-)^{x+y}_{N|G} + i^{x}_{o_N} \qquad 7.7$$

It should be pointed out that Equation 7.1 agrees with an ideal system, i.e. when $(HO_2^-)^{x+y}_{N|G} \rightarrow 0$, then

$$i^{x+y}_{o_{N|G}} = 2i^{y}_{o_G} + i^{x}_{o_N} \qquad 7.8$$

From Equation 7.7 the quantity of peroxide in a $NiCo_2O_4$/graphite electrode is given by

$$(HO_2^-)^{x+y}_{N|G} = \frac{2i^{y}_{o_G} + i^{x}_{o_N} - i^{x+y}_{o_{N|G}}}{2F} \qquad 7.9$$

It is to be noted that Equation 7.9 assumes that $NiCo_2O_4$ reduces oxygen to form peroxide (given by $i^{x}_{o_N}/2F$). This assumption is at present supported by the following evidence; (a) Many workers[134,135] have detected peroxide during oxygen reduction on $NiCo_2O_4$. (b) It was postulated (Chapter 6) that peroxide is formed as an intermediate during oxygen reduction on $NiCo_2O_4$. However, further analysis will prove that modification to the quantity, $i^{x}_{o_N}/2F$, in Equation 7.9 is necessary.

7.3.2 Further discussion

Figure 7.7 shows three plots, A, B and C. Plot A gives the quantity of peroxide in graphite electrodes at zero overpotential, in the absence of $NiCo_2O_4$. This plot was obtained using Equation 7.3, and the experimentally obtained $i^y_{o_G}$ values. As expected the quantity of peroxide decreased as the graphite loading ~~in~~decreased.

Plot B gives the quantity of HO_2^- in $NiCo_2O_4$/graphite electrodes. The plot was obtained using Equation 7.9 and the experimentally obtained pseudo-exchange current densities of $NiCo_2O_4$, graphite and $NiCo_2O_4$/graphite. According to Plot B, the quantity of peroxide, in $NiCo_2O_4$/graphite electrodes containing 30% and less $NiCo_2O_4$, is greater than the quantity of peroxide in the absence of $NiCo_2O_4$. However in electrodes, where the percentage of $NiCo_2O_4$ is greater than 30, the quantity of peroxide is lower than that of graphite, thus, showing expected trends. The discrepancy obtained for $NiCo_2O_4$/graphite electrode having $NiCo_2O_4$ < 30% could be explained. A greater pseudo-exchange current density in $NiCo_2O_4$/graphite electrodes compared to graphite is due to

(a) activity of $NiCo_2O_4$ for oxygen reduction, given by $i^x_{o_N}$

(b) synergism due to peroxide decomposition by $NiCo_2O_4$.

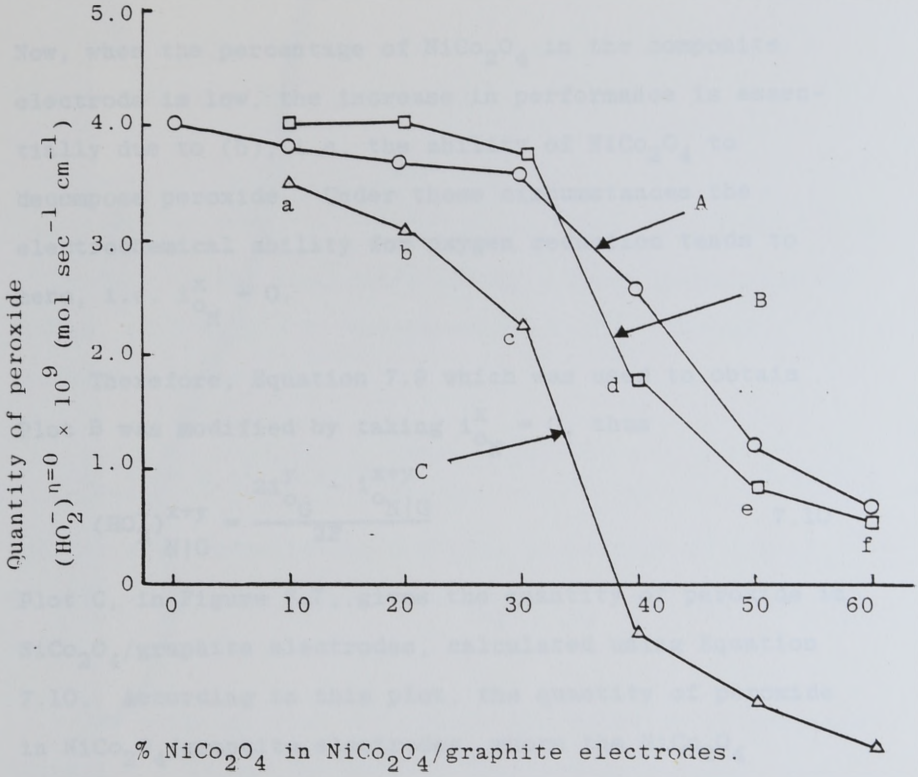

A in the absence of $NiCo_2O_4$ (equation 7.3).

B assuming $NiCo_2O_4$ to be active for electrochemical oxygen reduction (equation 7.9).

C assuming $NiCo_2O_4$ to be only active for the chemical decomposition of peroxide (equation 7.10).

a,b,c,d,e and f are the realistic quantities of peroxide.

Figure 7.7: Justification for inserting a coefficient L into the kinetic equation that predicts the quantity of peroxide at zero overpotential in composite $NiCo_2O_4$/graphite electrodes.

Now, when the percentage of $NiCo_2O_4$ in the composite electrode is low, the increase in performance is essentially due to (b), i.e. the ability of $NiCo_2O_4$ to decompose peroxide. Under these circumstances the electrochemical ability for oxygen reduction tends to zero, i.e. $i^x_{o_N} \rightarrow 0$.

Therefore, Equation 7.9 which was used to obtain Plot B was modified by taking $i^x_{o_N} = 0$, thus

$$(HO_2^-)^{x+y}_{N|G} = \frac{2i^y_{o_G} - i^{x+y}_{o_{N|G}}}{2F} \qquad 7.10$$

Plot C, in Figure 7.7, gives the quantity of peroxide in $NiCo_2O_4$/graphite electrodes, calculated using Equation 7.10. According to this plot, the quantity of peroxide in $NiCo_2O_4$/graphite electrodes where the $NiCo_2O_4$ composition is 30% and less are lower, compared to the quantity of peroxide in graphite electrodes. Furthermore, the quantity of peroxide decreases as the percentage of $NiCo_2O_4$ increases in the composite electrodes, within this range. However, the quantity of peroxide in composite electrodes, where the percentage of $NiCo_2O_4$ is greater than 30, is less than zero. This state of affairs cannot be valid. Therefore, it is argued that, as the percentage of $NiCo_2O_4$ in the composite electrode increases, $NiCo_2O_4$ reduces oxygen to form an appreciable quantity of peroxide (given by $i^x_{o_N}/2F$), thus, justifying the inclusion of $i^x_{o_N}$ in Equation 7.9.

In the light of the above discussion, Equation 7.7 is modified to a more general form

$$i_{o_{N|G}}^{x+y} = 2i_{o_G}^{y} - 2F(HO_2^-)_{N|G}^{x+y} + L\, i_{o_N}^{x} \qquad 7.11$$

For electrodes having a lower percentage of $NiCo_2O_4$ (< 30%) $L \rightarrow 0$, and therefore $L\, i_{o_N}^{x} \rightarrow 0$, and Equation 7.11 becomes

$$i_{o_{N|G}}^{x+y} = 2\, i_{o_G}^{y} - 2F(HO_2^-)_{N|G}^{x+y} \qquad 7.12$$

and for electrodes having a higher percentage of $NiCo_2O_4$ (< 40%), $L \rightarrow 1$ and therefore $L\, i_{o_N}^{x} \rightarrow i_{o_N}^{x}$ and Equation 7.7 holds.

The equation that determines the quantity of peroxide (Equation 7.9) for the $NiCo_2O_4$/graphite electrodes, when modified with the inclusion of the coefficient L, becomes

$$(HO_2^-)_{N|G}^{x+y} = \frac{2i_{o_G}^{y} + L\, i_{o_N}^{x} - i_{o_{N\,G}}^{x+y}}{2F} \qquad 7.13$$

A further conclusion that could be drawn from the above discussion relates to the mechanistic function of $NiCo_2O_4$ in composite graphite electrodes. It seems likely that function of $NiCo_2O_4$ differs depending on the graphite concentration in the electrode. With excess graphite concentration, its predominant function is peroxide decomposition, and at lower graphite concentration it has an added function of oxygen reduction, the product of

which is at least, partly, peroxide. The inactivity of $NiCo_2O_4$ for oxygen reduction at high graphite concentration may be due to, the same sites being active for peroxide decomposition and oxygen reduction. Other workers[175,176] have related the M^{2+}/M^{3+} redox system in oxides to peroxide decomposing ability and it was pointed out in the previous chapter the M^{2+}/M^{3+} sites may also be responsible for oxygen reduction.

The rest potentials and the quantity of peroxide in composite $NiCo_2O_4$/graphite electrodes; Goldstein and Tseung[12] related the peroxide ion concentration in composite $Co_xFe_{2-x}O_4$/graphite electrodes to their respective rest potentials by means of the Nernst equation and obtained good correlation. In this study although the rest potential of each $NiCo_2O_4$/graphite electrode was not related to its quantity of peroxide, a good correlation was obtained between the experimentally observed rest potentials, which increased with increase in $NiCo_2O_4$ and the calculated quantity of peroxide, which decreased with increase in $NiCo_2O_4$ in the composite electrode. This trend is shown in Figure 7.8.

The maximum performance that could be achieved on composite $NiCo_2O_4$/graphite electrodes; Plot A in Figure 7.9 gives the maximum pseudo-exchange current density that could be achieved in $NiCo_2O_4$/graphite electrodes.

Expression 7.11 was used to obtain Plot A. Also included in the figure, for comparison, the experimental pseudo-exchange current density (Plot B) that was achieved on the composite electrodes. Thus, the experimental values are very much lower than the maximum values that could be obtained.

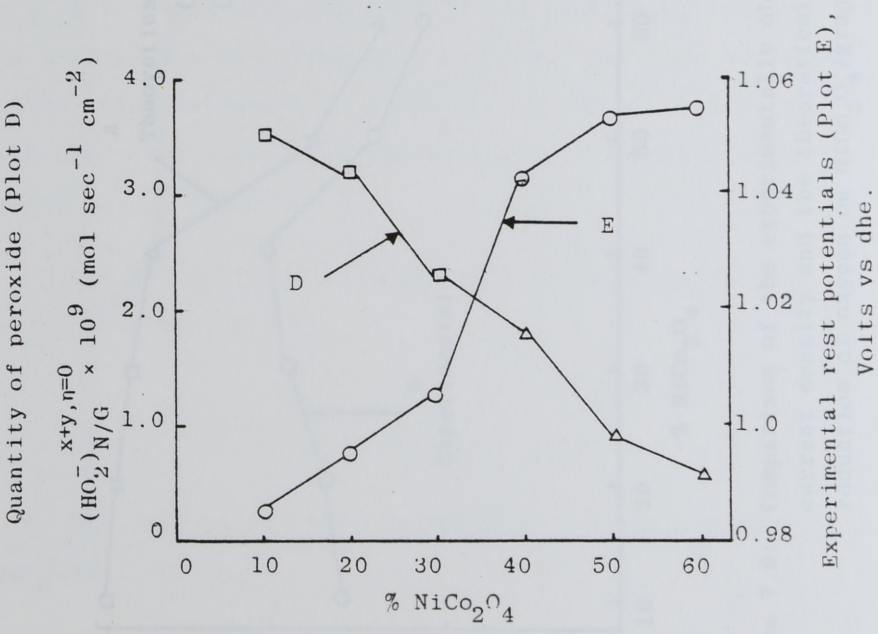

Plot D calculated from equation 7.13

(□), L → 0

(△), L → 1

Figure 7.8: Comparison of the calculated quantity of peroxide at zero overpotentials and the experimental rest potentials at 25°C for the composite $NiCo_2O_4$/graphite electrodes.

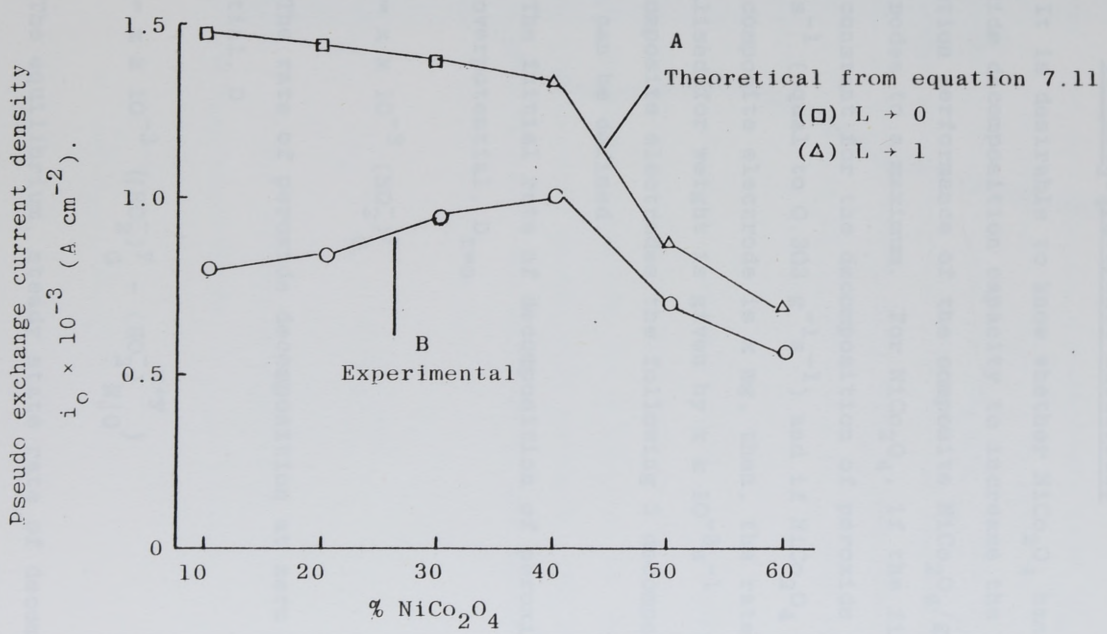

Figure 7.9: Comparison of the experimentally observed pseudo exchange current density and the theoretically predicted maximum for reduction of oxygen on $NiCo_2O_4$/graphite electrodes.

7.3.3 The Peroxide Decomposition Capacity of $NiCo_2O_4$, in $NiCo_2O_4$/graphite Electrodes

It is desirable to know whether $NiCo_2O_4$ has sufficient peroxide decomposition capacity to increase the oxygen reduction performance of the composite $NiCo_2O_4$/graphite electrodes to a maximum. For $NiCo_2O_4$, if the first order rate constant for the decomposition of peroxide is $k\ g^{-1}s^{-1}$ (equal to $0.303\ g^{-1}s^{-1}$) and if $NiCo_2O_4$ loading in a composite electrode is x mg, then, the rate constant normalised for weight is given by $x\ k\ 10^{-3}s^{-1}$. Now, for the composite electrodes the following 3 decomposition rates can be defined.

The initial rate of decomposition of peroxide at zero overpotential, $D_{t=o}$

$$= x\ k\ 10^{-3}\ (HO_2^-)^y_G \qquad 7.14$$

The rate of peroxide decomposition at zero overpotential, D

$$= x\ k\ 10^{-3}\ ((HO_2^-)^y_G - (HO_2^-)^{x+y}_{N|G}) \qquad 7.15$$

The equilibrium, steady state rate of decomposition at zero overpotential, D_{ss}

$$= x\ k\ 10^{-3}\ (HO_2^-)^{x+y}_{N|G} \qquad 7.16$$

The hypothetical rates $D_{t=o}$ and D will be expected to vary, depending on the initial quantity of peroxide. However, the equilibrium, steady-state rate, D_{ss}, will be expected to be constant. Thus, x in Equation 7.16 will be inversely proportional to $(HO_2)^{x+y}_{N|G}$. The D_{ss} values calculated using Equation 7.16 for the composite electrodes containing 10, 20 and 30 wt.% $NiCo_2O_4$ were found to be 1.1×10^{-11}, 2.0×10^{-11} and 2.0×10^{-11} mole sec^{-1} cm^{-2} respectively.

Figure 7.10 gives the calculated, percentage increase of the pseudo-exchange current density for the 30 wt.% $NiCo_2O_4$/graphite electrode, as a function of the equilibrium, steady state quantity of peroxide, $(HO_2^-)^{x+y}_{N|G}$, at zero overpotential. The increase in the pseudo-exchange current density is given by

$$i^{x+y}_{o_{N\,G}} - i^{y}_{o_G} = i^{y}_{o_G} - 2F(HO_2^-)^{x+y}_{N\,G} \qquad 7.17$$

Equation 7.17 was derived from Equation 7.12. Therefore the percentage increase is

$$= \frac{i^{x+y}_{o_{N\,G}} - i^{y}_{o_G}}{i^{y}_{o_G}} \times 100 \qquad 7.18$$

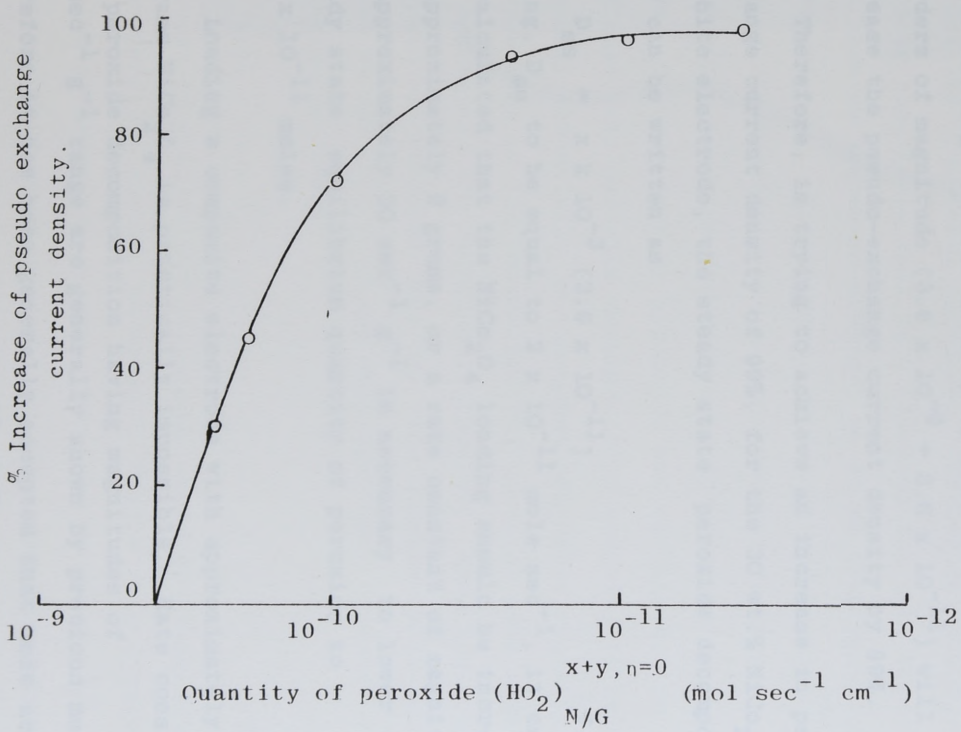

Figure 7.10: The % increase of the pseudo exchange current density for a graphite electrode (y = 70 mg cm^{-2}) as a function of its quantity of peroxide at zero overpotential.

According to Figure 7.10, the reduction of the steady state equilibrium quantity of peroxide by 1 order of magnitude ($3.6 \times 10^{-9} \rightarrow 3.6 \times 10^{-10}$) will increase the pseudo-exchange current density by 90%, and a decrease by 2 orders of magnitude ($3.6 \times 10^{-9} \rightarrow 3.6 \times 10^{-11}$) will increase the pseudo-exchange current density by 99%.

Therefore, in trying to achieve an increase in pseudo-exchange current density of 99%, for the 30 wt.% $NiCo_2O_4$/graphite electrode, the steady state peroxide decomposition rate can be written as

$$D_{ss} = x\ k\ 10^{-3}\ (3.6 \times 10^{-11}) \qquad 7.19$$

Taking, D_{ss} to be equal to 2×10^{-11} mole sec^{-1}, it could be calculated that the $NiCo_2O_4$ loading should be increased to approximately 2 grams, or a rate constant of magnitude of approximately 20 $sec^{-1}\ g^{-1}$ is necessary to lower the steady state equilibrium quantity of peroxide to 3.6×10^{-11} moles.

Loading a composite electrode with approximately 2 grams $NiCo_2O_4$ is practically impossible. Rate constant for peroxide decomposition having magnitudes of 20 $sec^{-1}\ g^{-1}$ range are generally shown by precious metals. Therefore it has been generally accepted that more active peroxide decomposition catalysts [12, 157] are required to maximise the performance of graphite electrodes.

In powders, particles are found in the form of aggregates. For oxides the aggregate diameter varies from 1 - 50 x 10^{-6}m[176]. When powders are mechanically mixed, it is the aggregates of powder that inter-mix, and not the individual particles. Therefore $NiCo_2O_4$/graphite electrodes that were prepared for this study will have an aggregate mixture, as shown diagrammatically in Figure 7.11. Furthermore, Goldstein and Tseung[176], studied the intrinsic and microstructural factors influencing peroxide decomposition activity on $Co_xFe_{3-x}O_4$, prepared by hydroxide and oxalate routes and concluded that peroxide decomposition activity to be dependent essentially on the outer aggregate specific surface area of the powder, and the internal pore area of the aggregates are relatively inactive. From their study it could be concluded that the rate constant k is proportional to the square of the mean aggregate diameter d_a, of the oxide powder

i.e. $k \propto d_a^2$ 7.20

However, if preparatory techniques could be devised to attain inter-particle mixing, as shown in Figure 7.12, rather than inter-aggregate mixing, then, the value of the rate constant could be increased. In this case the increase in the value of the rate constant, B, is given by

$$B = \frac{d_a^2}{d_p^2} \qquad 7.21$$

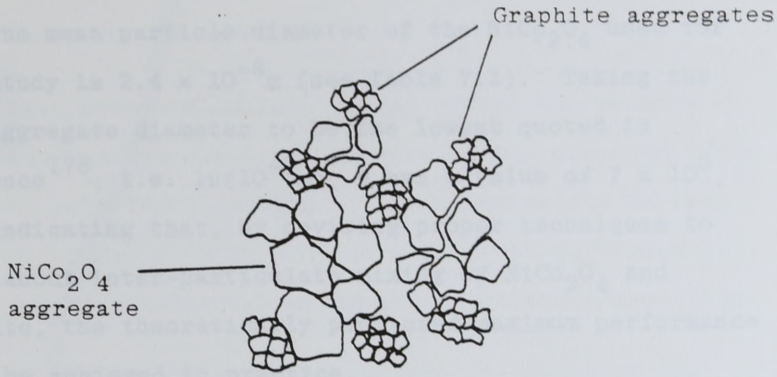

Figure 7.11: Diagrametic representation of a mixture of aggregates of $NiCo_2O_4$ and graphite powders.

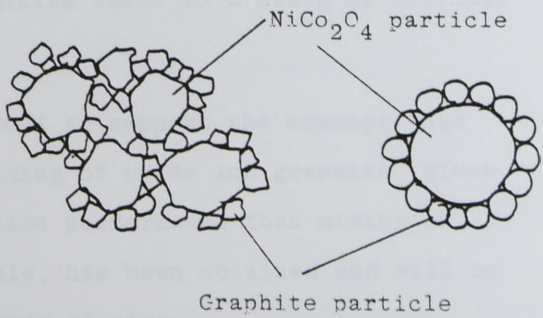

Diagrametic representation of a mixture of particles of $NiCo_2O_4$ and graphite powders.

Ideal arrangement for the calculation of A_G see section 7.3.4.

Figure 7.12

where B is the average number of particles per aggregate of $NiCo_2O_4$ and d_p is the mean particle diameter of $NiCo_2O_4$.

The mean particle diameter of the $NiCo_2O_4$ used for this study is 2.4×10^{-8}m (see Table 7.1). Taking the mean aggregate diameter to be the lowest quoted in reference[176], i.e. $1\mu(10^{-6}m)$, B has a value of 7×10^3, thus indicating that, by devising proper techniques to bring about inter-particulate mixing of $NiCo_2O_4$ and graphite, the theoretically predicted maximum performance could be achieved in practice.

Therefore, the equilibrium, steady state, rate of peroxide decomposition, at zero overpotential, for the $NiCo_2O_4$/graphite (or for any peroxide decomposition catalyst/graphite) system could be written as

$$D_{ss} = xk10^{-3}(1 + B) \quad (HO_2^-)^{x+y}_{N|G} \qquad 7.22$$

when the aggregate mixing tends to a state of intimate particulate mixing.

Experimental proof to support the concept that intimate particle mixing of oxide and graphite gives better oxygen reduction performance than mixing of aggregates of particle, has been obtained and will be described later in this chapter.

7.3.4 Factors that Govern the Attainment of Ideal Structure and Maximum Performance of Composite Oxide/Graphite

These factors are

(a) Inter-particulate mixing of the two powders

(b) Maximum electrode loading of the graphite. The electrode loading of the oxide should be such that, it will provide sufficient particles to be completely surrounded by graphite particles.

If the ideal inter-particulate structure of the $NiCo_2O_4$ and graphite can be represented as spherical spheres as shown in Figure 7.12, the number of smaller graphite particles, A_G, that surround a large $NiCo_2O_4$ particle is given by

$$A_G = \frac{4\pi(r_N + r_G)^2}{\pi r_G^2} \qquad 7.23$$

where r_N and r_G are the mean radii of the $NiCo_2O_4$ and graphite particles respectively. Assuming that $r_G^2 < r_N r_G << r_N^2$

$$A_G = \frac{4r_N^2}{r_G^2} \qquad 7.24$$

The ratios of the weight of the two powders, W_G/W_N, that will form the ideal arrangement as in Figure 7.12, is

$$\frac{W_N}{W_G} = \frac{r_N^3 \, P_N}{A_G \, r_G^3 \, P_G} \qquad 7.25$$

where, P_G and P_N are the densities of graphite and $NiCo_2O_4$ respectively. Equation 7.25 relates the particle characteristics that determine ideal distribution.

Table 7.1 gives the particle characteristics of $NiCo_2O_4$ and graphite. These characteristics were obtained from the experimentally determined specific surface areas and the densities of the two powders. A_G calculated using Equation 7.24 was found to be 38. The weight percent of $NiCo_2O_4$ that will have an 100% attainment of ideal arrangement was found to be 28.

If a hypothetical quantity E can be defined as the percentage of particles that can form the ideal arrangement in a $NiCo_2O_4$/graphite mixture. E can achieve a value of 100 for a 28 wt. percent $NiCo_2O_4$/graphite mixture. When the wt. percent of $NiCo_2O_4$ is less than 28, $NiCo_2O_4$ particles will limit the formation of the ideal arrangement. Thus,

$$E = \frac{\text{wt.\% } NiCo_2O_4}{28} \times 100 \qquad 7.26$$

However, when the wt. percent of $NiCo_2O_4$ exceeds 28, then the amount of graphite particles will limit the formation of the ideal arrangement, thus

$$E = \frac{\text{wt.\% graphite}}{72} \times 100 \qquad 7.27$$

Table 7.1: Mean Particle Characteristics of the $NiCo_2O_4$ and Graphite Powders.

Particle Characteristics	Formula	$NiCo_2O_4$	Graphite
Specific surface area $S\ (m^2\ g^{-1})$	Experimental	43	490
Denisty $\rho\ (g\ M^{-3})$	Experimental	5.81	1.57
Mean radius of particles $r_p\ (M)$	$\frac{3}{sp}$	1.2×10^{-8}	0.39×10^{-8}
Mean surface area of particles $a_p\ (M^2)$	$4\pi r_p^2$	1.81×10^{-15}	1.91×10^{-16}
Mean volume of particles $v_p\ (M^3)$	$\frac{4}{3}\pi r_p^3$	7.24×10^{-24}	2.48×10^{-25}
Mean mass of particles $m_p\ (g)$	$v_p \times p$	4.21×10^{-17} g	3.9×10^{-19}

Figure 7.13 gives the variation of E for different $NiCo_2O_4$/graphite ratios. Also included in the figure, for comparison, is the maximum pseudo-exchange current density that could be achieved on composite electrodes made of diffent ratios of the powders. Therefore, it could be seen from Figure 7.13 that the ideal performance predicted by electrochemical studies could be achieved by inter-particle mixing of the two powders.

The required characteristics of the oxide catalyst; this study has indicated that the electrochemical performance of the oxide does not contribute appreciably to the performance of the composite electrodes (that have low wt. percent oxides) of practical importance. Therefore, an oxide which is active for peroxide decomposition only is sufficient. It is also desirable for the oxide to have a low electrical resistivity (< 100 ohm-cm). The specific surface area of the oxide should be high, so that the W_G/W_N ratio (Equation 7.25) will be high, if this is so, the weight of oxide in the composite electrode can be minimized. The preparatory temperature of the oxide should be low (< $400^{o}C$) so that it could be prepared in a high surface area form, uniformly mixed with the graphite particles. Spinel oxides are known to have the above mentioned properties.

Techniques that could bring about an intimate contact of the oxide and graphite particles; an intimate mixing of the graphite and the oxide powders could be achieved

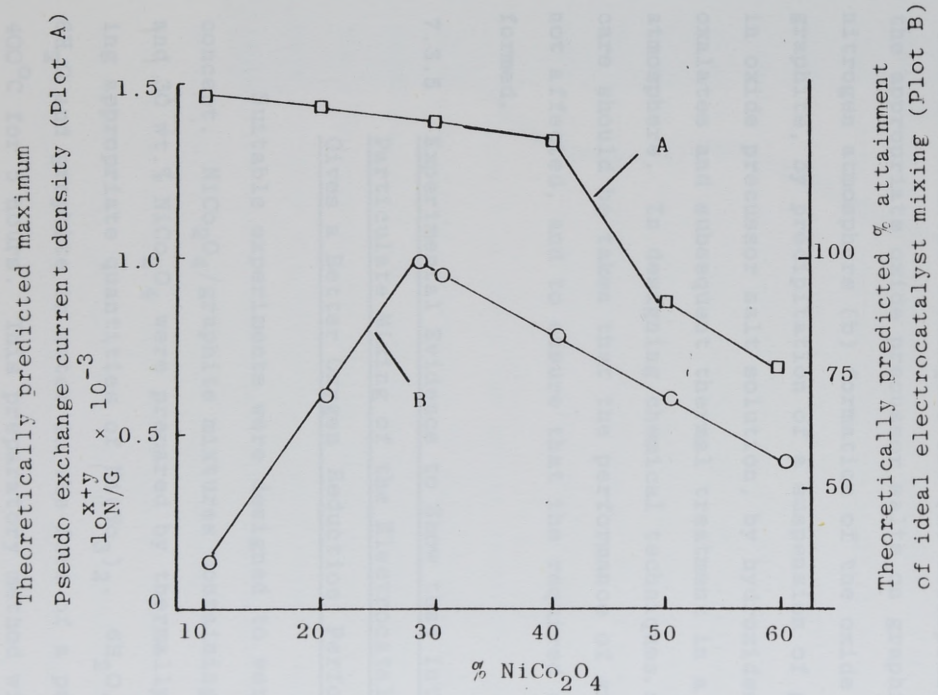

Figure 7.13: Comparison of the theoretically predicted percentage attainment of ideal electrocatalyst mixing of $NiCo_2O_4$ and graphite powders and the theoretically predicted maximum pseudo exchange current densities for the $NiCo_2O_4$/graphite electrodes.

either mechanically of chemically. A mechanical method is to ball mill a mixture of the oxide and graphite (low surface area) in a vibratory ball mill[158] for 10 - 14 hours. The oxide required for this purpose is prepared initially in a high surface area form[113, 116, 118]. Possible chemical techniques are (a) decomposition of the appropriate oxide precussor salts on graphite, in a nitrogen atmosphere (b) formation of the oxide on graphite, by precipitation of a suspension of graphite in oxide precussor salt solution, by hydroxides or oxalates and subsequent thermal treatment in a nitrogen atmosphere. In designing chemical techniques, sufficient care should be taken that the performance of graphite is not affected, and to ensure that the required oxide is formed.

7.3.5 Experimental Evidence to Show that Inter Particulate Mixing of the Electrocatalysts Gives a Better Oxygen Reduction Performance

Suitable experiments were designed to verify this concept. $NiCo_2O_4$/graphite mixtures containing 10 wt.% and 30 wt.% $NiCo_2O_4$ were prepared by thermally decomposing appropriate quantities of $Ni(No_3)_2 \cdot 6H_2O$, $Co(No_3)_2 \cdot 6H_2O$ and graphite in water in the form of a paste, at 400°C for 5 hours. This preparatory method will bring about an intimate mixing of the particles of the two electrocatalysts. Thermal treatment was carried out in a N_2 atmosphere, since graphite was found to ignite

when it was heated in air at 400°C. FEP bonded electrodes (electrocatalyst loading ∿ 15 mg cm^{-2}) of the two mixtures were fabricated and their electrochemical performances for oxygen reduction were evaluated in air, in 5 mol dm^{-3} KOH at 25°C. $NiCo_2O_4$ was also prepared under the same conditions and a suspension of graphite in water was also thermally treated under the same condition. FEP bonded electrodes of the $NiCo_2O_4$ and graphite powders, and a mechanical mixture of the two powders containing 10 and 30 wt.% $NiCo_2O_4$ were fabricated. The electrocatalyst loading of each of the 4 electrodes was ∿ 15 mg cm^{-2}. The oxygen reduction performance of the 4 electrodes were evaluated under the same conditions.

Figure 7.14 gives the oxygen reduction performance of 6 electrodes, according to which the electrochemical performance of the composite electrodes fabricated from the electrocatalysts having inter particulate mixing, gave a higher electrochemical performance than the respective electrodes where the electrocatalysts were mechanically mixed. This experimental evidence shows that when the oxide and the graphite powders are in a state of inter particulate mixing a considerable enhancement in performance could be obtained.

An experimental investigation carried out recently by Chou[177], in the author's laboratory confirmed the doubling of the pseudo-exchange current density for oxygen reduction on a composite electrode compared to

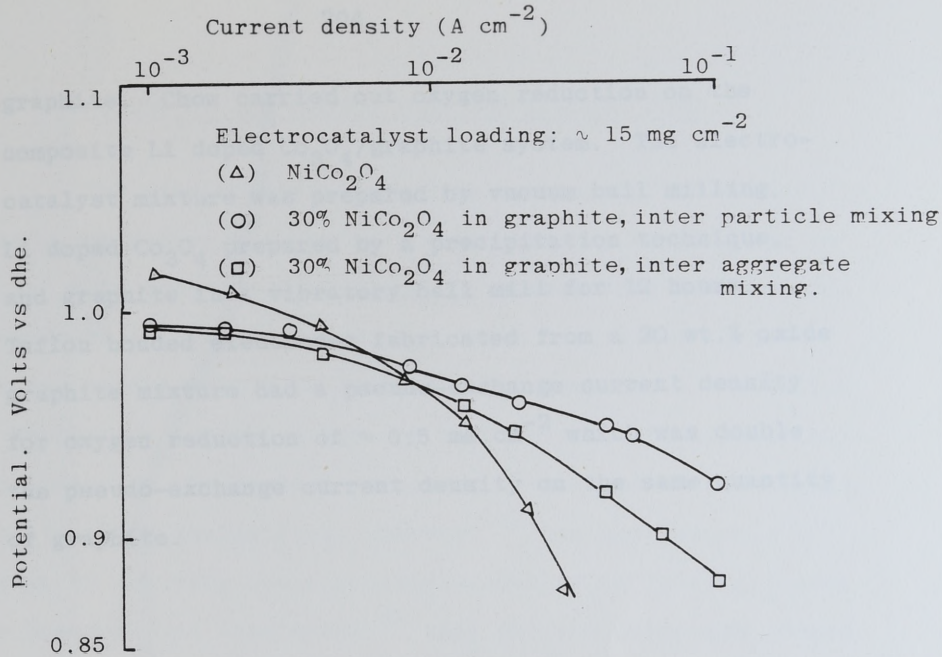

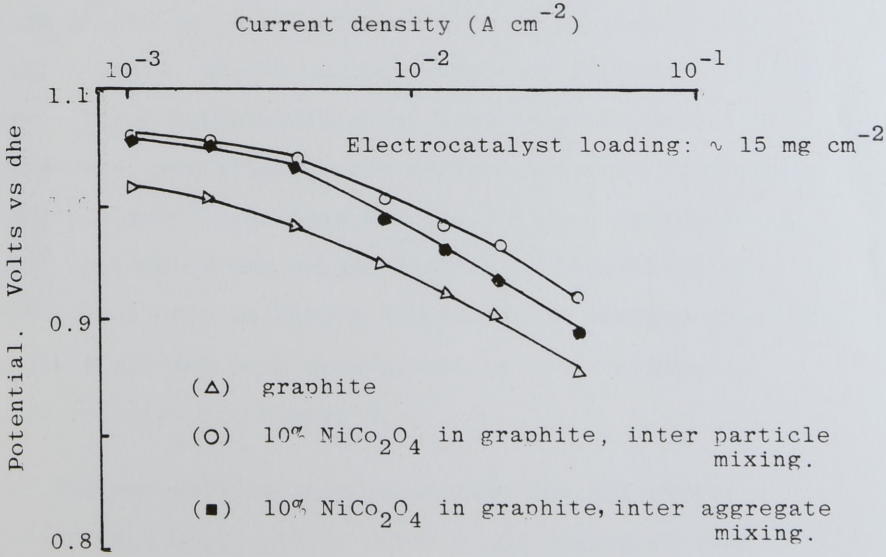

Figure 7.14: Evidence to show that inter particle mixing of electrocatalysts gives better oxygen reduction performance than inter aggregate mixing of electrocatalyst in composite electrodes (5 mol dm^{-3} KOH, air 25°C, FEP bonded electrodes).

graphite. Chow carried out oxygen reduction on the composite Li doped Co_3O_4/graphite system. The electrocatalyst mixture was prepared by vacuum ball milling, Li doped Co_3O_4 prepared by a precipitation technique, and graphite in a vibratory ball mill for 12 hours. Teflon bonded electrodes fabricated from a 20 wt.% oxide graphite mixture had a pseudo-exchange current density for oxygen reduction of ~ 0.5 mA cm^{-2} which was double the pseudo-exchange current density on the same quantity of graphite.

CONCLUSIONS AND SUGGESTIONS FOR FURTHER WORK

The electrochemical studies carried out at potentials below which oxygen evolution takes place on $NiCo_2O_4$ and on 4 at. % Li doped Co_3O_4 (chapter 3) showed that surface compounds of oxidation states of 3 and 4 are formed on both oxides before oxygen is evolved. The compound of oxidation 4 decomposes to give oxygen on both oxides. It is difficult to indentify the surface compounds by analytical techniques due to their instability. Hibbert[107] has conclusively shown by carrying out experiments similar to that performed by Rosental and Veselovskii[49] that surface compounds formed on $NiCo_2O_4$ decompose to give oxygen. However, similar types of experiments could also be carried out to confirm the oxidation states of the surface compounds formed on the two oxides. These experiments could involve polarising the electrodes at potentials where surface compound formation is complete in O^{18} enriched KOH electrolyte, and relating the O^{18} content of the oxygen evolved in unenriched KOH electrolyte to the oxidation states of the surface compounds which have already been established by electrochemical studies reported in Chapter 3.

The mechanistic studies carried out for oxygen evolution on $NiCo_2O_4$ and Li doped Co_3O_4 suggested that trivalent ions of Ni and Co are more active for oxygen evolution rather than the divalent ones. Mechanisms were proposed for both $NiCo_2O_4$ and 10 at. % Li doped Co_3O_4 and

these mechanisms were confirmed by reaction order studies. It could be stated that the mechanism on $NiCo_2O_4$ is

$$S + OH^- \rightarrow SOH + e$$

$$SOH + OH^- \rightarrow SO + H_2O + e$$

$$SO + S' \rightarrow S\overset{O}{\diagup\diagdown}S'$$

$$2\,S\overset{O}{\diagup\diagdown}S' \rightarrow 2S + 2S' + O_2$$

However, due to the high trivalent concentration of cations in 10 at. % Li doped Co_3O_4 step 2 and 3 had to be modified into

$$SOH + OH^- \rightarrow SO^- + H_2O$$

$$SO^- + S' \rightarrow S\overset{O}{\diagup\diagdown}S' + e$$

Further, the oxygen evolution performance of 10 at. % Li doped Co_3O_4 was found to be very good; Teflon bonded electrodes of 10 at. % Li doped Co_3O_4 gave an oxygen evolution performance of 1 A cm^{-2} at 1.52V vs dhe at 70^oC in 5 mol dm^{-3} KOH.

The percentage values of the Li dopant for the spinel oxides of Co (4,7 and 10 at .%) reported in this work are nominal percentages of Li. Previous work carried out on Li doped NiO by Tseung and Bevan[113] showed that the quantity of Li that enters the NiO lattice is always less

than the nominal quantity added during preparation. The difference is found as free Li on the surface. Therefore, chemical analysis similar to that carried out for Li doped NiO[113] should be carried out to estimate the percentage of Li that has been incorporated in to the Co_3O_4 lattice. A knowledge of this quantity will enable the quantitative linking of the percentage of Li in the lattice of Co oxides to the oxygen evolution performance.

This work also has produced experimental evidence based on 6 oxides, to show that minimum potential of oxygen evolution is governed by the magnitude of the lower oxide/ higher oxide couple. However the oxygen evolution performance will also depend on the magnitude of the Tafel slope. It will be very useful if the Tafel slopes of the six oxides reported in this work are analysed in relation to properties of the active site in each case. Such work will be similar to that carried out for $NiCo_2O_4$ and for the Li doped Co oxide reported in Chapters 3 and 4. General conclusions that could be drawn linking the Tafel slope to site properties will be useful in the selection of transition metal oxides for oxygen evolution.

Although the effectiveness factor of FEP bonded porous electrodes were found to be higher than non hydrophobic bonded porous electrodes, the effectiveness factor of FEP bonded electrodes was only in the region of 30-35%. However the effectiveness factor for hydrogen evolution on Teflon

bonded Pt black electrodes[168] was found to be 50-55%. Since the lower efficiency of the oxygen evolving electrode cannot be attributed to the difference in the type of hydrophobic binder, further optimisation studies could lead to increased performance.

Oxygen reduction studies carried out on $NiCo_2O_4$ suggested that the mode of oxygen adsorption is end on. A suitable mechanism has been proposed for oxygen reduction on $NiCo_2O_4$, which postulates the formation of peroxide as an intermediate. This mechanism was proposed by considering the different nature of the sites on $NiCo_2O_4$, the experimentally obtained electrochemical parameters, and some mechanistic evidence provided by literature. In this study it was assumed that oxygen adsorption is under limitingly low Langmuir conditions. This should be confirmed experimentally by transient oxygen stripping studies, similar to that reported in literature[154,187].

The work carried out on composite $NiCo_2O_4$/graphite electrodes indicated that if the two electrocatalyst powders are mixed so as to bring about inter particulate contact, then, the maximum oxygen reduction performance that is predicted by theory, could be achieved in practice. Recently Chou[177] mixed Li doped Co_3O_4 and graphite by a ball milling technique and carried out oxygen reduction studies on the mixed powders, and obtained the maximum efficiency for

oxygen reduction on the 20 wt.% Li doped Co_3O_4/Graphite mixture. Further work in this aspect will require studies to ascertain the stability of the oxygen reduction performance and the electrodes structure of the composite electrodes, on a long term basis.

REFERENCES

1. D.Gregory, P.J.Anderson, R.J.DuFour, R.H.Elkins, W.J.D.Escher, R.B.Foster, G.M.Long,J.Wurm and G.G.Yie, "The Hydrogen Energy System, prepared for American Gias Association by I.G.T., 1973.

2. J.O'M.Bockris in T.Nefat Veziroglu (Ed.), Hydrogen Energy, Port A, Plenum Press, 1975, p.371.

3. W.E.Winsche, E.C.Hoffman and F.J.Salzano, Secience 180, 1325 (1973).

4. R.R.Reeves and C.S.Girant in T.N.Veziroglu, K.Fueki and T.Ohta (Eds.) Hydrogen Energy Progress, Vol.4, Perganon Press 1981, p.1785.

5. T.Takahashi. in T.Ohta (Ed.), Solar-Hydrogen Energy Systems, Pergamon Press, 1979, p.35.

6. A.T.Kuhn, New Scientist, 36, 21 (1971).

7. A.C,C,Tseung, P.Rasiyah, M.C.M.Man and K.L.K.Yeung in Hydrogen as an Energy Vector, Commision of European Communities, (1980), p.199.

8. A.C.C.Tseung and S.C.Dhara, Electrochim. Acta 20, 681 (1975).

9. J.A.Bett, K.Kinoshita and P.Stonehart, J. of Catalysis 35, 307 (1974).

10. K.Kordesh. Austrian Patent No. 168 040 (1951).

11. K.Kordesh and F.Martinola, Monatsh., 84, 39 (1953).

12. J.R.Goldstein and A.C.C.Tseung, J.Physical Chem., 76, 3646 (1972).

13. M.Davis, M.Clark, E.Yeager, F.Hovorka, J. Electrochem. Soc., 106, 56 (1959).

14. A.C.C.Tseung and H.L.Bevan, Electroanalytical Chemistry and Interfacial Electrochemistry, 45, 429 (1973).

15. A.C.C.Tseung, B.S.Hobbs and A.D.S.Tantrain, Electrochim. Acta, 15, 473 (1970).

16. S.Gilman in A.J.Bard (Ed.), Electroanalytical Chemistry, Vol.2, Marcel Dekker, (1967).

17. S.Gilman, Electrochim. Acta, 9, 1205 (1964).

18. H.A.Laitinen and C.G.Enke, J.Electrochem. Soc., 107, 773 (1960).

19. W.Wisscher and M.A.V.Devanathan, J. Electroanal. Chem., 8, 127 (1964).

20. D.Gilroy and B.E.Conway, Can.J.Chem., 46, 2571 (1973).

21. J.W.Schultze and K.J.Vetter, Ber. Bunsenges Phys. Chem., 75, 470 (1971).

22. D.Dickertmann, J.W.Schultze and K.J.Vetter, J.Electroanal. Chem. 55, 429 (1974).

23. S.Shibata, Bull. Chem. Soc. Japan, 38, 1330 (1965).

24. A.Hickling and G.Vrjosek, Trans. Faraday Soc., 57, 123 (1961).

25. W.Bold and M.W.Breiter, Electrochem. Acta., 5, 169 (1961).

26. J.Llopis, I.M.Tordesillas and J.M.Alfayate, Electrochim. Acta, 11, 57 (1967).

27. J.Llopis, J.M.Giamboa and J.M.Alfayate, Electrochim. Acta, 12, 57 (1967).

28. D.A.J.Rand and R.Woods, J.Electroanal. Chem., 36, 57 (1972).

29. R.Woods, Electrochim. Acta, 16, 655 (1971).

30. U.R.Evans, Nature, 126, 130 (1930).

31. J.Kruger and J.P.Calvert, J.Electrochem. Soc., 114, 43 (1967).

32. B.Kabanov, R.Burshtein and A.N.Frunikin, Discussions Faraday Soc., 1, 259 (1947).

33. U.R.Evans. The Corrosion and Oxidation of Metals, Arnold (1960).

34. S.E.S.El.Wakkad, H.A.Rizk, and I.G.Ebaid, J.Phys. Chem., 59, 1004 (1955).

35. H.J.Boosz, Metall., 11, 511 (1957).

36. H.A.Johansen, G.B.Adams and P.Van Rysselberghe, J.Electrochem. Soc., 104, 339 (1957).

37. M. Stern and H.Wissenberg, J.Electrochem. Soc., 106, 755 (1959).

38. R.I.Agladze, and A.E.Legran, Zhur. fiz. Khim., 24, 1122 (1950).

39. G.W.D.Briggs, E.Jones, and W.F.K.Wynne-Jones, Trans. Faraday Soc., 62, 3217 (1966).

40. D.E.Davis and W.Barker, Corrosion, 20, 47 (1964).

41. R.D.Cowling and A.C. Riddiford, Electrochim. Acta. 14, 981 (1969).

42. K.Behl Wishvender and Jorge E. Toni, J. Electroanal. Chem. 31, 63 (1971).

43. T.P.Hoar, Proc. 8th Meeting CITCE, Madrid 19 56, Butterworths, London (1958).

44. M.Breiter in P.Delahay (Ed.), Advances in Electrochemistry and Electrochemical Engineering, Vol.1, Interscience,(1961),p.123.

45. W.Latimer, Oxidation states of Elements, MeGraw-Hill, NY. (1952), p.39

46. T.P.Hoar, Proc. Roy. Soc. (London) A142, 628, (1933).

47. J.O'M. Bockris, J.Phys.Chem., 24, 817 (1956).

48. A.Damjanovic, A.Dey and J.O'M.Bockris, Electrochim. Acta, 11, 791 (1966).

49. K.I.Rosental and V.I.Veselovskii, Doklady Akad. Navk S.S.S.R., 111, 637 (1956).

50. A.C.Riddiford, Electrochim. Acta 4, 170 (1961).

51. A.J.Krasilshichikov, Zh. fiz. Khim, 37, 531 (1963).

52. W.H.Wade and N.Hackerman, Trans. Faraday Soc., 53, 1636 (1957).

53. B.E.Conway and M.Saloman, Electrochim. Acta, 9, 1599 (1964).

54. J.O'M Bockris. in J.O'M. Bockris and B.E.Conway (Eds.), Modern Aspects of Electochemistry, Vol.1., Butterworths (1954) p.180.

55. E.Gileadi in J.O'M. Bockris and B.E.Conways (Eds.), Modern Aspects of Electrochemistry, Vol.3, Butterworths (1964) p.347.

56. B.E.Conway and P.L.Bourgault, Can.J.Chem., 40, 1960 (1962).

57. B.E.Conway and P.L.Bourgault, Trans. Faraday Soc., 58, 593 (1962).

58. A.Damjanovic in J.O'M. Bockris and B.E.Conway (Ed.), Modern Aspects of Electrochemistry, Vol.5., Plenum Press (1969), p.369.

59. J.P.Hoare. The Electrochemistry of Oxygen, Interscience, (1968).

60. J.O'M. Bockris and S.Srinivasan. Fuel Cells: Their Electrochemistry, McGraw Hill, (1969).

61. J.P.Hoare in P.Delahay (Ed.), Advances in Electrochemistry and Electrochemical Engineering, Vol.6., Interscience, 1967, p.201.

62. Tibor Erdey-Cruz. Kinetics of Electrode Processes, Adam Hilger Ltd., London, (1972).

63. C.Iwakura, K.Kukuda and H.Tamura, Electrochim. Acta, 21, 501 (1976).

64. G.Fiori, L.Formaro, C.M.Mari, P.V.Scolari and L.Vago in Seminar on Hydrogen as an Energy Vector, Commison of The European Communities, Luxembourg, (1978), p.194.

65. M.Morita, C.Iwakura and H.Tamura, Electrochim. Acta, 22, 325 (1977).

66. W.O'Grady, C.Iwakura, J.Huang And E.Yeager in M.W.Breiter (Ed.), Electrocatalysis, The Electrochemical Society, Princeton,(1974), p.284.

67. C.Iwakura, H.Tada and H.Tamura, Denki Kagaku, 45, 202 (1977).

68. Y.Motsumoto and E.Sato, Electrochim. Acta, 24 421 (1979).

69. Y.Matsumoto, H.Manabe and E.Sato, J. Electrochem. Soc., 127, 811 (1980).

70. Y.Matsumoto, H.Kurimoto and E.Sato, J.Electroanal. Chem., 102, 77 (1979).

71. J.Orehotsky, H. Huong, C.R.Davidson and S.Srinivasan, J.Electroanal. Chem. 95, 233 (1979).

72. S.Trasatti in E.Vecchi (Ed.), Proceeding of the 31st Meeting of the International Society of Electrochemistry, International Society of Electrochemistry, (1980), p.115.

73. B.E.Conway and E.Gileadi, Trans. Faraday Soc. 58, 2493 (1962).

74. E.Gileadi and B.E.Conway, J.Chem. Phys., 39, 3420 (1963).

75. G.Lodi, E.Sivieri, A de Battisti and S. Trasatti, J. Appl. Electrochem 8, 135 (1978).

76. R.U.Bondar and E.A.Kalinovskii, Electrokhimiya 14, 470 (1978).

77. D.V.Kokoulina, Yu. I.Frasovitskaya and V.T.Ivanova, Electrokhimiya 14, 470 (1978).

78. A.C.C.Tseung and S.Jasem, Electrochim. Acta, 22, 31 (1977).

79. H.Vandenborre and R. Leysen in E. Vecchi (Ed.), Proceedings of the 31st Meeting of the International Society of Electrochemistry, International Society of Electrochemistry,(1980), p.319.

80. G.Singh, M.H.Miles and S.Srinivasan in Electrocatalysis on Non-Metalic Surfaces, NBS special publication 455, (1975), p.289.

81. B.N.Efremov and S.R.Zhukov in II All-Union Conference on Electrocatalysis (Abstracts), Moscow, (1978), p.39.

82. S.M.Jasem and A.C.C.Tseung, J.Electrochem. Soc., 126, 1352 (1978).

83. P.Rasiyah, A.C.C.Tseung and D.B.Hibbert, J. Electrochem. Soc., 129, 1724 (1982).

84. M.H.Mites, Y.H.Huang and S.Srinivasan, J.Elechem. Soc., 125, 1931 (1978).

85. B.Cossec, J.Inor. Nucl. Chem., 8, 483 (1958).

86. J.W.Mellor. A Comprehensive Treatise on Inorganic and Theoretical Chemistry, Vol. XIV, (1957), p.558.

87. J.P.Suchet, Chemical Physics of Semiconductors, D.Van Nostrand, (1965), p.85.

88. L.Brewer, Chem. Rev., 52, 1 (1953).

89. Temkin, Zh. Fiz. Khim, 15, 296, (1941).

90. J.G.N.Thomas, Trans. Faraday Soc., 57, 1603 (1961).

91. A.C.C.Tseung, P.Rasiyah and D.B.Hibbert, Provisional British Patent Application No.804483,(1980).

92. A.C.C.Tseung, S.Jasem and M.N.Mahmood in T.N.Viziroglu and W.Zeifritz (Eds.), Hydrogen Energy Systems, Vol.1, Pergamon Press,(1978), p.214.

93. A.Hickling and S.Hill, Discussion Faraday Soc., 1, 236 (1974).

94. P.Ruetshi and P.Delahay, J.Chem.Phys., 23, 560, (1955).

95. A.K.Vijh, Electrochim. Acta., 17, 91 (1972).

96. K.J.King and A.C.C.Tseung, Electrochim. Acta., 19, 493 (1974).

97. M.Pourbaix. Atlas d'Equilibres Electrochemiques a 25°C, Gauthiers - Villars, Paris (1963).

98. V.M.Novakovskii and Yu.A.Likhachev, Zash. Metall, 7, 514 (1971).

99. J.E.O.Mayne and J.W.Menter, J.Chem. Soc. (1954),99.

100. M.Morita, C.Iwakura and H.Tamura, Electrochim, Acta, 23, 331 (1978).

101. M.Morita, C.Iwakura and H.Tomura, Electrochim. Acta, 24, 357 (1979).

102. G.Beni, L.M.Schiavone, J.L.Shay and W.C.Dautremont-Smith, Extended Abstracts, Electrochemical Society Meeting 80-1 (1980) p.1226.

103. C.Iwakura, K.Hirao and H.Tamura, Electrochim, Acta., 22, 335 (1977).

104. P.W.T.Lu and S.Srinivasan in S.Srinivasan, F.J.Salzano and A.R.Landgrebe (Eds.), Proceedings of the Symposium on Industrial Water Electrolysis, The Electrochemical Society, (1978), p.77.

105. J.P.Hoare, J.Electrochem Soc., 111, 610 (1964).

106. S.E.S.El. Wakkad and A.M.S.El. Din, J. Chem. Soc., (1954), 3094.

107. D.B.Hibbert, J. Chem. Soc. Chommun., 202 (1980).

108. Marcel Pourbaix. Lectures on Electrochemical Corrosion, Plenum Press, (1973).

109. A.K.Vijh, Electrochim. Acta, 14, 921 (1969).

110. L.J.J.Janssen, L.M.C.Starmans, J.G.Visser and E.Barendrecht. Electrochim. Acta., 22, 1093 (1977).

111. B.V.Tilak, J. Electrochem. Soc., 126, 1343 (1979).

112. G.Faita and G.Fiori, J.Appl. Electrochem, 2, 31 (1972).

113. A.C.C.Tseung and H.L.Bevan, J.Mater Sci., 5, 604 (1970).

114. J.Kelly, D.B.Hibbert and A.C.C.Tseung, J.Mater. Sci., 13, 1053 (1978).

115. D.B.Hibbert and A.C.C.Tseung, J. Mater. Sci. 14, 2665 (1979).

116. A.C.C.Tseung and J.R.Goldstein. J.Mater. Sci. 13, 531 (1973).

117. K.Kinoshita and P.Stonehart in J.O'M. Bockris and B.E.Conway (Eds.), Modern Aspects of Electrochemistry, No.12, Plenum Press, (1977), p.183.

118. T.Sato, M.Sugihara and M.Saito, Rev. Elec.Comm. Lab., 11, 26 (1963).

119. P.R.Vassi and A.C.C.Tseung, Electrochim. Acta., 20, 763 (1975).

120. B.S.Hobbs, P.R.Vassi and A.C.C.Tseung in J.D.Thornton (Ed.), Electrochemical Engineering Symposium, Institute of Chemical Engineers, 1, 123 (1971).

121. J.O'M. Bockris and A.K.M.S.Haj, Pro. Roy. Soc. (London), A 237, 277 (1956).

122. N.Watanabe and M.A.V.Devanathan, J. Electrochem. Soc., 111, 615 (1964).

123. J.P.Hoare, J.Electrochem. Soc., 109, 858 (1962).

124. M.Foex, Comptes Rend., 227, 193 (1948).

125. E.R.S.Winter, J. Catalysis, 6, 35(1966).

126. K.L.K.Yeung and A.C.C.Tseung, J. Electrochem. Soc., 125, 1660 (1978).

127. E.Yeager in Electrocatalysis on Non-Metalic Surfaces, NBS special publication 455, (1975), p.203.

128. J.S.Griffiths, Proc. Roy. Soc., A235, 23 (1956).

129. L.Pauling, Nature, 203, 182 (1964).

130. W.J.King and A.C.C.Tseung, Electrochim. Acta, 19, 485 (1974).

131. A.C.C.Tseung and K.L.K.Yeung, J. Electrochem. Soc., 125, 1003 (1978).

132. N.I.Ryasintseva, E.I.Khrusheva, N.A. Sumilova and A.M.Turnov, Elektrokhimiya 10, 822 (1974).

133. A.M.Trunov, V.A.Presnov, M.V.Uminskii, O.K.Rakityanskaya, T.S.Bakutina and A.N.Kotseruba, Elektrokhimiya 11, 552 (1975).

134. M.R.Tarasevich, V.S.Vilinskaya, A.M.Khutornoi, R.Kh.Burshtein, F.V.Makordei and Yu.A.Tkach, Elektrokhimiya 12, 504 (1976).

135. V.S.Bagotzky, N.A.Shumilova and E.I.Khrushchera, Electrochim. Acta, 21, 919 (1976).

136. M.Savy, Electrochim. Acta, 13, 1359 (1968).

137. E.I.Khrusheva, O.V.Moravskaya, N.A.Shumilova and I.I.Astakhov, Elektrokhi miya 14, 907 (1978).

138. R.Kh.Burshtein, M.R.Tarasevick, A.M.Khutornoi, V.S.Vilinskaya, F.Z. Sabirov, I.I.Astakhov and G.L.Teplitskaya, Elektrokhimiya 11, 1064 (1975).

139. D.M.Meadowcroft, Nature 226, 847 (1960).

140. T.Kudo, H.Obayashi and T.Giefo, J.Electrochem. Soc., 122, 159 (1975).

141. E.R.van Buren, G.H.J.Broers, A.J.Bouman, and C.Boesveld, J. Electroanal. Chem., 87, 389 (1978).

142. T. Kudo, H. Obayashi and M. Yoshida, J. Electrochem. Soc., 124, 321 (1977).

143. Y. Matsumoto, H. Yoneyama and H.Tamura, J. Electroanal. Chem., 79, 319 (1977).

144. Y. Matsumoto, H. Yoneyama and H. Tamura, Bull,Chem. Soc., Jap., 51, 1927 (1978).

145. J.P.Hoar, J. Electrochem. Soc., 112, 849 (1965).

146. J.L.Lambert, J.Chem. Educ., 41, (1964).

147. O.Holmes and D.S.McClure, J.Chem.Phys., 26, 1686 (1956).

148. J.D.Dunitz and L.E.Orgel, J.Phys. Chem. Solids 3, 318 (1957).

149. D.S.McClure, J.Phys.Chem. Solids 3, 311 (1957).

150. J.E.Huheey. Inorganic Chemistry, Haper and Row, 1975, p.294-337.

151. L.E.Orgel. An Introduction To Transitional-Metal Chemistry, Methuen, (1960), p.46.

152. A.F.Wells. Structural Inorganic Chemistry, Oxford University Press, (1975), p.483.

153. S.Minomura and H.G.J.Drickamer, J. Chem. Phys., 34, 3043 (1963).

154. K.L.K.Yeung, Ph.D. Thesis 1978, The City University, London.

155. C.Iwakura, H.Tada and H.Tamura, Electrochim. Acta., 22, 217 (1977).

156. J.Giner and L.Swette, Nature, 211, 1291 (1961).

157. S.M.Jasem, Ph.D. Thesis, 1978, The City University, London.

158. M.J.Kent, Ph.D. Thesis, 1972, The City University, London.

159. H.L.Bevan, Ph.D. Thesis, 1970, The City University, London.

160. S.Brunaver, P.Emmett and E.Teller, J.Am. Chem. Soc., 60, 309 (1938).

161. J.R.Goldstein, Ph.D. Thesis 1970, The City University, London.

162. M.A.Brown, X-Ray Methods, Merrow, (1971).

163. J.Giner, J.Electrochem. Soc., 111, 376 (1964).

164. A.D.S.Tantram and A.C.C.Tseung, Nature, 221, 167 (1969).

165. W.J.King, Ph.D. Thesis, 1974, The City University, London.

166. K.R.Williams, An Introduction to Fuel Cells, Elsevier, 1966, p.58.

167. J.S.Newman and C.W.Tobias, J. of Electrochem. Soc., 109, 1183 (1962).

168. A.C,C.Tseung and P.R.Vassie, Electrochim. Acta., 21, 315 (1976).

169. P.R.Vassi, Ph.D. Thesis, 1972, The City University, London.

170. C.Bramell and A.C.C. Tseung, Oxygen Evolution Studies on Teflon bonded Silicates, Unpublished.

171. W.S.Wu and A.C.C,Tseung, Chlorine evolution studies on Teflon bonded Perovskite Oxdies, Unpublished.

172. P.Delahay, New Instrumental Methods in Electrochemistry, Interscience, 1966, Ch.3, p.67.

173. P.Delahay, Advances in Electrochemistry and Electrochemical Engineering, Interscience, Vol.1, (1961) p.247.

174. G.M.Clark. The Structure of Non-Molecular Solids, Applied Science Publishers, (1972).

175. H.M.Cota, J.Katan, M.Chin and F.J.Schoenweis, Nature 203, 1281 (1964).

176. J.R.Goldstein and A.C.C.Tseung, J. of Catalysis 32, 452 (1974).

177, Y.H.Chou, A.C.C.Tseung and P.Rasiyah, Fall Meeting of The Electrochemical Society, 1981, Extended Abstracts, Vol. 81-2, The Electrochemical Society, 1981, Abstract 109, p.276.

178. M.C.M.Mann, S.Jasem, K.L.K.Yeung and A.C.C.Tseung in Seminar on Hydrogen as an Energy Vector, Commission of the European Communities, Luxemburg, (1978), p.255.

179. D.B.Rogers, R.D.Shannon, A.W.Sleight and J.L.Gillson, J.Inorg. Chem 8, 841 (1969).

180. H.Schafer, G.Schneidereit and W.Gerhardt, Z.Anorg. Allgem. Chem., 319, 327 (1963).

181. D.B.Rogers, R.D.Shannon and J.L.J.Gillson, Solid State Chem., 3, 314 (1971).

182. Handbook of Chemistry and Physics, 58th Edition, 1977-1978, CRC Press, p.B84-B178.

183. E.W.Gorter, Philips. Res. Rept., 9, 245 (1954).

184. G.Blasse, Philips. Res. Rept., 3, 1 (1964).

185. K.Kugimiya and H. Steinfink, Inorg. Chem., 7, 1762 (1968).

186. R.Parsons, Quoted by T.P.Hoar, Proc. 8th Meeting CITCE, Madrid, 1956, Butterworths. (1958).

187. A.C.C. Tseung and S.C. Dhara, Electrochim. Acta, 19, 845 (1974).

188. M.C.M.Ball and A.H.Norbury. Physical Data for Inorganic Chemists, Longman, 1974, p.40.

189. A.B.Hart and G.J.Womack. Fuel Cells: Theory and Application, Chapman and Hall, London, 1967, p.73,101.